

Reports of the Department of Geodetic Science and Surveying

Report No. 355

A STUDY OF TERRAIN REDUCTIONS, DENSITY ANOMALIES
AND GEOPHYSICAL INVERSION METHODS IN GRAVITY FIELD MODELLING

by

Rene Forsberg

The Ohio State University
Department of Geodetic Science and Surveying
1958 Neil Avenue
Columbus, Ohio 43210

April 1984

ABSTRACT

The general principles of the use of known density anomalies for gravity field modelling are reviewed with special emphasis on local applications and utilization of high degree and order spherical harmonic reference fields. The natural extension to include also unknown density anomalies will be studied within the framework of geophysical inversion methods, and the prospects for "hybrid" gravity field modelling/inversion methods will be outlined. A very simple case of such methods is the determination of representative topographic densities through collocation with parameters.

The topography, being the dominant density anomaly, together with the isostatic compensation, may be taken into account by various types of terrain reductions. Special attention is given to residual terrain reductions, i.e. using spherical harmonic expansions of the topography as a reference. The auxiliary quantity "the terrain correction" is investigated in detail, and possibilities for approximations (so called "linear approximation") in terrain effect computations are evaluated through models and actual data. Frequency domain methods using the Fast Fourier Transform are studied on a theoretical base, and used for error studies to investigate the resolution of topographic data versus the attainable accuracies of computed terrain effects.

Actual topography and gravity field data is analyzed by FFT for many different areas of USA and two areas of the Pacific, yielding power spectra, degree-variances and covariance functions for the topography and the gravity field. Results show topographic covariance functions to be of exponential type, and that use of terrain reductions as expected produce a gravity field of less variance, longer correlation length and higher degree of isotropy.

FOREWORD

This report was prepared by Rene Forsberg, Geodetic Institute, Denmark, and Research Associate, Department of Geodetic Science and Surveying, The Ohio State University, under Air Force Contract No. F19628-82-K-0022, The Ohio State University Project No. 714274. The contract covering this research is administered by the Air Force Geophysics Laboratory, Hanscom Air Force Base, Massachusetts, with Dr. Christopher Jekeli, Scientific Program Officer.

Certain computer funds used in this study were supplied by the Instruction and Research Computer Center through the Department of Geodetic Science and Surveying.

This report is a contribution to a gravity field modelling project supported by NATO grant no. 320/82. Travel support for the author's stay at The Ohio State University have been provided by a NATO Science Fellowship grant.

The author wishes to thank Dr. Richard H. Rapp for hosting me at OSU and valuable discussions, Laura Brumfield for typing the report and finally a special thanks to the many graduate students of the Department who have helped me, through fruitful discussions and through practical advice, especially how to tackle the computer system at OSU. An additional thanks to Jaime Cruz for putting to my disposal some of his plots.

The reproduction and distribution of this report was carried out through funds supplied by the Department of Geodetic Science and Surveying. This report was also distributed by the Air Force Geophysics Laboratory as document AFGL-TR-84-0174, Scientific Report No. 5, under Contract No. F19628-K-0022.

CONTENTS

1.	Introduction	1
2.	The Anomalous Gravity Field and Density Anomalies	6
3.	On the Use of Spherical Harmonic Expansions	9
4.	Utilization of Known Density Anomalies	14
5.	Unknown Densities - Geophysical Inversion	16
6.	Density Modelling Using Rectangular Prisms	24
	6.1 Space Domain	24
	6.2 Frequency Domain	28
7.	Terrain Reductions	33
	7.1 Terrain Effects and Associated Density Anomalies	34
	7.2 Practical Terrain Reductions in Gravity Field Modelling	40
	7.3 The Linear Approximation for topographic Effects	42
	7.4 Accuracy of the Linear Approximation	46
	7.5 The Terrain Correction as Convolution Integrals	50
	7.6 The Use of FFT for Terrain Effect Computations	52
	7.7 The Linear Approximation and Error Studies	57
	7.8 Error Studies of DTM Resolution Requirements	60
8.	Spectral Characteristics and Covariance Functions for Local Topography and Terrain Effects	68
	8.1 Topographic Covariance Functions for U.S. Sample Areas	73
	8.2 Magnitude of the Gravimetric Terrain Correction - Colorado Area	78
	8.3 RTM Geoid Effects - Colorado Area	82
9.	Terrain Reductions: Spectral Characteristics and Covariance Functions For Local Gravity in U.S. Sample Areas	85
10.	Isostatic Reductions of Satellite Altimetry Data in Two Areas of the Pacific	94
11.	Summary and Conclusions	107
	Appendix: TC - A FORTRAN Program for General Terrain Effect Computations	111
	References	127

1. Introduction

With the term "gravity field modelling" we usually, in the geodetic community mean methods for representing the external potential of the earth, in order to be able to estimate quantities related to the gravity field from a given set of "observed" quantities. Such methods include spherical harmonic expansions, integral formulas such as Stokes' and Vening-Meinesz' formulas and "spatial" approximation methods such as collocation and generalized point mass modelling (e.g. Bjerhammar's methods). Common for all of these methods is that they are approximation methods for harmonic functions, all rely on the assumption that the anomalous potential T fulfills Laplace's equation $\nabla^2 T = 0$ at least outside the surface of the earth. No assumption is made regarding the density distribution actually generating the gravity field.

In contrast the term "gravity field modelling" as used in geophysics stands for the process of determining internal density distributions of the earth, consistent with the observed outer field. This inversion is non-unique, and to get reasonable answers the geophysicist must introduce constraints, through selection of a finite dimensional representation of the structures (density values, depth parameters, etc.), through "fixing" some of these parameters based on independent geophysical information (well data, seismic interpretations) and through subjective choices of the most "realistic" models in terms of geology. At the basis of the geophysical gravity field modelling is the "direct problem" of potential field theory: to calculate the gravity potential and its derivatives in space due to given density distributions.

When the prime interest is in "external" gravity field modelling, any geophysical density model, realistic or not, may in principle be used to represent a part of the external field through a direct computation of the effects of the assumed

density distribution. If the density distribution is realistic we would expect the remaining field to be more smooth, in some cases the fit would be so close that we would have no use for any external gravity field modelling at all. Usually, however, our knowledge of density anomalies is confined to more shallow structures of crustal and upper mantle origin, thus mainly contributing to the shorter wavelengths of the variation of the gravity field. Longer wavelength parts of the signal are more conveniently treated using "external" modelling, such as high degree and order spherical harmonic expansions of the geopotential.

The "external" and "internal" modelling may conveniently be done simultaneously in some cases, using e.g. combined versions of collocation and geophysical inversion procedures. Thus we will at the same time estimate both the external gravity field and density values inside the earth. This approach has the advantage that it allows fairly easy use of independent geologic/geophysical information as data for the construction of external gravity field models. Due to the difficult choice of geologically "reasonable" density parameters it will, however, hardly ever be a "hands-off" automatic method like standard collocation.

Combined collocation/inversion will probably prove itself useful for inversion of future "multisensor" gravity data, as e.g. gravity vector measurements by inertial survey systems and gravity gradiometer measurements. In conventional geophysical inversion we have an inherent arbitrary choice of the "regional" field, representing the effects of all other sources than the density structures of interest. This regional/residual - separation is done using more or less crude forms of filtering and trend fitting. When we have several different types of gravity field data containing information about the same mass body, it is essential that the filtering is consistent between the various gravity field data types, such that the filter output still represent quantities related to the same harmonic function. This will be assured using combined collocation/inversion and similar methods.

In this report the utilization of density anomalies for generalized gravity field modelling will be treated in the first chapters in a rather broad way.

The bulk of the report will, however, be concerned about the most important and also best known density anomalies on the earth, namely density anomalies associated with the topography.

The density anomalies relating to the topography include the direct gravitational effects of the visual topography on the continents, the ocean bathymetry, ice cap effects and the isostatic compensation. These effects together represent a major part of the variation of the earth's gravity field, especially at shorter wavelengths (less than, say, a few hundred kilometers), where the direct computed topographic effects only to a low degree are counteracted by the isostatic compensation effects. In mountainous areas the topographic effects completely dominate the local variation of the gravity field, and some kind of terrain reduction is indispensable when attempting gravity field modelling in such areas. The most well-known terrain reduction is the Bouguer reduction, which is well-suited for geophysical work and prediction of mean free-air anomalies (for use e.g. in traditional geodetic gravity field modelling), but is not applicable for reduction of geoid undulations. Isostatic reductions provide the smoothest possible residual fields on a global basis, and are easily applicable to all the various types of gravity field data available. The computation of topographic/isostatic effects is facilitated by high-degree spherical harmonic expansions of the isostatic reduction potential (Rapp, 1982), but for local applications the computations are still relatively laborious. Since the usual Airy-type isostasy does not operate on a local scale (the short wavelength topography is supported by the finite strength of the earth's crust) we might not like to introduce the somewhat arbitrary isostatic reduction mass anomalies at the crust/mantle boundary. Instead we might just simply try to take only the short wavelength variations of the topography into

account, introducing an arbitrary smooth mean elevation surface ("model" earth) as a "reference" topography, the gravitational influence of which is not directly taken into account in the gravity field modelling. For gravity anomalies such a residual terrain correction corresponds closely to the formation of regional mean free-air anomalies, and by choice of a proper reference elevation surface, such as defined through a spherical harmonic expansion of the earth's topography to degree and order 180, we end up with a reduction which would be expected to give somewhat similar results as conventional isostatic reductions.

For local modelling of the gravity field - on which the main emphasis is put in this report - the availability of high degree and order spherical harmonic expansions of the geopotential (Lerch et al., 1981; Rapp, 1982) has proven itself to be a major break-through of big practical value. For a region like Scandinavia with reliable $1^\circ \times 1^\circ$ mean gravity data, the r.m.s. variation of the gravity anomalies is roughly reduced to half the original value, and geoid undulations may be computed with an accuracy around 1 m using such spherical harmonic expansions (Tscherning, 1983). Thus by using long-wavelength information from such expansions and combining with short and medium wavelength topographic effects computed using a residual terrain model with respect to a corresponding spherical harmonic expansion of the topography itself, the "remaining" signal will be smooth, its variance low and its degree of anisotropy usually less. This will be demonstrated later in this report, through investigations of local empirical covariance functions and power spectra of the gravity field in areas with different types of topography.

The computation of terrain effects, using digital terrain models, is basically a problem of numerical integration. However, it is by no means a simple problem. The integration kernels are usually singular at the evaluation points, and the influence of the "inner zone" - the topography in the immediate vicinity of the evaluation point - is very critical for quantities like gravity anomalies and second

order derivatives. A FORTRAN program for computing terrain effects on geoid undulations, deflections of the vertical and gravity anomalies, based on the rectangular prism as integration element, will be given in the appendix.

For gravity anomalies a type of topographic effect - the conventional gravimetric terrain correction - is of special interest. The terrain correction is basically not a terrain reduction, used in conjunction with a general gravity field modelling procedure it represents no unique density anomaly distribution to be removed from the observations. Rather the terrain correction should be viewed as a mathematical convenience, representing the - usually small - nonlinear part of the total terrain effect. Unfortunately terrain corrections have from time to time been confused with terrain reductions proper. The application of terrain corrections alone does usually not improve results of the gravity field modelling in mountainous areas significantly, since the bulk of the topographic density anomaly distribution, causing short wavelength "noise" in the gravity field, is not removed. The application of terrain corrected free-air anomalies does, however, make good sense for integral formula applications, since the application of the terrain correction to free-air anomalies represents a first (and rather crude) approximation to the problem of downward continuation of gravity observations from the surface of the topography to the geoid, the terrain correction being an approximation to Molodensky's G_1 -term, see e.g. Heiskanen and Moritz (1967) and Moritz (1966). The role of the terrain correction will be given attention later in this report, and some examples of its magnitude will be given.

To summarize, the emphasis in this report will be on the utilization of density anomalies in local gravity field modelling - especially collocation and related methods. The first part will review principles for the utilization of known and unknown density anomalies, then the practical computation of such effects - especially topographic effects - will be outlined, and finally the influence of

the topography will be studied through investigations of empirical covariance functions for various test areas in the United States. No major examples of actual applications of the methods for gravity field modelling will presently be given. For earlier results of gravity field modeling by collocation using some of the terrain reduction concepts presented, the reader is referred to e.g. Forsberg and Tscherning (1981), Forsberg and Madsen (1981), and Tscherning and Forsberg (1983).

2. The Anomalous Gravity Field and Density Anomalies

The gravity field of the earth is traditionally described using the anomalous potential T

$$T = W - U \quad (2.1)$$

representing the difference between the actual geopotential W and a normal potential U , corresponding to chosen reference ellipsoid parameters. In U is also included the centrifugal, tidal and atmospheric potentials, and thus T is a harmonic function.

$$\nabla^2 T = 0 \quad (2.2)$$

outside the surface of the earth, and may be expanded in spherical harmonics

$$T(r, \phi, \lambda) = \frac{GM}{r} \sum_{\ell=2}^{\infty} \sum_{m=-\ell}^{\ell} a_{\ell m} \left(\frac{R}{r}\right)^{\ell} \bar{Y}_{\ell m}(\phi, \lambda) \quad (2.3)$$

$$\bar{Y}_{\ell m}(\phi, \lambda) = \begin{cases} \bar{P}_{\ell m}(\sin \phi) \cos m\lambda & (m \geq 0) \\ \bar{P}_{\ell m}(\sin \phi) \sin m\lambda & (m < 0) \end{cases}$$

Here G is the gravitational constant, M the mass of the earth and R the radius of a reference earth sphere (Bjerhammar sphere).

The observable gravity field quantities may in the usual spherical approximation be expressed as linear functionals $L(T)$, the most important quantities being point and area mean values of

$$\zeta = \frac{T}{\gamma} \quad \text{Height anomalies/geoid undulations} \quad (2.4)$$

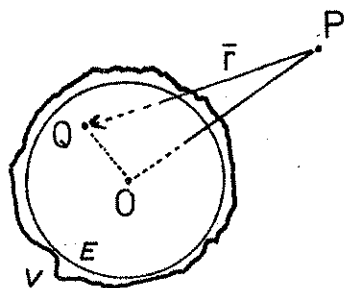
$$\left. \begin{aligned} \xi &= -\frac{1}{r\gamma} \frac{\partial T}{\partial \phi} \\ \eta &= -\frac{1}{r\gamma \cos \phi} \frac{\partial T}{\partial \lambda} \end{aligned} \right\} \quad \text{Deflections of the vertical} \quad (2.5)$$

$$\Delta g = \frac{\partial T}{\partial r} - \frac{2}{r} T \quad \text{Free-air anomaly} \quad (2.6)$$

$$\delta g = -\frac{\partial T}{\partial r} \quad \text{Gravity disturbance} \quad (2.7)$$

where γ is normal gravity.

Similarly, density anomalies $\Delta\rho$ may be defined as the difference between the actual density distribution ρ inside the earth and a normal density distribution ρ_0 , generating U :



$$\Delta\rho = \rho - \rho_0 \quad (2.8)$$

$$W = \int_V \frac{\rho}{r} dV_Q + \phi, \quad r = |\bar{r}| \quad (2.9)$$

$$U = \int_E \frac{\rho_0}{r} dV_Q + \phi \quad (2.10)$$

Figure 1.

where ϕ is the centrifugal potential, V the interior of the earth and E the reference ellipsoid. We thus have

$$T(P) = \int_V \frac{\Delta\rho}{r} dV_Q \quad (2.11)$$

In other words, $\Delta\rho$ is a density distribution generating the anomalous gravity field.

Due to the fundamental ambiguity of potential field theory, an infinite variety of density distributions satisfying (2.10) exists. If a spherical normal potential U is chosen, indeed any radial symmetric density distribution, having the correct GM-value, generates U . It is therefore clear that the observed gravity field is of no use in determining a realistic normal density ρ_0 . Instead we must get information on ρ_0 from other geophysical sources: seismic body-wave travel times, surface wave dispersion curves, eigen periods of the earth's free oscillations and the moment of inertia. Examples of current earth models, applicable for "defining" ρ_0 , is the HB-I (Haddon & Bullen, 1969) model and the PEM-models (Dziewonski et al., 1976).

To account for the non-spherical part of ρ_0 , we may resort to perturbing the interior density distribution by small amounts, given by the hydrostatic equilibrium theory. The flattening of the interior density discontinuities will thus be decreasing downwards, from 1/298 at the surface to 1/390 at the core/mantle boundary. Alternatively we may resort to a stringent analytic representation of the normal density distributions using ellipsoidal coordinates (where the flattening increase with depth), and more or less arbitrary mathematical constraints to secure a unique solution (Moritz, 1968; Tscherning & Sunkel, 1980). In any way, however, the non-spherical perturbations are very small, much less than the errors in the geophysical earth models, and we may thus for all practical purposes simply disregard these.

We are thus free to choose "convenient" reference density distributions when working in given regions: a typical continental choice would be e.g. a density starting at 2.67 g/cm^3 at sea level, increasing to 2.9 at the base of the crust, jumping to 3.3 across the moho at 32 km depth and increasing through the mantle with major "discontinuities" at the phase transition zones at ~420 km (olivine-spinel) and at ~700 km. At the base of the mantle the PEM-model gives a density of 5.4, and for the earth's core values from 9.9 to 13.0 at the center, the density of the inner core being still very uncertain. For an oceanic area we might change this model above the low velocity zone, e.g. choosing a reference model with 4 km of water (density 1.03), a thin, dense crust (2.9) extending to 12-18 km depth and an "undepleted", oceanic upper mantle at 3.4 g/cm^3 .

3. On the Use of Spherical Harmonic Expansions

When we use a spherical harmonic expansion as a first step in gravity field modelling, the "wanted" approximation \tilde{T} to T is split into

$$\tilde{T} = \tilde{T}_1 + \tilde{T}_2 \quad (3.1)$$

with \tilde{T}_1 given by the expansion

$$\tilde{T}_1(r, \phi, \lambda) = \frac{GM}{r} \sum_{\ell=2}^{\ell_{\max}} \sum_{m=-\ell}^{\ell} a_{\ell m} \left(\frac{R}{r}\right)^{\ell} Y_{\ell m}(\phi, \lambda) \quad (3.2)$$

The currently available high degree-and-order models ($\ell_{\max} = 180$) provides the bulk of \tilde{T} . They suffer, however, of a minor problem relating to the continental topography: information on the higher-degree coefficients stem from analysis of $1^\circ \times 1^\circ \Delta g$ (used directly in the Rapp models (Rapp, 1981) and through Stokes' formula in GEM10C (Lerch et al., 1981)), treated as data on a sphere, neglecting that the continental anomalies are actually anomalies at altitude. This fact gives rise to a small correction, completely corresponding to Molodensky's G_1 -term, but in the frequency domain.

Let the standard surface harmonic expansion of the mean anomalies be

$$\overline{\Delta g}(\phi, \lambda) = \frac{GM}{R^2} \sum_{\ell} \sum_m (\ell-1) a'_{\ell m} \overline{Y}_{\ell m}(\phi, \lambda) \quad (3.3)$$

To first order these anomalies correspond to elevation $\overline{h}(\phi, \lambda)$, defined through a similar expansion of the continental topography (0 at oceans). Using the correct spatial expansion (3.2) we get

$$\overline{\Delta g} = \frac{GM}{(R+\overline{h})^2} \sum_{\ell} \sum_m (\ell-1) a_{\ell m} \left(\frac{R}{R+\overline{h}}\right)^{\ell} \overline{Y}_{\ell m} \quad (3.4)$$

$$\approx \frac{GM}{R^2} \left(1 - 2\frac{\overline{h}}{R}\right) \sum_{\ell} \sum_m (\ell-1) a_{\ell m} \left(1 - \ell\frac{\overline{h}}{R}\right) \overline{Y}_{\ell m} \quad (3.5)$$

$$\approx \overline{\Delta g}^* - \frac{GM}{R^3} \overline{h} \sum_{\ell} \sum_m (\ell-1)(\ell+2) a_{\ell m} \overline{Y}_{\ell m} \quad (3.6)$$

where $\overline{\Delta g}^*$ is the gravity anomalies harmonically downward continued to the Bjerhammar sphere. Since $a_{\ell m} \approx a'_{\ell m}$, the second term in (3.6) may be evaluated with sufficient accuracy from existing solutions, representing essentially $\overline{h} \cdot T_{zz}$. Expanding this correction term in surface spherical harmonics $b_{\ell m}$, we obtain

$$\overline{\Delta g} = \overline{\Delta g}^* - \frac{GM}{R^3} \sum_{\ell} \sum_m b_{\ell m} \overline{Y}_{\ell m} \quad (3.7)$$

which by (3.3) and expansion of $\overline{\Delta g}^*$ gives

$$a_{\ell m} = a'_{\ell m} + \frac{1}{\ell-1} b_{\ell m} \quad (3.8)$$

The correction term has for gravity anomalies a maximum value of c. 19 mgal (Rapp, 1983). For local gravity field modelling the above has the practical application that elevations of the individual (ground) observation points should be used properly when evaluating (2.3), otherwise elevations should rather be set to zero.

Corresponding to (3.1) also the density anomaly may be split in a spherical harmonic reference part and a residual

$$\Delta\rho = \Delta\rho_1 + \Delta\rho_2 \quad (3.9)$$

The reference density distribution $\Delta\rho_1$ poses some problems, especially for high degree-and-order fields ($\ell_{\max} \geq 180$), since many of the major crustal - upper-mantle structures (trenches, rifts, etc.) will indeed have a significant part of their gravitational signal in the reference part $\Delta\rho_1$. When working with residuals (" T_2 ") only, the response from assumed $\Delta\rho$ -models must thus be split, either by introducing a "formal" $\Delta\rho_1$, or by high-pass filtering the response. In this case we will, however, lose important information about the structure.

For more local gravity field modelling, we may totally neglect the density split (3.9). Many of the typical intracrustal density anomalies would have only small long-wavelength effects. By removing such density anomalies computationally, the remaining part of the residual potential T_2 would in principle be "contaminated" with these long wavelength errors, but they will usually not be very significant compared to e.g. the errors in the reference field \tilde{T}_1 .

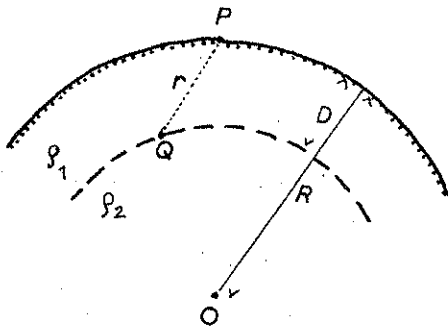
For the topography, the natural choice of $\Delta\rho_1$ would be a model corresponding to an analogous expansion in spherical harmonics of the topographic elevations:

$$\bar{h}(\phi, \lambda) = \frac{1}{R} \sum_{\ell=1}^{\ell_{\max}} \sum_{m=-\ell}^{\ell} h_{\ell m} \bar{Y}_{\ell m}(\phi, \lambda) \quad (3.10)$$

The reference density model in this case would have density $\sim 2.67 \text{ g/cm}^3$ below the mean elevation surface $\bar{h}(\phi, \lambda)$ on the continents. More on this (i.e., the residual terrain correction) later.

Formal introduction of spherical harmonic reference density anomalies may be done using simple analytical inversion methods. Consider e.g. a two-layer

earth model with a interface at depth D (Figure 2). The effect of undulations $h(\phi, \lambda)$ of this interface may be approximated by a mass coating of density $\kappa = (\rho_2 - \rho_1)h$. We thus have:



$$T_1(P) = G \int_{\sigma_i} \frac{\kappa(Q)}{r(P,Q)} d\sigma(Q) \quad (3.11)$$

where σ_i is the interface sphere.

Figure 2

(3.11) represents a spherical convolution, and we have the simple well-known expression in the frequency domain for the dimensionless coefficients (3.2) of the generated potential

$$a_{\ell m} = \frac{4\pi R^2}{M} \frac{1}{2\ell+1} \left(1 - \frac{D}{R}\right)^\ell \kappa_{\ell m} \quad (3.12)$$

see e.g. (Sunkel, 1981b). Just a single interface thus provides a unique inversion. For real applications, however, several layers will be needed in order that the derived interface undulations be reasonable and the corresponding stress levels within accepted limits. Typically the lower harmonics could be modelled as "topography" on the mantle/core interface and the deeper mantle phase transition zones, the higher harmonics on discontinuities in the upper mantle and the moho. Such a model makes reasonable physical sense, it has e.g. been hypothesized that major global features of the geoid corresponds to thermally induced shifts in the olivine-spinel transition zone.

Alternatively, unique "spatial" density anomaly models may be obtained by imposing "analytic" constraints on the possible density distributions. If e.g. the density distribution fulfills the condition

$$\nabla^2(r^n \rho) = 0 \quad (3.13)$$

where n is an arbitrary integer constant, the density solution is found by an expansion in internal spherical harmonics as

$$\rho(r, \phi, \lambda) = r^{-n} \sum_{\ell} \sum_m b_{\ell m} \left(\frac{r}{R}\right)^{\ell} Y_{\ell m}(\phi, \lambda) \quad (3.14)$$

with

$$b_{\ell m} = \frac{(2\ell - n + 3)(2\ell + 1)}{4\pi GR^{3-n}} a_{\ell m} \quad (3.15)$$

for $2\ell > n - 3$ (Tscherning, 1974). The drawback of this method is that the condition (3.13) is completely arbitrary without any physical meaning. The resultant density distribution will have its extremes at the surface of the sphere, and the actual density variations will be very low - e.g. order-of-magnitude 0.004 g/cm^3 for GEM10B ($\ell_{\text{max}} = 36$) (Tscherning & Sunkel, 1980). Attempts to find other constraints like (3.13) corresponding to some simple physical minimum principle have been fruitless (Tscherning, personal communication). - it is obviously not possible to find "state equations" for the earth's interior relating only to the density distribution.

4. Utilization of Known Density Anomalies

In external gravity field modelling known (or assumed) density anomalies may be taken into account by a simple remove-restore technique: the influence of the anomalous masses is subtracted from the given data ("observations"), then

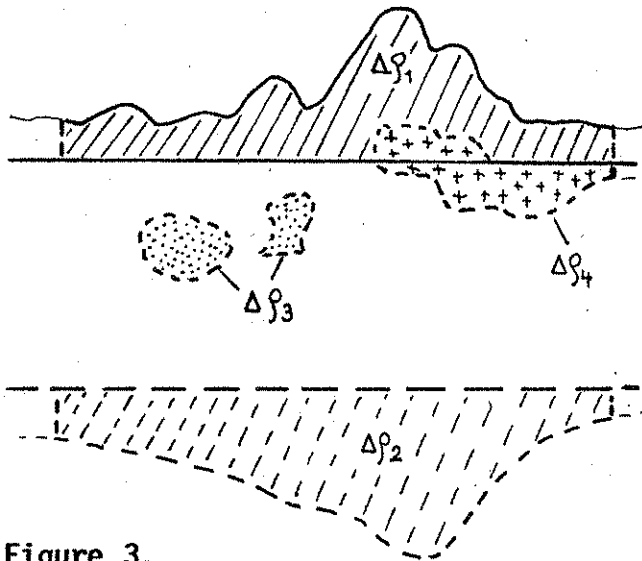


Figure 3.

the gravity field modelling technique is applied on these terrain reduced data, and the final results ("predictions") are obtained by adding back the terrain effects to the predicted anomalies.

Let V be the volume enclosing the given density anomalies.

Then in a point P

$$T_m(P) = G \int_V \frac{\Delta\rho}{r} dV_Q, \quad r = |\bar{r}_Q - \bar{r}_P| \quad (4.1)$$

is the terrain effect potential, and for a gravity field quantity $L(T)$ we have the "terrain" effect (including "geologic" effects)

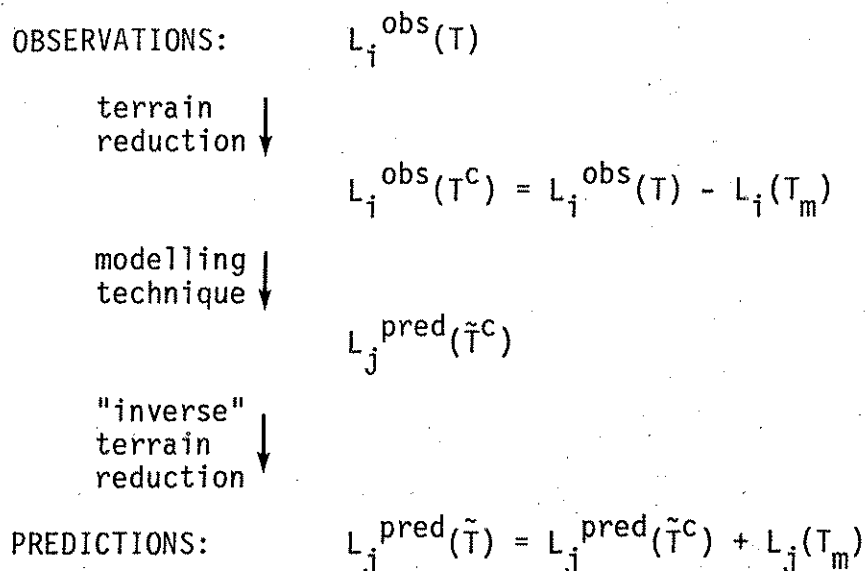
$$L(T_m) = G \int_V \Delta\rho L\left(\frac{1}{r}\right) dV \quad (4.2)$$

e.g. for the gravity disturbance vector

$$\delta\bar{g}_m = -\nabla T_m = -G \int_V \Delta\rho \nabla\left(\frac{1}{r}\right) dV = G \int_V \Delta\rho \frac{\bar{r}}{r^3} dV \approx \sum_i G \Delta\rho_i \int_{V_i} \frac{\bar{r}}{r^3} dV \quad (4.3)$$

For practical computations "building blocks" of constant density are traditionally used, as expressed by the last term of (4.3).

The remove-restore technique may schematically be written as:



Irrespectively of the gravity field modelling technique actually used (Integral formulas, Collocation etc.), T^c must be a harmonic function. This is secured if T_m represents the gravitational effects of a given, fixed mass model, e.g. the density anomalies within a given geographical area. The same mass model must naturally be used for both the observed and predicted quantities. For topographic/isostatic effects and - especially - "residual" topographic effects, a global mass model is often appropriate: formally we thus have to extend the integral (4.2) all around the earth, but in practice it is sufficient to integrate out to a certain distance from the computation point - depending on the type of gravity field quantity and thus the "sharpness" of the integral kernel $L(\frac{1}{r})$ - the effect of the distant topography being either negligible or obtainable from e.g. spherical harmonic expansions.

When using a remove-restore technique like outlined here, it is important to know that the assumed density anomalies need not be realistic - any density distribution may be used as long as T_m and thus T^c is harmonic outside the topography. But naturally the most smooth T^c is expected when the most realistic mass model is applied. For "geologic" density anomalies - e.g. salt domes, intrusions, faults

where the function f_p is generally non-linear and must be linearized

$$(L_p(T) - L_p^0(T)) = \sum_i \left. \frac{\partial f_p}{\partial x_i} \right|_0 \Delta x_i \quad (5.2)$$

by assuming an initial model x_i^0 . Since geophysical inversion problems are often highly nonlinear, a large number of iterations (5.2) are often necessary. The model parameters x_i may be generally classified in two types:

- 1) geometric parameters (interface depths etc.)
- 2) density value parameters

The main emphasis in traditional geophysical modelling has been in terms of structural geometric parameters (see e.g. Burkhard & Jackson, 1976; Pedersen, 1979), to directly represent interfaces such as the top basement in sedimentary basins or the moho, exemplified in Figure 4 (left). The advantage of the geometric parameters is that they directly reflect simplified geologic models, and additional data such as well control is easily including by e.g. fixing one or more parameters. The drawback of choosing "structural" parameters is the inherent nonlinearities.

Opposed to this, models with density value parameters only (Figure 4, right) are perfectly linear, but the computational advantage of the linearity is usually counterweighted by the greater number of parameters needed to represent a wanted geologic scenario. Also it is less simple to include the non-gravity constraints. The commonly applied point mass modelling in geodesy may be viewed as a special case of such geophysical inversion, using the simplest possible finite element representation (delta spikes) of the subsurface density distribution. However, this simplest possible case of inversion gives results that are amazingly close to results obtained using improved (spatial) density representations (Figure 5).

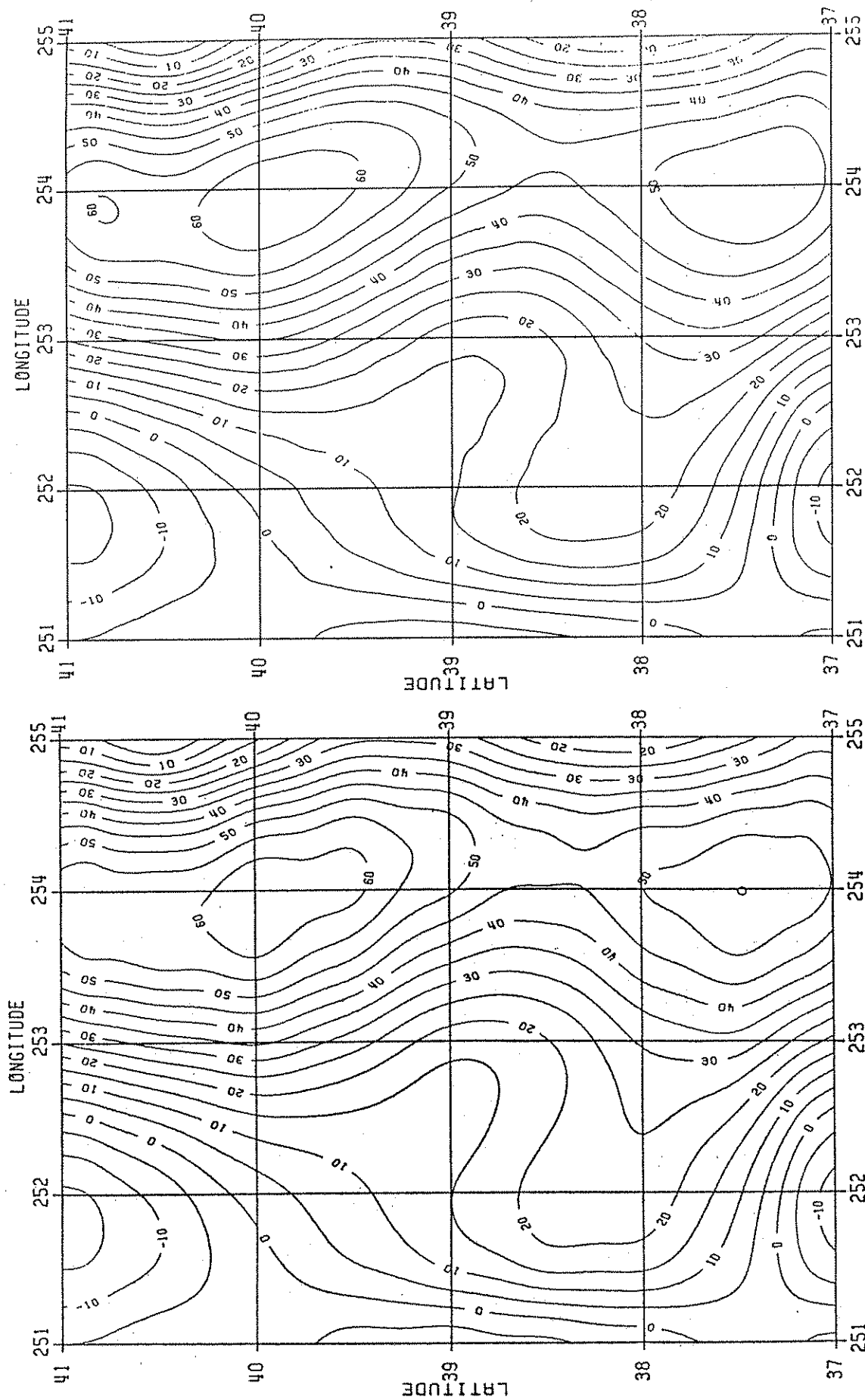


Figure 5 Example of gravity field modelling using inversion. From a $\frac{1}{4}^{\circ} \times \frac{1}{2}^{\circ}$ grid of smooth free-air anomalies in the Colorado area (from the Rapp (1981) 180x180 expansion), density parameters were solved for on a $\frac{1}{2}^{\circ} \times \frac{1}{2}^{\circ}$ grid. Figures show the computed "model" field at the surface, using
LEFT: density spikes, point masses in depth 50 km,
RIGHT: spatial density distribution, using prisms of constant density at depth 25-75 km.

Assuming a set of observations $y_i = L_i(T)$, $i = 1, \dots, n$ the (linearized) inversion geophysical problem may be written as

$$y = Ax \quad (5.3)$$

where A is the response matrix. This problem is generally ill-conditioned or improperly posed, and generalized inversion must not be used.

One popular technique is the use of the singular value decomposition:

$$A = U\Lambda V^T, \quad \Lambda = \begin{pmatrix} \lambda_1 & & 0 \\ & \ddots & \\ 0 & & \lambda_p \end{pmatrix} \quad (5.4)$$

with the U and V being orthonormal matrices defined through

$$\begin{aligned} A^T A v_j &= \lambda_j^2 v_j & V &= \{v_j\} \\ A A^T u_j &= \lambda_j^2 u_j & U &= \{u_j\} \end{aligned} \quad (5.5)$$

See e.g. Pedersen (1979) or Rummel et al. (1979). p is the number of non-zero eigen values, i.e. the number of degrees of freedom of the problem. A solution \tilde{x} to (5.3) is given by the Lanczos inverse,

$$\tilde{x} = V\Lambda^{-1}U^T y \quad (5.6)$$

minimizing as well $y^T y$ as $x^T x$. To prevent the eigen values of ill-conditioned problems to induce large changes in the parameters x , the eigen value spectrum λ_i may be truncated by removing eigen values smaller than a suitable threshold, giving the traditional trade-off between resolution and variance.

Alternatively to the explicit use of the singular value decomposition, essentially the same solution may be obtained using Tikhonov regularization. In this case we seek to minimize a combination.

$$\|y - Ax\|^2 + \alpha \|x\|^2, \quad \alpha > 0 \quad (5.7)$$

Assuming a noise covariance matrix D for the observations and an a priori covariance matrix C for the "signal" x (both matrices usually assumed to be diagonal), we obtain the solution by solving the normal equations.

$$(A^T D^{-1} A + \alpha C^{-1}) \tilde{x} = A^T D^{-1} y \quad (5.8)$$

(Rummel et al., 1979). The constant α is arbitrary and may be chosen to obtain a desired smoothness of the parameters, again with the price to be paid being a degraded fit of the model.

Independent geologic information may be taken into account using linear constraints of the form

$$Bx = C \quad (5.9)$$

where B and C are constant. Such constraints can be used to fix certain parameters (e.g. representing known depths to an interface), to fix differences in density values (e.g. forcing parameters of type "2" to represent layers, faults, etc.) and to introduce special geometric constraints on the anomalous mass body based on geologic experience (e.g. assuming a dike to have parallel sides). The constraint (5.9) is taken into account in the minimization problem (5.8) using Lagrange multipliers, obtaining somewhat more complicated normal equations. Details may be found e.g. in Burkhard & Jackson (1976).

The methods outlined above represent conventional geophysical inversion techniques. They are usually applied only for one type of gravity field quantity (gravity anomalies or - at times - altimeter geoid undulations), but there is of course no restriction in the model formulation to utilize heterogeneous data (e.g. simultaneous gravity and geoid information) as we are commonly used to in geodesy. The problem with the heterogeneous data lies in the regional/residual separation: the gravity field contains information about density anomalies at

all depths, but the model parameters x are typically restricted to describe simplified rather shallow structures - a filtering is therefore done to remove the unwanted parts of the signal. This filtering is often very crude (e.g. graphical determination of a "regional") and not applicable for heterogeneous data, for such data we must make sure that the filtering of the different data types are consistent - the "regional" must be a harmonic function.

In some cases high degree and order spherical harmonic expansions might be valuable as "regionals" - e.g. when trying to model total crustal density distributions-but we should then also have a well-defined spherical harmonic reference density distribution (c.f. Section 3). Alternatively we can utilize "general" gravity field modelling techniques to represent the regional, e.g. by introducing arbitrary (deep) model point-masses or by doing the inversion within the framework of least squares collocation with parameters.

In this case we have the following observation equations for an observation y_i with associated linear functional L_i and noise n_i :

$$y_i = \{Ax\}_i + L_i(T) + n_i \quad (5.10)$$

for which we get the well-known collocation solution (see e.g. Moritz, 1980)

$$\begin{aligned} \tilde{T}(Q) &= L_i K(\cdot, Q)^T C^{-1} \\ \tilde{x} &= (A^T C^{-1} A)^{-1} A^T C^{-1} y \\ C &= \{L_i L_j K(\cdot, \cdot) + D_{ij}\} \end{aligned} \quad (5.11)$$

where D again is the noise covariance matrix, $K(P, Q)$ the potential covariance function of the gravity field. Note that this covariance function should not be the observed, empirical covariance function but rather the covariance function of the field after the model influence have been subtracted - i.e. the covariance function of the "regional". We would expect this field to have less variance and greater correlation length than the original field. Since the model results

depend on the covariance parameters, these must ultimately be determined through trials or through considerations of the wanted characteristics of the regional/residual filter.

Least squares collocation with parameters will be especially well-suited for the determination of optimum topographic reduction densities in mountainous areas. In this case our model parameters x will just be a single value (or a few, if the geology is changing), and the observation equation (5.10) will look like

$$y_i = \{G \int_V L_i(\frac{1}{r})dV\} \Delta\rho + L_i(T) + n_i \quad (5.12)$$

where the term in the bracket represents the terrain effect of a topography with unit density, cf. (4.2). This problem is well-conditioned for sufficiently varying topography, and represents a straight forward generalization of Nettletons density profiling method to heterogeneous data. More reliable density estimates are obtained with (5.12) than with the more traditional approaches such as regression analysis of the variation of free-air anomalies with elevation, as pointed out by Sunkel (1981a). Application of (5.12) will probably be even better than using real measurements of sample rock densities: everybody who has tried this knows how difficult it is to estimate average formation densities from samples of individual rock formations, especially for sedimentary rocks with their varying porosity and water saturation.

When estimating more complex structural models of the density anomalies, stabilization of the parameters \tilde{x} in (5.11) will be needed, and we will have to make a combined collocation/generalized inverse approach. Collocation by itself may be viewed as an inversion problem (Moritz, 1976): the simple collocation approximation \tilde{T} is built up from the kernel function $K(P, Q)$ in the observation points:

$$\tilde{T}(Q) = \sum_j a_j L_j K(\cdot, Q) \quad (5.13)$$

where the coefficient a_j is the solution for the "normal equations" corresponding to (5.11). Expressing (5.6) in terms of these coefficients we have:

$$\begin{aligned} y_i &= Ax + \sum_j L_i L_j K(\cdot, \cdot) \cdot a_j + n_i \\ &= \left\{ A \mid \{L_i L_j K(\cdot, \cdot)\} \right\} \left\{ \begin{matrix} x \\ \{a_j\} \end{matrix} \right\} + n_i \end{aligned} \quad (5.14)$$

which clearly shows our problem as a "double" generalized inverse problem with unknowns x_j (geophysical parameters) and a_j (kernel coefficients). The solution is obtained by minimizing a combination:

$$\|x\|^2 + \alpha \|T\|_H^2 \quad (5.15)$$

where α is a positive constant and $\|\cdot\|_H$ the Hilbert space norm associated with the chosen covariance function K . The constant α is arbitrary, and must be chosen based on empirical investigations. The constant determines how much variation is put "into" the structure and how much is retained in the outer, residual field, and acts like the "trade-off" parameter in (5.7). By combining the well-known methods of collocation and geophysical generalized inversion like outlined here, we have in fact obtained a discrete version of the so-called "mixed collocation", suggested by Sanso and Tscherning (1982).

The practical applicability of hybrid gravity field modelling/geophysical inversion methods remains to be seen. For geodesy and external gravity field modelling the obvious application would lie in the determination of only a few key parameters: topographic densities, density contrasts across major known discontinuities (e.g. for moho at continental margins) and density anomalies of well-known geologic bodies (e.g. salt domes), avoiding unlinear structural parameters requiring iteration. The computational burden would not be significantly increased using

such a limited set of parameters, and by choosing "good" geologically reasonable parameters, one could hope in many cases to get significant improvements in the characteristics of the "background" field: less power, more stationarity and a higher degree of isotropy.

Probably the geophysical exploration would benefit more from the hybrid collocation/inversion scheme. With the technological advances heterogeneous gravity field data will be more common - through the development of high-precision inertial survey systems measuring the complete gravity vector, through airborne gradiometry and through geoid undulations from GPS and satellite altimetry in addition to terrestrial or airborne gravity. To perform quantitative interpretations with error analysis etc. for such data, some kind of "hybrid" inversion method will be necessary, to stringently handle model oversimplifications, regional/residual separations etc.

With these remarks the general discussion of density anomalies and inversion techniques will be concluded. In the next section formulas for actual computations will be given, and then the main density anomaly - the topography - will be treated in detail.

6. Density Modelling Using Rectangular Prisms

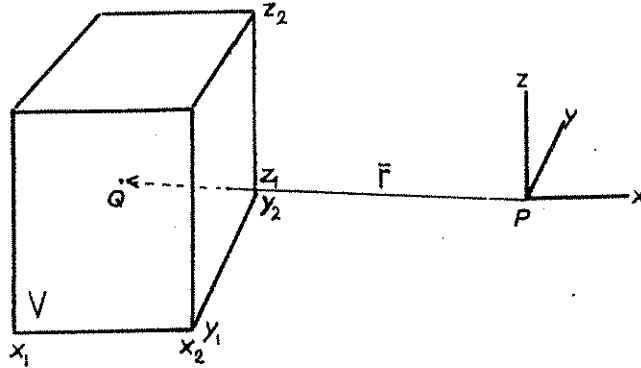
6.1 Space Domain

For the practical evaluation of gravitational effects of density anomalies, integrals of the type:

$$L(T_m) = G \int_V \Delta\rho L\left(\frac{1}{r}\right) dV \quad (6.1)$$

must be computed numerically. This computation is most naturally done using the simplest form of finite element representation of the density distribution: assuming the density anomaly $\Delta\rho$ to be constant in subblocks, each such finite element

(subblock) being a rectangular prism. For terrain reductions using digital models, these subblocks e.g. naturally correspond to the subdivision defined by the elevation data grid. The evaluation of integrals (6.1) over each finite element is synonymous with the formulas for the gravitational effects of the rectangular prism of constant density.



To integrate spherical symmetric function like $\frac{1}{r}$ over an interval with Cartesian symmetry is doomed to give some very complicated integrals, this being indeed the case for the rectangular prism formulas. Let the coordinate system used have axes parallel to the prism sides and origin in the computation point \$P\$, as indicated in Figure 6. In the sequel \$\vec{r} = (x, y, z)\$ is the coordinate of the integration point \$Q\$ in this system. We have in \$P\$ for various gravimetric quantities:

$$T = G\Delta\rho \int_V \frac{1}{r} dV = G\Delta\rho \int_{x_1}^{x_2} \int_{y_1}^{y_2} \int_{z_1}^{z_2} \frac{1}{r} dx dy dz, \quad r = \sqrt{x^2 + y^2 + z^2} \quad (6.2)$$

$$\delta g = -G\Delta\rho \int_V \frac{\partial}{\partial z_P} \left(\frac{1}{r} \right) dV = G\Delta\rho \int_V \frac{\partial}{\partial z_Q} \left(\frac{1}{r} \right) dV = -G\Delta\rho \int_V \frac{z}{r^3} dV \quad (6.3)$$

$$T_{zz} = -\frac{\partial}{\partial z_P} (\delta g) = -G\Delta\rho \int_V \frac{\partial}{\partial z_Q} \left(\frac{z}{r^3} \right) dV = -G\Delta\rho \int_V \frac{r^2 - 3z^2}{r^5} dV \quad (6.4)$$

$$T_{xz} = -\frac{\partial}{\partial x_P} (\delta g) = G\Delta\rho \int_V \frac{3xz}{r^5} dV \quad (6.5)$$

Since differentiations occur under the integrals for the higher order derivatives, these will give the simplest formulas. Let the formulas (6.2) - (6.5) be evaluated

as undefinite integrals to keep the notation simple. We have then for the second order derivatives

$$\underline{T_{zz}}: -G\Delta\rho \int \int_{x,y} \frac{z}{r^3} dx dy = -G\Delta\rho z \int_y \frac{1}{y^2+z^2} \frac{x}{r} dy = G\Delta\rho z \arctan \left(\frac{xy}{zr} \right) \quad (6.6)$$

$$\underline{T_{xz}}: G\Delta\rho \int \int_{y,z} \frac{z}{r^3} dx dy = G\Delta\rho \int_y \frac{1}{r} dy = G\Delta\rho \log (y+r) \quad (6.7)$$

For the first order derivative a non-trivial integration of (6.7) with respect to x is obtained (Jung, 1961):

$$\underline{\delta g}: -G\Delta\rho \int \int_{x,y} \frac{1}{r} dx dy = G\Delta\rho \int_x \log (y+r) dx = G\Delta\rho (x \log (y+r) + y \log (x+r) - z \arctan \left(\frac{xy}{zr} \right)) \quad (6.8)$$

Finally the formula for geoid undulations (height anomalies) are obtained by integrating (6.8) with respect to z (MacMillan, 1958):

$$\underline{T}: G\Delta\rho [xy \log (z+r) + xz \log (y+r) + yz \log (x+r) - \frac{x^2}{2} \arctan \frac{yz}{xr} - \frac{y^2}{2} \arctan \frac{xz}{yr} - \frac{z^2}{2} \arctan \frac{xy}{zr}] \quad (6.9)$$

The final formulas for the rectangular prisms are obtained by summing the expressions (6.6) - (6.9) over the corners of the prisms with alternating signs, e.g. $T = \sum_{i=1}^2 \sum_{j=1}^2 \sum_{k=1}^2 (-1)^{i+j+k} T_{ijk}$, where T_{ijk} is (6.9) evaluated at (x_i, y_j, z_k) . The formulas for the remaining derivatives (deflections of the vertical, other second order gradients) are simply obtained by coordinate permutations, see Forsberg and Tscherning (1981).

Although some simplifications of the final formulas are possible using addition theorems for logarithms and \arctan ($\arctan a + \arctan b = \arctan \frac{a+b}{1-ab}$), the formulas

are still very complex and time consuming. In the terrain effect computation program (see appendix) an approximative formula, where the mass of the prism is condensed as a mass layer on the xy-plane through the center of the prism, is used for geoid undulations instead of (6.9). In this case we get an integral similar to (6.8):

$$\begin{aligned}
 T &\approx G\Delta\rho(z_2 - z_1) \int \int_{x,y} \frac{1}{r_{z=z_m}} dx dy \\
 &= G\Delta\rho(z_2 - z_1) \left[x \log(y+r) + y \log(x+r) - z_m \arctan \frac{xy}{z_m r} \right]_{x_1}^{x_2} \left[y_1 \right]^{y_2}, \\
 z_m &= \frac{z_1 + z_2}{2}, \quad r = \sqrt{x^2 + y^2 + z_m^2}
 \end{aligned} \tag{6.10}$$

For terrain effect computations, this formula has negligible error (typically corresponding to millimeters in ζ).

In larger distances from the prism, the formulas (6.6) - (6.9) may be substituted by much simpler series expressions of the gravity field, obtained using a spherical harmonic expansion of the prism field. Since the spherical harmonics expressed in cartesian coordinates are simple homogeneous polynomials in x , y , and z , the resulting series expansions are simple. In a prism-centered coordinate system we have for the potential

$$\begin{aligned}
 T = G\Delta\rho \Delta x \Delta y \Delta z \left\{ \frac{1}{r} + \frac{1}{24r^5} [(2\Delta x^2 - \Delta y^2 - \Delta z^2)x^2 + (-\Delta x^2 + 2\Delta y^2 - \Delta z^2)y^2 \right. \\
 \left. + (-\Delta x^2 - \Delta y^2 + 2\Delta z^2)z^2] + \frac{1}{288r^9} [\alpha_1 x^4 + \alpha_2 y^4 + \dots] + \dots \right\},
 \end{aligned} \tag{6.11}$$

$$\Delta x = x_2 - x_1, \Delta y = y_2 - y_1, \Delta z = z_2 - z_1$$

(MacMillan, 1958), from which gravity, second order derivatives etc. are easily found by differentiation. The first term in (6.11) is simply the point mass approximation. The second term takes into account the different dimensions of the prism - it is zero for a cube.

In the terrain effect computation programme given in the appendix, a subroutine "PRISM" forms the nucleus of the calculations. This subroutine uses the exact prism formulas when the computation point P is near the prism, in an intermediate zone the MacMillan formula (6.11) is used, and finally in very large distances the point mass approximation is used. The shift between the formulas is automatic, determined by accuracy levels wanted by the user. (cf. Figure 7). It is through the additional use of the approximate formulas that the prism method becomes feasible for "routine" gravity field modelling in mountainous areas, otherwise evaluation of the complex exact prism formulas would often become prohibitive in terms of computer time. Furthermore, in large distances the formulas (6.6)-(6.10) become numerically unstable, requiring extended precision due to the differencing of the evaluated "corner" - functions entering the formulas.

6.2 Frequency Domain

While the prism formulas are complicated in the space domain, they are surprisingly simple in the frequency domain. Since the basics of Fourier analysis of potential fields is not generally well known in geodesy, a short outline will be given first.

The Fourier spectral analysis is applied in the flat-earth approximation. Let π be the reference plane (e.g. sea level) with coordinates (x, y) , and $\tilde{\pi}$ the associated spectral plane with spatial frequencies (u, v) . Then the Fourier transformation is given by (" $\tilde{\cdot}$ " denotes transformed quantities):

$$\tilde{T}(u, v) = \int_{\pi} T(x, y) e^{-i(ux+vy)} dx dy \quad (6.12)$$

$$T(x, y) = \frac{1}{4\pi^2} \int_{\tilde{\pi}} \tilde{T}(u, v) e^{i(ux+vy)} du dv \quad (6.13)$$

Upward continuation of the field to elevation z is obtained by a filtering

$$\tilde{T}(u, v, z) = \tilde{T}(u, v) e^{-\omega z}, \quad \omega = \sqrt{u^2 + v^2} \quad (6.14)$$

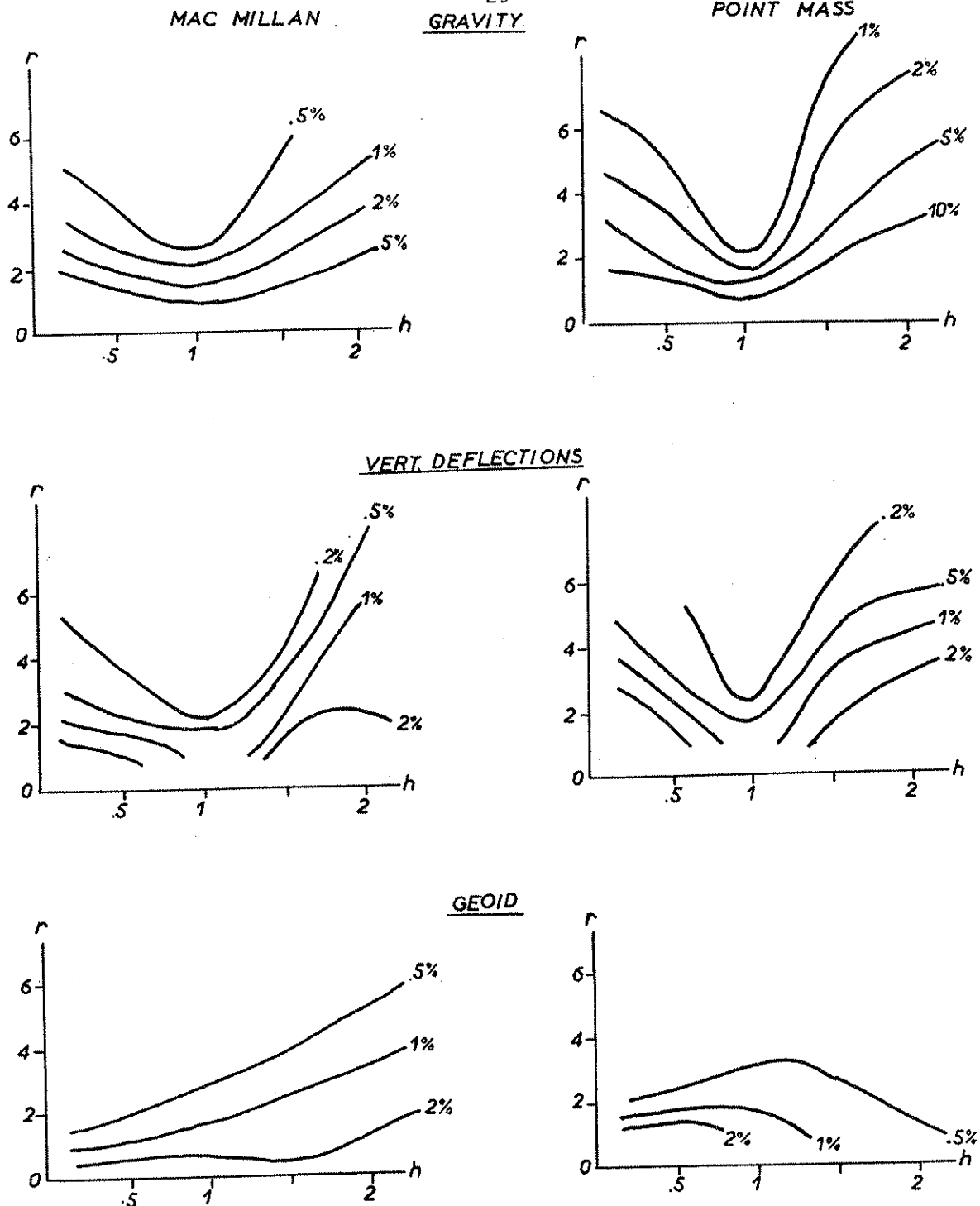


Figure 7 Approximate maximal approximation error between the prism formulas ((6.8), (6.10)) and the simpler MacMillan and point mass formulas (6.11). Errors given in percent as a function of normalized distance to prism (r) and height (h) for a square sector, i.e. graphs show errors in computed terrain effects from a rectangular mountain, with unit side lengths and height h in distance r from the center. For a cube ($h=1$) the MacMillan and point mass formulas are identical. Note that for the geoid the comparison is against the "mass plane" formula (6.10). The graphs are intended as a guide for deciding the accuracy of the terrain effect computation program (appendix), which essentially uses the value of r to discriminate between the various formulas. (Example: if topography is given on a 1000 m grid with elevations up to 2000 m ($h=2$), a maximal 1% error requires $r \sim 5$, i.e. the MacMillan formula can be used for topography more than 5 km away from the computation point).

and similarly for the gravity field functionals (2.5)-(2.7) simple linear filters transform the quantities in the spectral domain:

$$\tilde{\xi}(u, v) = -\frac{iv}{\gamma} \tilde{T}(u, v) \quad (6.15)$$

$$\tilde{\eta}(u, v) = -\frac{i u}{\gamma} \tilde{T}(u, v) \quad (6.16)$$

$$\tilde{\Delta g}(u, v) = (-\omega - \frac{2}{R}) \tilde{T}(u, v) \approx -\omega \tilde{T}(u, v) \quad (6.17)$$

where R in (6.17) is the radius of the earth.

For radial symmetric functions, $f(x, y) = f(r')$, $r' = \sqrt{x^2 + y^2}$, the Fourier transform (6.12) becomes a Hankel transform (Papoulis, 1968):

$$\tilde{f}(u, v) = 2\pi \bar{f}(\omega) \quad \omega = \sqrt{u^2 + v^2} \quad (6.18)$$

where the Hankel transform pair (transform denoted by a bar) is given by:

$$\bar{f}(\omega) = \int_0^\infty r' f(r') J_0(\omega r') dr' \quad (6.19)$$

$$f(r') = \int_0^\infty \omega \bar{f}(\omega) J_0(\omega r') d\omega \quad (6.20)$$

Here $J_0(\cdot)$ is the Bessel function of order zero. Of special importance is the Hankel transform of the inverse distance:

$$\frac{1}{r} = \frac{1}{\sqrt{r'^2 + z^2}} \quad \xleftrightarrow{\text{Hankel}} \quad \frac{1}{\omega} e^{-\omega z} \quad (6.21)$$

(Papoulis, 1968, p. 145).

Now, for a rectangular prism (Figure 6), situated below the x-y plane, we have:

$$T(x, y, 0) = G\Delta\rho \int_V \frac{1}{r} dx' dy' dz' \quad (6.22)$$

$$r = \sqrt{(x-x')^2 + (y-y')^2 + z'^2}$$

giving the transform

$$\begin{aligned}
 \tilde{T}(u, v) &= G_{\Delta\rho} \int_{\pi} \int_V \frac{1}{r} e^{-i(ux+vy)} dx'dy'dz'dxdy \\
 &= 2\pi G_{\Delta\rho} \int_V \frac{1}{\omega} e^{-\omega z'} e^{-i(ux'+vy')} dx'dy'dz' \\
 &= 2\pi G_{\Delta\rho} \frac{1}{\omega^2} \frac{1}{uv} (e^{-\omega z_2} - e^{-\omega z_1}) \left| \begin{matrix} e^{-i(ux+vy)} & \left| \begin{matrix} x_2 \\ x_1 \end{matrix} \right| & \left| \begin{matrix} y_2 \\ y_1 \end{matrix} \right| \end{matrix} \right. \quad (6.23)
 \end{aligned}$$

Results for gravity and deflections may be obtained from (6.23) using (6.15)-(6.17) and using (6.18) and (6.21) by interchanging the order of integration. Formulas like (6.23) have been used for a number of years in geophysical exploration, especially for the magnetic field (Bhattacharyya, 1964).

The advantage of the formula (6.23) is that it allows the use of the fast fourier transform (FFT) when computing the gravity effects from a regular grid of prisms, e.g. defined through a digital terrain model. If we have a set of $n \times m$ prisms, the corners of the prisms, projected on the x - y plane, will form a $(n+1) \times (m+1)$ grid mesh. By rearranging the sum (6.23) as sums over this grid, the general expression for the total effect of all prisms will have the form

$$\tilde{T}(u, v) = \sum_{j=1}^{n+1} \sum_{k=1}^{m+1} f(\omega, x_j, y_k) e^{-i(ux_j+vy_k)} \quad (6.24)$$

where f contains sums and differences of $e^{-\omega z}$ for the prisms adjoining the grid point (x_j, y_k) . Sums like (6.24) is exactly what is obtained by the FFT algorithm - had it not been for the dependence of f with ω . This dependence is due to the basic fact that the prism integral (6.22) is fundamentally unlinear, not being a convolution. We are thus forced to evaluate (6.24) on a frequency-by-frequency basis by FFT, for each value of ω a separate spectrum T is obtained and the final spectrum must then be "constructed" by carefully selection and interpolation in this set of spectra. The thus obtained final spectrum may then be transformed back into the space domain by an inverse FFT.

It is important to stress, that (6.24) is exact. Therefore the spectral values obtained using (6.24) are not influenced by window effects etc., the obtained spectrum represents the spectrum of a transient signal, this signal decreasing quickly to zero outside the area covered by the prisms. The only "errors" occurring in this FFT technique is in the ω -interpolation scheme to obtain the final spectrum, and in the final synthesis of the frequencies, since FFT only gives the sums (6.24) for a finite, discrete number of frequencies, the highest frequencies being the Nyquist frequencies for the prism grid. This secures, however, a nice smoothness of the computed field, since e.g. a representation of the topography with flat-topped prisms is anyway a rather poor representation, causing unwanted high frequency spectral "ripple" effects from the edges.

To estimate the gain in computing speed, consider as an example a $n \times m$ grid of prisms (with varying top and base levels), and assume we want to compute the gravitational effects in the same grid at a fixed altitude. Then the operations will be (orders of magnitude):

SPACE DOMAIN:	$n^2 \times n^2$ calls of "PRISM" subroutine (no computation-saving grid symmetries exists for "exact" formulas)
FREQUENCY DOMAIN:	$n/2$ spectra (6.24) of n^2 coefficients f , FFT speed $\sim n^2 \log N$, spectral selection, inverse FFT. Combined order of magnitude: $n^3 \log N$

The gain is thus moderate, a consequence of the nonlinearity of (6.22).

A real significant gain in computation speed is obtained if the basic volume integral (6.1) is approximated with surface convolution integrals. This is e.g. possible for "thin" prism layers at near constant depth, and to some degree also for terrain effects (so-called "linear topographic approximation"), involving integrals of the topographic elevations and their squares (more details in next section). In the case of a "thin layer" at average depth D , we obtain

$$T(x, y, 0) = G \int_V \frac{\Delta \rho}{r} dx' dy' dz'$$

$$\approx G \int_{\pi} \frac{\kappa(x', y')}{[(x-x')^2 + (y-y')^2 + D^2]^{\frac{1}{2}}} dx' dy' \quad (6.25)$$

where $\kappa = \Delta \rho (z_2 - z_1)$ is the surface density. The transform is obtained simply by utilizing (6.21) again, giving

$$\tilde{T}(u, v) = 2\pi G \frac{1}{\omega} e^{-\omega D} \tilde{\kappa}(u, v) \quad (6.26)$$

In this case the order-of-magnitude computation speed of the previous example will be only $n^2 \log n$ if FFT is utilized, but opposed to the "exact" spectral formulation "window effects" due to finite data lengths must now be given full attention.

The frequency domain methods have as common restrictions that data and computation points must be in a grid, the computation points being in a plane (important exception: gravimetric terrain corrections, cf. next section). Obvious applications could be e.g. for geoid computations at sea level (especially for satellite altimetry) and upward continuation studies (airborne gravimetry and gradiometry). The importance of spectral methods in geophysical inversion may be inferred from (6.26): if a particular spectrum (e.g. white noise) is expected for the source κ , then the depth D to the source may be found directly from the observed gravity field spectrum. This is the base of the widespread "statistical inversion techniques", dominating in the analysis of aeromagnetic data.

7. Terrain Reductions

For the remainder of this report, emphasis will now concentrate on topographic and isostatic reductions - a synonym for computational elimination of the effects of the two most dominant and best known density anomalies of the earth: the visible topography and its associated compensation at depth. For such gravity field effects the general term "terrain effects" will be used in the present context.

The commonly applied term "terrain corrections" will be reserved for the narrow meaning, i.e. a correction to the Bouguer reduction, to give the true (unlinear) effect of the topography on gravity anomalies (and deflections of the vertical as well).

7.1 Terrain Effects and Associated Density Anomalies

The various terrain reductions in use is illustrated in Figure 8. To use terrain reduced data in a "remove-restore" technique for gravity field modelling (Section 4), it should be remembered that the density models indicated by Figure 8 should either cover a given, fixed geographical area, or - or at least in principle - be global.

The topographic reduction or complete Bouguer reduction consists of removing the visible topography. Conventionally a density of 2.67 g/cm^3 is used. This density, which represents a typical density of granite and many Paleozoic and Pre-Cambrian sediments, is fairly good in mountainous areas. However, one should not hesitate to use other density values, since the density may range from below 2.0 g/cm^3 in moraine hills to 3.0 g/cm^3 in volcanics. Average density values could be chosen from geological considerations or using the inversion techniques of the last section. At the oceans the topographic density anomalies are formally negative, the standard density 2.67 corresponding to $1.03 - 2.67 = -1.64 \text{ g/cm}^3$, 1.03 being the density of sea water.

The topographic reduction may formally be split into a Bouguer term, the effect of an infinite plate, plus the terrain correction, which takes into account the topographic irregularities. For gravity disturbances we have

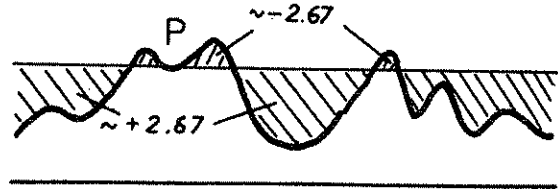
$$\delta g_{\text{topo}} = 2\pi G \rho h_p - t_c \quad (7.1)$$

where $2\pi G \rho h_p$ is the gravity due to a (plane) Bouguer plate of thickness h_p (if the computation point P is situated above the topography, h_p is the topographic elevation at the surface point below P), and t_c is the terrain correction.

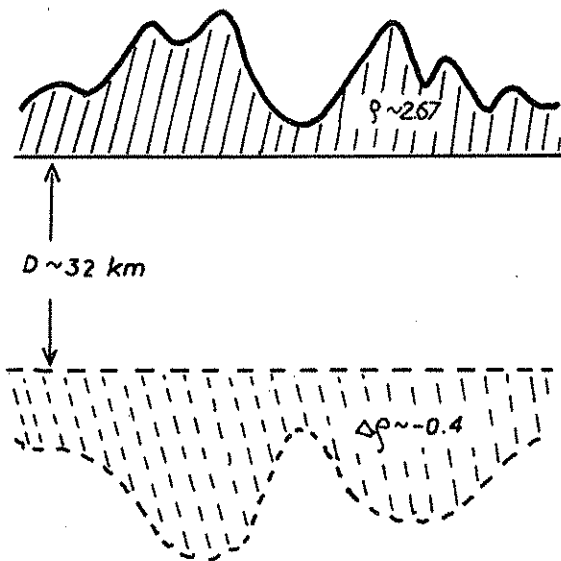
A) TOPOGRAPHY



B) TERRAIN CORRECTION



C) ISOSTATIC



D) RESIDUAL TERRAIN MODEL

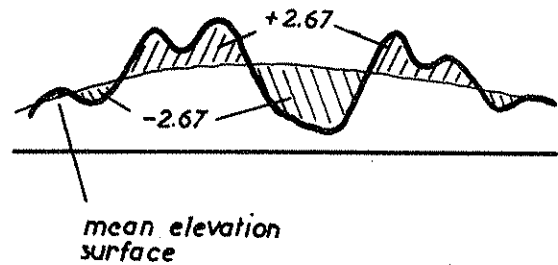


Figure 8. Density anomalies associated with various terrain reductions (continental area). A: topographic effect, i.e. the "complete" Bouguer reduction (consisting of the effects of a Bouguer plate minus the terrain correction "B"), C: conventional Airy-isostatic model, D: Residual terrain model (RTM), the mean elevation surface e.g. given by a 180×180 spherical harmonic expansion.

The terrain correction is always positive (in the plane approximation) due to the conventional minus sign in (7.1).

For deflections of the vertical the terrain correction and the topographic effect are identical (except the signs), since the Bouguer plate effect is zero. For height anomalies, however, the infinite Bouguer plane can not be used, the effect being infinite. Instead one could think of using a spherical Bouguer plate: the effects typically computed, will however, still be very large and often much larger than the observed geoid undulations themselves (on a global basis). Topographic reductions are therefore not very applicable to general gravity field modelling: the large model geoid effects and biased Bouguer anomalies at oceans and mountainous areas necessitates some kind of negative density anomalies being introduced, e.g through an isostatic compensation hypothesis. Needless to say, the topographic reduction is naturally very well suited for problems such as gravity interpolation and geophysical inversion.

Isostatic reduction formalizes the prevailing tendency of the earth's topography to be compensated at depth. The standard Airy scheme assumes local compensation through a root system (Figure 8D), the thickness of the root being

$$t = \frac{\rho}{\Delta\rho} h \approx 6.7 h \quad (7.2)$$

where ρ is the density of the topography ($\sim 2.67 \text{ g/cm}^3$) and $\Delta\rho$ the density contrast between the crust and the mantle ($\sim 0.4 \text{ g/cm}^3$). The normal density model has a crust of thickness D ($\sim 32 \text{ km}$).

Naturally the earth does not fully follow this simple principle. Although (7.2) approximates the overall isostatic compensation fairly good, many exceptions occur: first of all the strength of the earth's crust supports short-wavelength topographic features, isostasy being primarily a regional phenomena. Second, many regions are either uncompensated or compensated at deeper levels (through

anomalous density values in the upper mantle), most noticeably the deep-sea trenches and mid-oceanic ridges. However, since the computed isostatic effects are very insensitive to the actual isostatic formulation and parameters used, even the simplest formulations (e.g. (7-2)) gives excellent results, the results being "good" when the remaining field after isostatic reduction is smooth and with low variance. Global isostatic reductions attain maximal values for the geoid in the range 10-20 m. It is therefore necessary to compute isostatic effects also on spherical harmonic coefficients for the geopotential, e.g. using the simple formula (3.12).

A drawback of the isostatic reduction is that it primarily should be global. If only a fixed, localized area is taken into account, the computed isostatic gravity field effects will be influenced by "edge effects": the computed isostatic gravity and deflections of vertical would change rapidly near the boundary for non-zero elevations. For the geoid an overall bias, dependent on the chosen size of the reduction area, will result if the area mean elevation is different from zero (see e.g. Forsberg & Tscherning, 1981, Figure 1).

Since the main problem in external gravity field modelling in mountainous areas is short-wavelength topographic "gravity field noise", a terrain reduction method avoiding the "global" computations of isostatic reductions, but capable of approximating isostatic conditions, would be ideal:

For a residual terrain model (RTM) reduction only the short wavelength of the topography is taken into account. This is done by choosing a smooth mean elevation surface, and computationally remove masses above this surface and fill up valleys below (Figure 8D). The mean elevation surface could be any smooth surface, representing mean elevations of the area, e.g. an interpolation in 30'x30' mean heights or - especially - defined through a high-order spherical harmonic expansion of the topography of the earth. In this case the RTM density anomalies correspond to a normal density distribution (normal earth) with smooth topography and bathymetry defined through the spherical harmonic expansion, and thus

corresponds to the residual gravity field after removal of a similar spherical harmonic expansion of the geopotential.

The advantages of the RTM-reduction are many: since the density anomalies have oscillating positive and negative values, the integrations for gravity field effects need only be done out to some suitable distance from the computation point, the influence of distant topography cancelling out. Also, terrain effects on height anomalies will be small (often negligible if a short-wavelength reference elevation surface is chosen), and especially for e.g. 180 x 180 height expansions the reduction gives results close to isostatic reductions.

The similarity between RTM and isostatic reductions are analogous to the similarity between mean free-air gravity anomalies and isostatic anomalies. Indeed, by a special choice of mean elevation surface nearly complete correspondence may be obtained: If we define the mean elevations through the low-pass filter (plane approximation)

$$h_{\text{ref}}(P) = \frac{D}{2\pi} \int_{\pi} \frac{h(Q)}{[r^2 + D^2]^{3/2}} d\pi Q, \quad r = \text{dist}(P, Q) \quad (7.3)$$

then Moritz has shown that the associated RTM-reduction corresponds to an isostatic reduction with a (surface layer) compensation depth D (Moritz, 1968a). Note that (7.3) is nothing but the well-known Poisson integral for upward continuation of harmonic functions.

The RTM-reduction may be viewed as a difference between two Bouguer reductions: first the visible topography is removed, and then the smoothed topography is added back (Figure 9):

$$L(T)_{\text{RTM}} = L(T)_{\text{TOPO}} - L(T)_{\text{REF} \cdot \text{TOPO}} \quad (7.4)$$

Each term in (7.4) may formally be split in a Bouguer plate effect and a terrain correction. Table 1 shows sample terrain corrections for a 180 x 180 spherical harmonic reference surface in two 4° x 4° fixed areas in the Rocky Mountains.

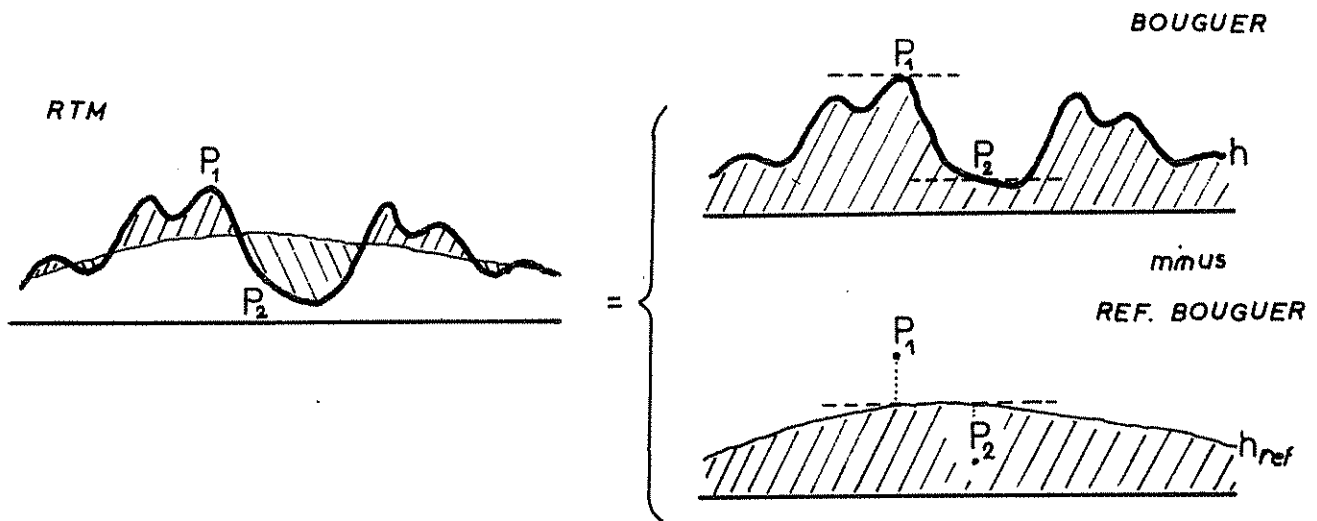


Figure 9. Residual reduction expressed as a difference between the effects of the topography and the reference topography.

Area	$\delta g_{\text{REF.TC}} (\text{mgal})$		$\xi_{\text{REF.TC}} (")$		$\eta_{\text{REF.TC}} (")$		$\zeta_{\text{REF.TC}} (\text{m})$	
Colorado	0.6	1.0	3.5	5.7	7.1	9.9	5.7	10.3
New Mexico	0.3	0.6	4.9	7.2	4.2	8.2	3.5	5.2

Table 1. R.M.S. and absolute maximal terrain corrections for a 180 x 180 spherical harmonic reference topography (4° x 4° fixed area, 9 sample points).

From the table it is seen that the gravity reference terrain corrections are very small - below 1 mgal*. We may therefore for gravity anomalies simply state

$$\Delta g_{\text{RTM180}} = 2\pi G\rho (h - h_{\text{ref}}) - tc \quad (7.5)$$

i.e., when using a RTM reduction with 180 x 180 reference heights (RTM180) the terrain effect is simply a terrain corrected (tc) Bouguer reduction to the level h_{ref} . This has the important practical advantage that available, terrain-corrected Bouguer anomalies (being still the bulk of the available local gravity field data)

*Additional verification on actual data: see Section 7.4.

may be applied directly for RTM-reduction using (7.5). For deflections of the vertical, however, the time-consuming "prism"-integrations can not be avoided, the deflection terrain effects due to the changing reference level being much too large.

When performing the RTM-reduction "directly" (e.g. using rectangular prism integration), stations above the reference level are left "hanging in the air", while observations below this level are reduced to their values inside the mass (Figure 9). However, for external gravity field modelling, we need not the value inside the mass, but the harmonically downward continued value, corresponding to the outer, "reduced" field. In other words, what would the reduced observation be at the point P_2 in Figure 9, if we treated the mean topography as non-existent?

An approximate answer to this question is simple: if the density above a plane through P_2 is condensed in a mass plane layer immediately below P_2 , deflections of the vertical and geoid undulations would remain nearly unchanged due to the smooth, low-slope reference surface. For gravity anomalies, however, we would see a change

$$\Delta g_{\text{harmonic}}^c - \Delta g_{\text{in mass}}^c = 4\pi G_p \Delta h \quad (7.6)$$

corresponding to a "double" Bouguer reduction with plate thickness $\Delta h = h_{\text{ref}} - h_p$. This "harmonic correction" must be applied for all gravity stations below the reference level when "direct" prism integration of RTM density anomalies (Figure 8D) is performed. If instead (7.5) is used, the correction is taken into account "implicitly".

7.2 Practical Terrain Reductions in Gravity Field Modelling

A FORTRAN 77 program for computation of any of the four types of terrain effects (and corrections) mentioned (Figure 8) are listed in the appendix.

The program uses rectangular prisms for a direct integration of geoid undulations, deflections of the vertical or gravity anomalies from digital terrain models given on a geographic grid.

Special precautions have been taken to evaluate the inner zone effect, i.e. the influence of the topography adjacent (say, within 1 km) to the computation point. These inner zone effects may be very large, especially for gravity terrain corrections. To represent the inner zone, a bicubic spline interpolation of the topography is utilized. However, since gravity topographic effects to first order depends linearly on the gravity station elevation, it is clear that the station elevation itself should be utilized in the inner zone interpolation. An option in the program allows the height interpolation procedure to give the correct elevation at a station, through a smooth "adjustment" of the digital terrain model elevations in the inner zone. For deflections and height anomalies, where the station height dependence is weak, use of this option is not necessary.

Actual examples of use of the various terrain reductions in connection with gravity field modelling by collocation can be found in e.g. Forsberg and Tscherning (1981). Here gravity and deflections were modelled with an accuracy around 4 mgal and 1" respectively, in a mountainous area (New Mexico), using gravity data spaced c. 6' apart and a 0.5'x0.5' digital terrain model. When applied properly, nearly the same results were obtained for all types of terrain reductions.

As an outline example, let us consider upward continuation of gravity data in a mountainous area. Using a "spatial" modelling technique like collocation or point mass modelling the application of the remove-restore technique for a RTM180-reduction (and a 180 x 180 reference field) is simple:

1. Compute terrain corrections for local gravity stations if not already given.
2. Obtain terrain-reduced residual gravity values by subtracting the reference Bouguer anomalies $\Delta g_{REF} - 2\pi G \rho h_{REF}$ from the local, terrain-corrected Bouguer anomalies.
3. Apply upward continuation method,
4. Add back RTM-effects computed at altitude (prism integration),
5. Add back 180 x 180 gravity computed at altitude.

For already gridded gravity data (e.g. 5'x5' mean free-air anomalies) this remove-restore technique may be used with some caution. For a mean block we would need the mean terrain correction, as we have from (7.5)

$$\overline{\Delta g}_{\text{RTM180}} = 2\pi G\rho (\bar{h} - \bar{h}_{\text{REF}}) - \overline{tc} \quad (7.7)$$

Such mean terrain corrections \overline{tc} are difficult to estimate. They are, however, very important since they play an essential role in the harmonic downward continuation of gravity data from the surface of the topography to the geoid, a necessary prerequisite for the application of e.g. the classical integral methods. Apart from direct computation of \overline{tc} by averaging, its magnitude may be estimated from the covariance function of the topography

$$\overline{tc} \approx 3\pi G\rho \frac{\sigma_h^2}{d}$$

where σ_h^2 is the terrain variance and d the correlation length, as pointed out by Sunkel (1981a).

7.3 The Linear Approximation for Topographic Effects

Approximate formulas for RTM-effects, especially applicable for error studies and frequency domain methods, may be obtained using functional expansions of the topographic volume integral kernels ($\frac{1}{r}$, $\frac{z}{r^3}$ etc.). In the sequel a "long wavelength" reference elevation surface e.g. 180 x 180 spherical harmonic expansion is assumed to be used.

In the plane approximation we have for the RTM potential effect when a constant topographic density is used:

$$T_m = G \int \frac{\Delta\rho}{r} dV = G\rho \int_{\pi} \int_{z=h_{\text{ref}}}^h \frac{1}{r} dzd\pi \quad (7.8)$$

where

$$\frac{1}{r} = [r_0^2 + (z - h_p)^2]^{-\frac{1}{2}} = \frac{1}{r_0} \left[1 + \frac{(z - h_p)^2}{r_0^2} \right]^{-\frac{1}{2}} = \frac{1}{r_0} [1 + \tan^2 \beta]^{-\frac{1}{2}} \quad (7.9)$$

V is the volume of non-zero (positive or negative) density anomalies $\Delta\rho$, shown hatched in Figure 10. A series expansion for T_m is obtained by expanding (7.9)

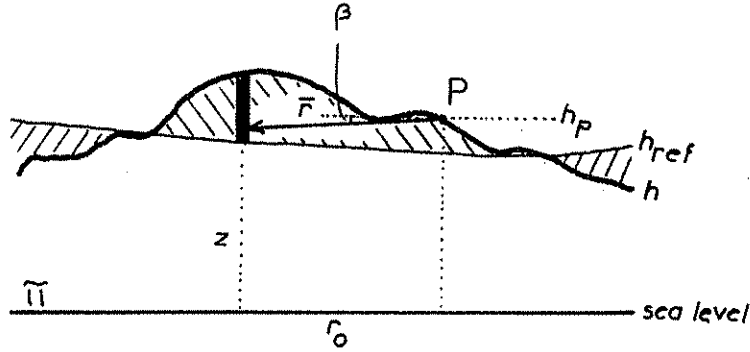


Figure 10

with respect to the inclination β , which is always small except for the inner zone in rugged topography (and geoid innerzone effects are very small). Thus,

$$\frac{1}{r} \approx \frac{1}{r_0} - \frac{1}{2} \frac{(z - h_p)^2}{r_0^3} + \dots \quad (7.10)$$

and by inserting (7.10) in (7.8) and integrating with respect to z

$$T_m = G\rho \int_{\pi} \frac{h - h_{ref}}{r_0} d\pi - \frac{1}{6} G\rho \int_{\pi} \frac{(h - h_p)^3 - (h_{ref} - h_p)^3}{r_0^3} d\pi + \dots \quad (7.11)$$

The first term in (7.11) has been called the linear approximation by Moritz (1968a).

It is seen that this term represents nothing but the potential of a mass coating $\kappa = \rho(h - h_{ref}) = \rho\Delta h$. Within the accuracy of the linear approximation we may view this mass coating as a surface density layer at the height reference surface. The higher order terms in (7.11) may similarly be viewed as successive coatings of dipoles, quadrupoles, etc.

For deflections of the vertical we have

$$\left. \begin{matrix} \xi_m \\ \eta_m \end{matrix} \right\} = -\frac{G}{\gamma} \int_V \left\{ \begin{matrix} y - y_p \\ x - x_p \end{matrix} \right\} \frac{\Delta \rho}{r^3} dV = -\frac{G\rho}{\gamma} \int_{\pi} \int_{z=h_{ref}}^h \frac{r_0}{r^3} dz \left\{ \begin{matrix} \cos \alpha \\ \sin \alpha \end{matrix} \right\} d\pi \quad (7.12)$$

which by expansion $r^{-3} = r_0^{-3} - \frac{3}{2} r_0^{-5} (z - h_p)^2 + \dots$ and integration analogous to the potential case gives

$$\left. \begin{matrix} \xi_m \\ \eta_m \end{matrix} \right\} = -\frac{G\rho}{\gamma} \int_{\pi} \frac{(h-h_{ref})}{r_0^2} \left\{ \begin{matrix} \cos \alpha \\ \sin \alpha \end{matrix} \right\} d\pi + \frac{1}{2} \frac{G\rho}{\gamma} \int_{\pi} \frac{(h-h_p)^3 - (h_{ref}-h_p)^3}{r_0^4} \left\{ \begin{matrix} \cos \alpha \\ \sin \alpha \end{matrix} \right\} d\pi \quad (7.13)$$

Again, the first term (the linear approximation) may be interpreted as the effect of a mass coating.

The RTM gravity anomalies are given by

$$\Delta g_m = -G\rho \int_{\pi} \int_{z=h_{ref}}^h \frac{z-h_p}{r^3} dz d\pi - \frac{2}{R} T_m \quad (7.14)$$

The last term in (7.14) - the indirect effect - will usually be below 1 mgal for a 180 x 180 reference surface and may be neglected. For gravity anomalies it is advantageous to use (7.5)

$$\Delta g_m \approx 2\pi G\rho (h - h_{ref}) - tc \quad (7.15)$$

and then only expand the terrain correction

$$tc = G\rho \int_{\pi} \int_{z=h_p}^h \frac{z - h_p}{r^3} dz d\pi \quad (7.16)$$

$$= \frac{1}{2} G\rho \int_{\pi} \frac{(h - h_p)^2}{r_0^3} d\pi + \dots \quad (7.17)$$

In (7.15) the Bouguer term is on the average one order of magnitude larger than the terrain corrections themselves. In some cases -e.g. error studies - it would therefore be sufficient only to use this simple term. For gravity field modelling with heterogeneous data it is, however, very dangerous not to include the best possible terrain corrections: since t_c is always positive, a systematic bias will be introduced in Δg_m , a bias which often would seriously affect computed geoid undulations.

For frequency domain formulas we note, that the linear approximations in (7.11) and (7.13) are convolutions, i.e. expressions of the form

$$L(T_m)_P = k * \Delta h = \int_{\pi} k(x_P - x_Q, y_P - y_Q) \Delta h(x_Q, y_Q) d\pi_Q \quad (7.18)$$

and thus in principle for the Fourier transform using the well-known convolution theorem

$$L(\tilde{T}_m) = \tilde{k} \Delta \tilde{h} \quad (7.19)$$

The function k is traditionally called the impulse response, \tilde{k} the transfer function. $\Delta h = h - h_{ref}$ will be termed the residual height hereafter.

For the potential we have from (6.26)

$$\tilde{T}_m(u, v) = 2\pi G\rho \frac{1}{\omega} \Delta \tilde{h}(u, v), \quad \omega = \sqrt{u^2 + v^2} \quad (7.20)$$

and since (also) in the linear approximation $\xi_m = -\frac{1}{\gamma} \frac{\partial T_m}{\partial y}$ we have

$$\left. \begin{matrix} \tilde{\xi}_m \\ \tilde{\eta}_m \end{matrix} \right\} (u, v) = -\frac{2\pi G\rho}{\gamma} i \begin{Bmatrix} v \\ u \end{Bmatrix} \frac{1}{\omega} \Delta \tilde{h}(u, v) \quad (7.21)$$

and by (7.15)

$$\Delta \tilde{g}_m(u, v) = 2\pi G\rho \Delta \tilde{h}(u, v) - \tilde{t}_c(u, v) \quad (7.22)$$

Note, that (7.20) and (7.21) may be derived from the Bouguer term of (7.22), excluding the terrain correction. However, we might expect the linear approximation for potential and deflections to be "better" than the Bouguer approximation for gravity: intuitively the condensation of the "rod" of Figure 10 to a point at the mean elevation surface would have a large effect on gravity but nearly none on potential and deflections. More formally, from the expansions of the impulse responses in terms of the inclination β :

$$\text{potential and deflections: } k_1\beta + k_3\beta^3 + \dots$$

$$\text{gravity: } k_0 + k_2\beta^2 + k_4\beta^4 + \dots$$

it is seen that the "condensation" interpretation (Bouguer term for gravity) corresponds to a first order expansion in β . By including the terrain correction for gravity anomalies, a second order expansion in β is obtained. It is this expansion which Moritz (1968a) has termed the "linear" approximation, in order to have the same accuracy level as in the well-known linearized Molodensky approach to the geodetic boundary value problem.

7.4 Accuracy of the Linear Approximation

If the linear approximation is sufficiently accurate, much faster techniques for the evaluation of terrain effects in grids are available (FFT and space domain filtering methods).

As a simple analytical example, consider the terrain correction at the summit of a cone shaped mountain.

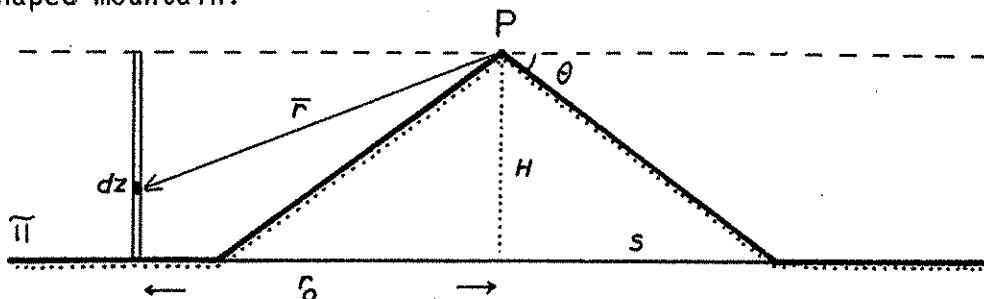


Figure 11

The exact terrain correction at P is:

$$tc = G_p \int_{\pi} \int_H^h \frac{z-H}{r^3} dz d\pi = G_p \int_{\pi} \left(\frac{1}{r_0} - \frac{1}{\sqrt{r_0^2 + h^2}} \right) d\pi \quad (7.23)$$

$$\begin{aligned} &= G_p \int_0^S 2\pi r_0 \left(\frac{1}{r_0} - \frac{1}{r_0 \sqrt{1 + \tan^2 \theta}} \right) dr_0 + G_p \int_S^{\infty} 2\pi r_0 \left(\frac{1}{r_0} - \frac{1}{\sqrt{r_0^2 + H^2}} \right) dr_0 \\ &= 2\pi g_p H \sin \theta \end{aligned} \quad (7.24)$$

while the linear approximation gives

$$\begin{aligned} tc &= \frac{1}{2} G_p \int_{\pi} \frac{(h-H)^2}{r_0^3} d\pi \\ &= \frac{1}{2} G_p \int_0^S \frac{(r_0 \tan \theta)^2}{r_0^3} 2\pi r_0 dr_0 + \frac{1}{2} G_p \int_S^{\infty} \frac{H^2}{r_0^3} 2\pi r_0 dr_0 = 2\pi G_p H \tan \theta \end{aligned} \quad (7.25)$$

The relative error for some slope values θ are:

θ	tc	Δg_m (total topographic effect)
15°	3.5%	1.2%
30°	15%	15%
45°	41%	100%

For common slopes the linear approximation thus seems somewhat reasonable, since the cone mountain is a "worst-case" model.

For a practical evaluation of the linear approximation (and the error associated with the "Bouguer-split" (7.5) for gravity anomalies), an alpine 1°x1° block in Colorado has been chosen (Figure 12). Comparisons have been performed in 36 stations, located in a 12'x12' grid at the surface of the topography. As elevation data 0.5'x0.5' heights were used, covering totally a 4°x4° area surrounding the comparison area. To get the linear approximation results, the "prism" sub-

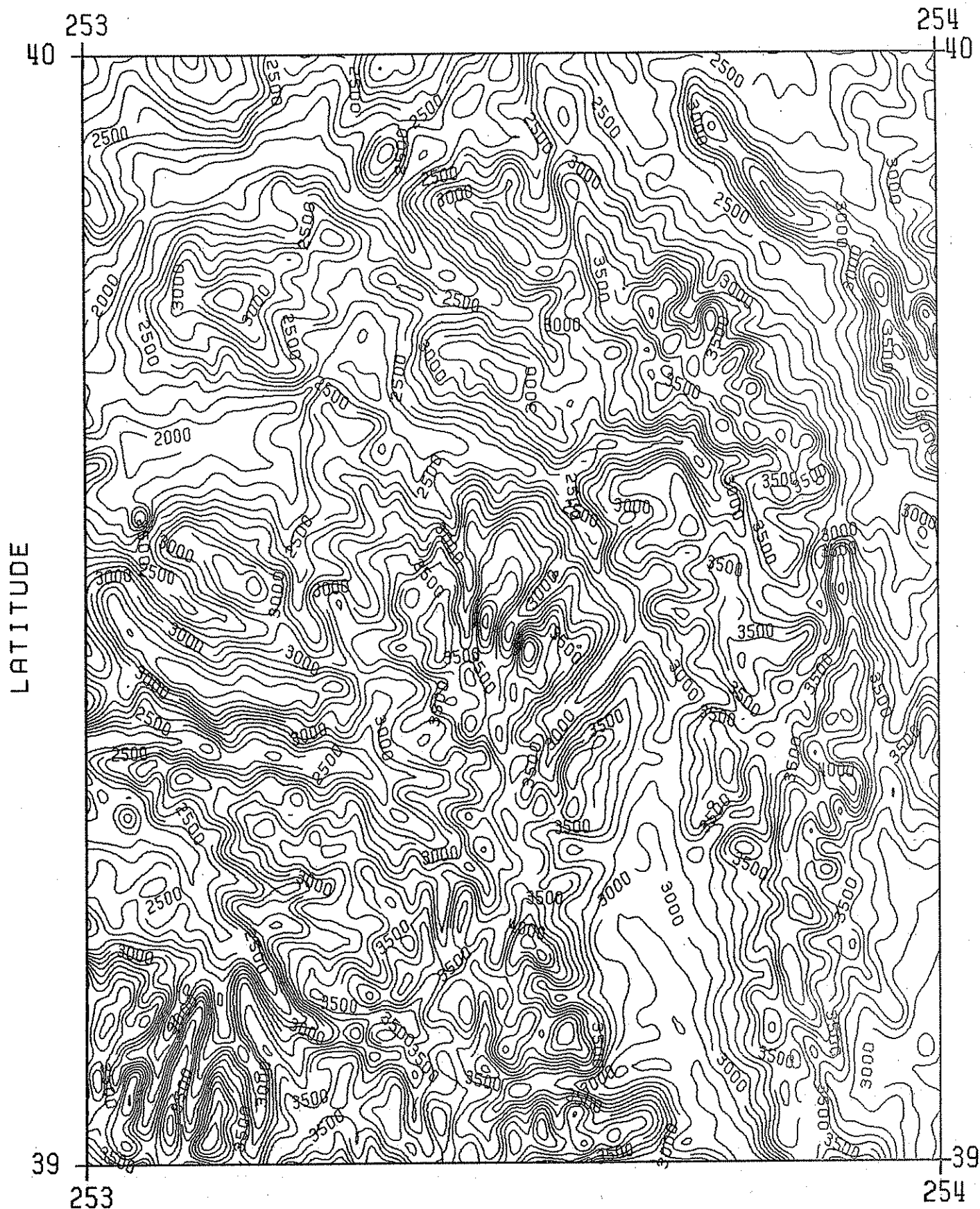


Figure 12. Rocky Mountain test area used for evaluation of the "linear approximation". The 111 x 86 km² area topography shown with a contour interval of 100 m contoured from 1' x 1' mean heights. The highest point is Mt. Elbert, 4399 m.

routine of the terrain effect computation program (cf. appendix) was changed to give instead only mass plane results (for formulas see Forsberg & Tscherning, 1981). For the linear approximation to the terrain correction, we have for a prism element at position x_1 to x_2 , y_1 to y_2 relative to the computation point:

$$tc = \frac{1}{2} G_p \int_{x_1}^{x_2} \int_{y_1}^{y_2} \frac{(h-h_p)^2}{r^3} dx dy, \quad r = \sqrt{x^2 + y^2} \quad (7.26)$$

which by simple integration gives

$$\begin{aligned} tc &= \frac{1}{2} G_p (h-h_p)^2 \left| \int_{x_1}^{x_2} \frac{1}{x^2} \frac{y}{r} dx \right|_{y_1}^{y_2} \\ &= -\frac{1}{2} G_p (h-h_p)^2 \left| \left| \frac{r}{xy} \right|_{x_1}^{x_2} \right|_{y_1}^{y_2} \end{aligned} \quad (7.27)$$

The following results were obtained:

Table 3. Comparison "exact" RTM-reduction versus linear approximation, Colorado/Mt. Evans area:

Quantity	Exact		Linear Approximation		Difference		Abs. Max.
	Mean	Std. Dev.	Mean	Std. Dev.	Mean	Std.	
ζ_m (meter)	0.82	0.65	0.82	0.65	0.00	0.01	0.04
ξ_m (arcsec)	0.68	6.85	0.60	6.59	0.09	0.69	-1.47
η_m (arcsec)	-0.21	7.06	-0.34	6.78	0.13	0.72	2.79
Δg_m (mgal)	-7.45	43.61	-7.74	43.49	0.29	0.60	3.24
tc (mgal)	6.01	4.41	6.33	4.94	-0.29	0.60	-3.24

Δg_m in Table 3 are computed using (7.5). A comparison between a rigorous RTM prism computation of Δg_m and (7.5) gave as a result an r.m.s. difference of only 0.3 mgal (maximal value 0.7 mgal), thus supporting the simple "Bouguer" - formula (7.5).

From Table 3 it is seen that the linear approximation errors are insignificant for geoid undulations and also rather small on the average for gravity, but with a possibility for rather large outliers. For deflections the error might not always be acceptable, and higher order expansions might be necessary. Considering the extreme ruggedness of the test area, other "milder" areas will be expected to give better results, and certainly the linear approximation will always be very useful since it allows the use of FFT methods for terrain effect computations.

7.5 The Terrain Correction as Convolution Integrals

From (7.17) we have in the linear approximation

$$tc = \frac{1}{2}G_p \int_{\pi} \frac{(h-h_p)^2}{r_0^3} d\pi \quad (7.28)$$

which may be expressed as convolutions of h and h^2 :

$$tc = \frac{1}{2}G_p \left[\int_{\pi} \frac{h^2}{r_0^3} d\pi + \int_{\pi} \frac{h_p^2}{r_0^3} d\pi - \int_{\pi} \frac{2hh_p}{r_0^3} d\pi \right] \quad (7.29)$$

since h_p is constant with respect to the integration, we obtain

$$tc = \frac{1}{2}G_p \left[(h^2 * f) + h_p^2 \int_{\pi} f d\pi - 2h_p (h * f) \right] \quad (7.30)$$

where $f = \frac{1}{(x^2+y^2)^{3/2}}$. Now, the function f does not have a fourier spectrum, but it may be regularized very simply: Instead of f consider $f' = \frac{1}{(x^2+y^2+a^2)^{3/2}}$ where a is a small constant. Using f' instead of f as kernel in (7.28), this corresponds to a computational upward continuation to a distance a , and when a is chosen sufficiently small the error will be insignificant and only affect an innerzone roughly of radius a . We thus have:

$$tc \approx \frac{1}{2}G_p \left[(h^2 * f') + \frac{2\pi}{a} h_p^2 - 2h_p (h * f') \right] \quad (7.31)$$

where the center integral of (7.30) has been evaluated analytically (the integral is nothing but the well-known Bouguer-plate integral).

The two convolutions in (7.31) may with advantage be evaluated using frequency domain methods, we have e.g.

$$\text{transform of } (h^2 * f') = \tilde{h}^2 \tilde{f}' = \frac{2\pi}{a} e^{-\omega a} \tilde{h}^2 \quad (7.32)$$

see Papoulis (1968), p. 145. With the split of the terrain correction (7.31) it is clear, that for practical applications there will be a lower limit for "a", since the terrain correction is expressed as a (small) difference between two large numbers, and thus unstable numerically.

Since "a" can not be chosen arbitrarily small, a small error Δ_{tc} is made, by using integral kernel f' instead of f , representing the "suppressed" effect of the local innerzone just around the computation point. If the regularization distance "a" is chosen somewhat smaller than the finest resolution of the given elevation data, a quantitative estimate of this "regularization error" Δ_{tc} may be obtained as follows: The error is

$$\Delta_{tc} = \frac{1}{2} G \rho \int_{\pi} \left(\frac{(h-h_p)^2}{r_0^3} - \frac{(h-h_p)^2}{[r_0^2 + a^2]^{3/2}} \right) d\pi \quad (7.33)$$

Since this error is dominated by a very local innerzone effect, a Taylor expansion of the topography is adequate, keeping only the first terms to represent a sloping plane. Then by assuming the computation point to be at origo we have

$$(h-h_p)^2 = r_0^2 \tan^2 \theta \cos^2 \alpha \quad (7.34)$$

where θ is the slope of the plane and α the azimuth from the direction of maximal slope. Insertion of (7.34) into (7.33) gives

$$\begin{aligned} \Delta_{tc} &= \frac{1}{2} G \rho \int_0^{\infty} \frac{2\pi r_0}{2} \left(\frac{r_0^2 \tan^2 \theta}{r_0^3} - \frac{r_0^2 \tan^2 \theta}{[r_0^2 + a^2]^{3/2}} \right) dr_0 \\ &= \frac{1}{2} \pi G \rho \tan^2 \theta \int_0^{\infty} \left(1 - \frac{r_0^2}{[r_0^2 + a^2]^{3/2}} \right) dr_0 \end{aligned} \quad (7.35)$$

This integral may be tackled by substitution of r_0^2 , giving

$$\begin{aligned}\Delta tc &= \frac{1}{2}\pi G\rho \tan^2\theta \left| r_0 - \frac{r_0^2 + 2a^2}{\sqrt{r_0^2 + a^2}} \right|_0^\infty \\ &= \pi G\rho \tan^2\theta a\end{aligned}\quad (7.36)$$

This is exactly the (linear approximation) terrain correction of a sloping innerzone of radius $2a$ (it is evident from (7.34) that this terrain correction must be half the corresponding cone terrain correction (7.25)). A numerical example: if $a = 100$ m and $\theta = 30^\circ$, the regularization error will be 1.8 mgal. This illustrates the critical importance of the very local station surroundings for gravity terrain corrections, and the fact that "a" can not be chosen too large - reasonable values must be chosen based on empirical investigations.

7.6 The Use of FFT for Terrain Effect Computations

In the previous sections frequency-domain formulas for terrain effects on height anomalies, deflections of the vertical and gravity anomalies have been discussed. These expressions are very useful since digital terrain models are naturally given in grids, suitable for direct use of the Fast Fourier Transform (FFT). The speed of FFT ($\sim n \log_2 n$ if the number of points n is a power of 2, otherwise somewhat slower depending on the prime factorization of n) certainly makes the application of frequency domain methods attractive especially when large volumes of data need to be terrain reduced. However, before applying the method, it is essential to realize the limitations inherent when using FFT.

FFT is basically a fast algorithm to determine the discrete transform of periodic data. The two-dimensional discrete Fourier transform pair may be expressed as

$$\tilde{h}(p\Delta u, q\Delta v) = \frac{\Delta x \Delta y}{nm} \sum_{j=0}^{n-1} \sum_{k=0}^{m-1} h(j\Delta x, k\Delta y) e^{-2\pi i \left(\frac{pj}{n} + \frac{qk}{m} \right)} \quad (7.37)$$

$$h(j\Delta x, k\Delta y) = \frac{1}{\Delta x \Delta y} \sum_{p=0}^{n-1} \sum_{q=0}^{m-1} \tilde{h}(p\Delta u, q\Delta v) e^{2\pi i \left(\frac{pj}{n} + \frac{qk}{m} \right)} \quad (7.38)$$

where Δx and Δy are gridspacing in the given elevation grid of $n \times m$ points, and the normalization factors have been chosen to be in accordance with the continuous transform (6.12-6.13). The frequency spacings are given by

$$\Delta u = \frac{2\pi}{n\Delta x}, \quad \Delta v = \frac{2\pi}{m\Delta y} \quad (7.39)$$

The spectrum \tilde{h} as well as the original data h must be viewed as infinitely periodically extended in space. Since the Nyquist frequencies

$$u_N = \frac{n}{2} \Delta u = \frac{\pi}{\Delta x}, \quad v_N = \frac{m}{2} \Delta v = \frac{\pi}{\Delta y} \quad (7.40)$$

represent the highest frequencies obtainable from the gridded data, frequencies above (u_N, v_N) in (7.37) will correspond to negative frequencies. For more details on FFT see e.g. Kanasewich (1975).

When applying FFT for convolutions of the form (7.18) or (7.31), the periodic extension means that for a data point near an edge, the convolution will actually "use" data from around the opposite edge as well. The convolution kernel will in effect be truncated (and periodically extended) when applying the analytical terrain effect filters at the discrete frequencies of the FFT (Figure 13), and this means in common words that the terrain effects computed using the FFT method will be terrain effects from a "running area" of size $(n\Delta x, m\Delta y)$, centered at the computation point. At the center point of the grid the computed effect will exactly be the effect of the given area - at a corner point the result will be completely erroneous, since 3 of the 4 quadrants around the corner will be integrated with the "non-existent" periodically extended heights.

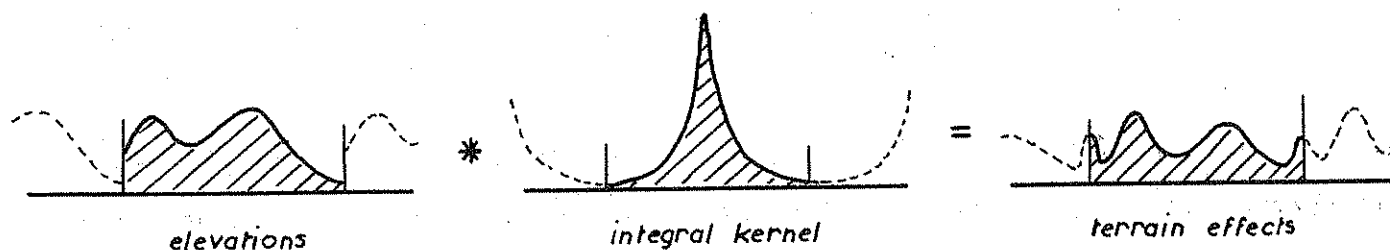


Figure 13

For terrain reductions in connection with general gravity field modelling, it has earlier been stressed that to preserve consistency and harmonicity either a fixed mass model must in principle be taken into account, or - especially for residual terrain reductions - the terrain effect integrations must be carried out to a sufficient distance from the computation points, so that the influence of the remote zones will be negligible for all quantities (gravity, deflections, height anomalies etc.). The FFT methods will in principle only be applicable for general terrain reductions when either sufficiently large areas of elevation data surrounding the target area is transformed, or the given elevation grid is extended with a "border" of zero-values on all sides (of "width" $\frac{1}{2}n\Delta x$ and $\frac{1}{2}m\Delta y$ respectively) to obtain a "true" fixed area reduction at the price of a quadrupling of the elevation data. In both cases computer limitations in storage might be prohibitive. Consider e.g. RTM-reduction, with a 180×180 spherical harmonic reference surface. If (as is very common) $1 \text{ km} \times 1 \text{ km}$ elevation data is available, an area of dimension 300-400 km must be taken into account for complete reduction of deflections and height anomalies in a $1^\circ \times 1^\circ$ block, necessitating a complex array of size "region" 1440 k-2560 k in double precision IBM FORTRAN. Furthermore, when the interest is concentrated in a rather small area, like the $1^\circ \times 1^\circ$ area, it seems somewhat unnecessary to take into account every tiny topographic irregularity at large distances, which is in principle done in the simple FFT approach.

These drawbacks may be overcome by using a "hierarchical" set of FFT terrain reductions, utilizing more and more coarse mean elevation grids. In effect, the terrain computations are split into various "wavelength bands". This split may

be done either in the space domain or the frequency domain. Consider the simple case of two elevation grids, a detailed DTM (e.g 1 x 1 km) covering the target area with a rather small margin, and a coarse DTM (e.g. 10 x 10 km mean heights) covering a much larger area.

In the space domain the terrain effect convolution kernel f may be split in two parts, a near-zone and a far-zone effect, symbolically

$$\text{terrain effect} \sim f * \Delta h = (f_1 + f_2) * \Delta h = f_1 * \Delta h + f_2 * \Delta h \quad (7.41)$$

f_1 being the integral from zero to a certain distance d , f_2 the integral from d to infinity (Figure 14). (For gravity terrain corrections two convolutions of h and h^2 are needed, as discussed in the last section). By choosing a suitable d , f_2 may be computed by sufficient accuracy from the coarse elevation grid and interpolated to the points of the detailed elevation grid, where the inner zone contributions are evaluated from f_1 . The drawback of the space domain split is that the "truncated" transfer functions \tilde{f}_1 and \tilde{f}_2 do not have simple analytical expressions, and a numerical transform must be made to obtain \tilde{f}_1 and \tilde{f}_2 .

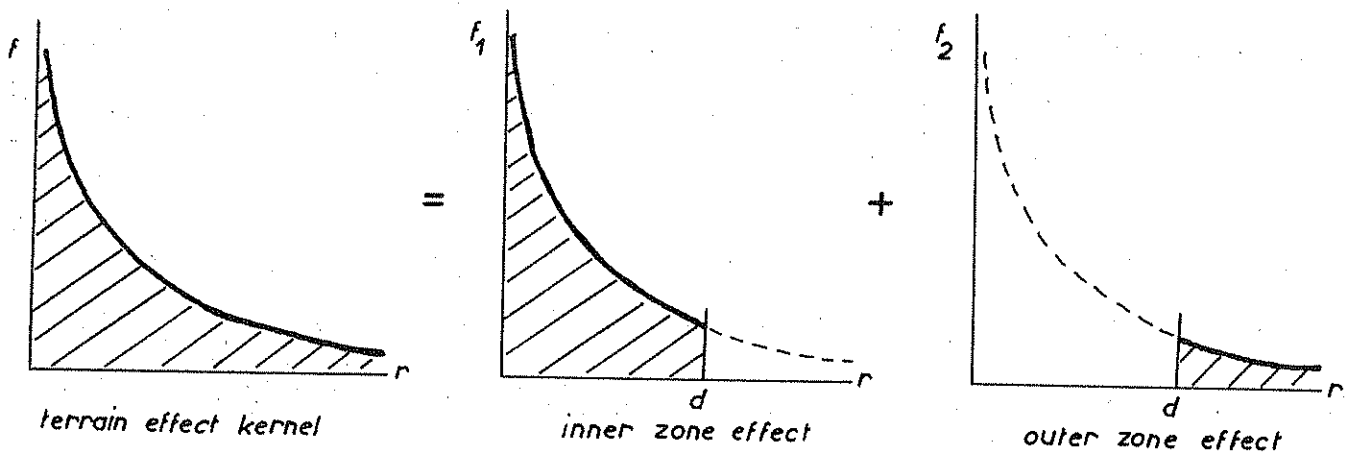


Figure 14

Alternatively a frequency domain split may be attempted as follows:

$$\text{terrain effect} \sim f * \Delta h = f * (\Delta h_1 + \Delta h_2) = f * \Delta h_1 + f * \Delta h_2 \quad (7.42)$$

where the elevation Δh is split into a smooth mean elevation surface Δh_2 , e.g. obtained by interpolation in the coarse elevation grid, and a residual height Δh_1 - analogous to the RTM-reduction. In other words, the terrain effect is split into a long-wavelength part from the mean elevations and a short-wavelength part from the detailed elevations. Ideally, the Δh_2 -surface should be a low-pass filtered version of Δh , so that Δh_1 contains only frequencies above the Nyquist frequencies for the coarse grid, and Δh_2 only frequencies below. Otherwise errors due to aliasing will occur. This may be illustrated as follows:

Let Δh_2 be defined through a running average:

$$\Delta h_2(x, y) = \frac{1}{\Delta x_2 \Delta y_2} \int_{x-\frac{1}{2}\Delta x_2}^{x+\frac{1}{2}\Delta x_2} \int_{y-\frac{1}{2}\Delta y_2}^{y+\frac{1}{2}\Delta y_2} \Delta h(x', y') dx' dy' \quad (7.43)$$

where $(\Delta x_2, \Delta y_2)$ are the grid spacings of the coarse grid. Then Δh_2 may be expressed as

$$\Delta h_2 = \frac{1}{\Delta x_2 \Delta y_2} g * \Delta h, \quad g = \begin{cases} 1 & |x| < \frac{1}{2}\Delta x_2, |y| < \frac{1}{2}\Delta y_2 \\ 0 & \text{otherwise} \end{cases} \quad (7.44)$$

which can have energy at all frequencies since

$$\tilde{g}(u, v) = \frac{1}{4} \frac{\sin(\frac{\pi}{2} u / u_N)}{u} \frac{\sin(\frac{\pi}{2} v / v_N)}{v} \quad (7.45)$$

where (u_N, v_N) are the Nyquist frequencies (7.40) for the coarse grid. (See e.g. Papoulis, 1968). Now, if FFT is directly applied on the coarse (averaged) heights, the non-zero spectrum of Δh_2 above (u_N, v_N) will by (7.44) and (7.45) result in a non-zero spectrum of Δh_2 above this interval, which "folds" erroneously into the low frequencies ("aliasing") by FFT, to give long-wavelength errors in the coarse terrain effect. In addition, minor errors occur when interpolating from points in the coarse grid to the dense, detailed elevation points. The aliasing error may be estimated from the spectrum above (u_N, v_N) for the detailed grid -

but only at the subset of the "coarse" frequencies. For practical applications it would therefore probably be more valuable simply to test various interpolation procedures (e.g. spline functions) for Δh_2 -construction and the subsequent interpolation of the computed far-zone effects, and choose the method with least high-frequency leakage. Such an "optimum" interpolation method is necessary anyway in order to interpolate results from the FFT computation grids to actual station locations.

Time has not allowed actual implementation of the FFT methods for terrain effect computations within the present project. However, recent results obtained by Sideris (1984) seem very promising: in a small test area of the Rocky Mountains (tc range 4-22 mgal), gravity terrain corrections computed with FFT showed sub-mgal accuracies when compared to a space-domain prism integration, using a 1km x 1km elevation grid.

7.7 The Linear Approximation and Error Studies

In addition to allowing the use of FFT for the evaluation of general terrain effects, the linear approximation also comes in very handy in the study of error propagation, e.g. used for answering questions of the type: given a certain statistical behavior of the gravity field and the topography, to what extent will it be beneficial to take the topography into account? and how detailed will the height information be needed? etc.

In this report emphasis is on residual terrain reductions - with respect to a 180 x 180 spherical harmonic expansion. It is therefore natural to work with planar (flat earth approximation) error analysis, briefly outlined in the sequel as it is not too familiar to many geodesists. The basic descriptor of the statistical properties of the variations of the gravity field (and the elevations) is the covariance function, e.g. for gravity anomalies at a reference level.

$$C(x, y) = E\{\Delta g(x', y') \Delta g(x' + x, y' + y)\} \quad (7.46)$$

where E is the ensemble expectation operator. Within the area of interest - approximated by an infinite plane - the signal (Δg) is assumed to be stationary. Fourier transformation of C yields the power spectrum (or, rather, power spectral density)

$$\phi_{\Delta g, \Delta g}(u, v) = E \left\{ |\tilde{g}(u, v)|^2 \right\} = \int_{\pi} C(x, y) e^{-i(ux+vy)} dx dy \quad (7.47)$$

For an isotropic process, $C(x, y) = C(r)$, $r = \sqrt{x^2+y^2}$, (7.47) will as earlier mentioned be a Hankel transform

$$\phi_{\Delta g, \Delta g}(\omega) = 2\pi \bar{C}(r) = 2\pi \int_0^{\infty} r C(r) J_0(\omega r) dr \quad (7.48)$$

Of special importance for error studies is Parsevals formula for Hankel transforms (Papoulis, 1968):

$$\int_0^{\infty} r |f(r)|^2 dr = \int_0^{\infty} \omega |\bar{f}(\omega)|^2 d\omega \quad (7.49)$$

Thus, given a power spectrum $\phi(\omega)$, the variance of the signal may be obtained as:

$$\sigma^2 = C(0) = \frac{1}{2\pi} \int_0^{\infty} \omega \phi(\omega) d\omega \quad (7.50)$$

Spatial extensions are obtained by upward continuation (6.14), e.g. for the potential

$$\phi_{TT}(\omega, z_1, z_2) = \phi_{TT}(\omega) e^{-\omega(z_1+z_2)} \quad (7.51)$$

$$C_{TT}(r, z_1, z_2) = \frac{1}{2\pi} \int_0^{\infty} \omega \phi_{TT}(\omega) e^{-\omega(z_1+z_2)} J_0(\omega r) d\omega \quad (7.52)$$

See e.g. (Nash and Jordan, 1978). The last formula - which is simply the inverse transform of (7.48) - is analogous to the well-known spherical covariance function expansion in Legendre polynomials

$$C_{TT}(\psi, r_1, r_2) = \sum_{\ell=2}^{\infty} \sigma_{\ell} \left[\frac{R^2}{r_1 r_2} \right]^{\ell+1} P_{\ell}(\cos \psi) \quad (7.53)$$

where σ_ℓ is the degree variances ("spherical power spectrum"), R the radius of the earth reference sphere etc. The degree-variances and power spectrum are closely related, and a unique asymptotic correspondence exists (Dorman and Lewis, 1970)

$$\sigma_\ell \approx \frac{1}{2\pi R^2} (\ell + \frac{1}{2}) \phi_{TT}(\frac{\ell + \frac{1}{2}}{R}) \quad (7.54)$$

More details will be given in a subsequent OSU report.

Power spectra and covariance functions for other quantities are easily derived by using the expressions of the quantities in frequency domain, e.g. from (6.15)-(6.17):

$$\phi_{\Delta g, \Delta g} \approx \omega^2 \phi_{TT} \quad (7.55)$$

$$\phi_{\xi\xi} = \left(\frac{v}{\gamma}\right)^2 \phi_{TT}, \quad \phi_{\eta\eta} = \left(\frac{u}{\gamma}\right)^2 \phi_{TT} \quad (7.56)$$

For an isotropic field (that is $\phi_{\Delta g, \Delta g}$ isotropic) these equations and Parsevals equation gives the important corollary that

$$\sigma_{\Delta g}^2 = \gamma^2(\sigma_\xi^2 + \sigma_\eta^2) = 2\gamma^2\sigma_\xi^2 \quad (7.57)$$

In other words, the gravity variance is double the variance of each of the deflection components. Thus $\sigma_\xi = \sigma_\eta = 1''$ corresponds to $\sigma_{\Delta g} \sim 6.7$ mgal.

To describe the covariance function in a given area, simple analytical expressions are traditionally used. The "Poisson" and "inverse distance" covariance functions of Moritz (1980) are especially important for gravity, since they have simple analytical spatial extensions. For topography, however, empirical investigations of U.S. data (cf. next section) indicates that better overall fits are obtained using exponential covariance functions (so-called first order Markov models). The basics of these three simple models may be outlined as (See Moritz (1980).

Name	$C(r)$	$\phi(\omega)$	Correlation Length
1) "Poisson"	$\frac{\sigma^2}{[1+(r/D^2)]^{3/2}}$	$2\pi\sigma^2 D^2 e^{-\omega D}$	$x_{1/2} = 0.77 D$
2) "Rec. distance"	$\frac{\sigma^2}{[1+(r/D)^2]^{1/2}}$	$2\pi\sigma^2 D \frac{e^{-\omega D}}{\omega}$	$x_{1/2} = 1.73 D$
3) "Markov"	$\sigma^2 e^{-r/D}$	$2\pi\sigma^2 D^2 \frac{1}{[1+\omega^2 D^2]^{3/2}}$	$x_{1/2} = 0.69 D$

These functions are shown in Figure 15 together with an actual topographic data example.

7.8 Error Studies of DTM Resolution Requirements

To give an example of error analysis in terrain reductions, the representation error for terrain effects on gravity and deflections at altitude will first be studied. In other words, the resolution requirements for a digital terrain model to give terrain effects of a certain accuracy will be studied.

Assume topographic mean elevations to be given on a grid of spacing $(\Delta x, \Delta y)$. If the grid elements are reasonably "square", then the mean may be approximated with a mean over a circle. This is advantageous, as isotropy then will be "conserved". Then to first order the terrain effect computed from the mean elevations (neglecting known station elevations) may be expressed as:

$$\Delta g' = 2\pi G_p \Delta h_{\text{mean}} \approx 2\pi G_p \frac{1}{\pi a^2} \int_C \Delta h(x', y') dx' dy', \quad a \approx 0.56 \sqrt{\Delta x \Delta y} \quad (7.51)$$

where $\Delta h = h - h_{\text{ref}}$ is the residual elevation and C a circle of radius a , centered at the computation point. (7.51) is again a convolution

$$\Delta g' = \frac{2G_p}{a^2} (f * \Delta h), \quad f(r) = \begin{cases} 1 & r < a \\ 0 & \text{otherwise} \end{cases} \quad (7.52)$$

with transfer function (Papoulis, 1968)

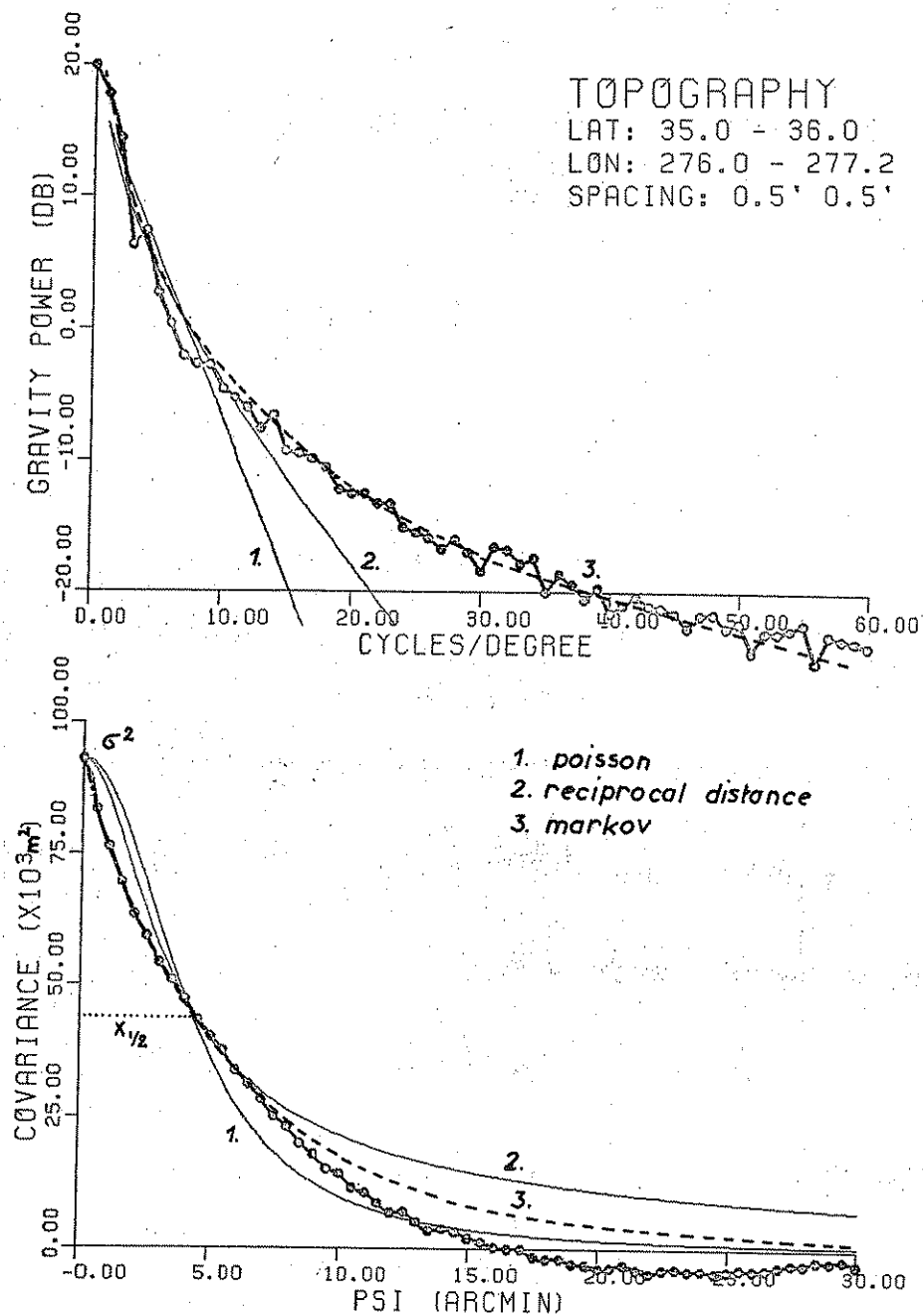


Figure 15 Empirical power spectrum and covariance function for elevations Δh in a 110x110 km area in the Smoky Mountains, eastern USA, and fit with 3 simple two parameter covariance models. An excellent fit is obtained with the exponential (Markov model).

$$\tilde{f}(\omega) = 2\pi \bar{f}(\omega) = 2\pi \frac{a J_1(a\omega)}{\omega} \quad (7.53)$$

J_1 is the Bessel function of order 1. The shape of the function \tilde{f} is shown in Figure 16.

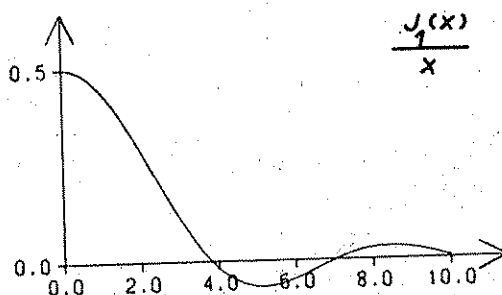


Figure 16

By upward continuation to elevation H the spectrum then becomes

$$\tilde{\Delta g}'(u, v) = 4\pi G\rho \frac{J_1(a\omega)}{a\omega} e^{-\omega H} \tilde{h}(u, v) \quad (7.54)$$

By comparison to the "exact" terrain effect

$$\Delta \tilde{g}(u, v) = 2\pi G\rho e^{-\omega H} \tilde{h}(u, v) \quad (7.55)$$

the representation error $\epsilon = \Delta g' - \Delta g$ is seen to be

$$\tilde{\epsilon}(u, v) = 2\pi G\rho \left(1 - 2 \frac{J_1(a\omega)}{a\omega}\right) e^{-\omega H} \tilde{h}(u, v) \quad (7.56)$$

and thus

$$\phi_{\epsilon\epsilon}(\omega) = (2\pi G\rho)^2 \left(1 - 2 \frac{J_1(a\omega)}{a\omega}\right)^2 e^{-2\omega H} \phi_{hh}(\omega) \quad (7.57)$$

For deflections of the vertical essentially the same formula holds. From formula (7.21) it is seen that the deflection error expressions corresponding to (7.56) will be simply

$$\left. \begin{array}{l} \tilde{\epsilon}_\xi(u, v) \\ \tilde{\epsilon}_\eta(u, v) \end{array} \right\} = -\frac{i}{\gamma} \left\{ \begin{array}{l} v \\ u \end{array} \right\} \frac{1}{\omega} \tilde{\epsilon}(u, v) \quad (7.58)$$

For an isotropic field, $\phi_{\xi\xi} = \phi_{\eta\eta}$, we get directly using the statistical independence of ξ and η ;

$$\phi_{\xi\xi}(\omega) = \phi_{\eta\eta}(\omega) = \frac{1}{2}E\{|\tilde{\epsilon}_{\xi}|^2 + |\tilde{\epsilon}_{\eta}|^2\} = \frac{1}{2\gamma^2} \phi_{\epsilon\epsilon}(u, v) \quad (7.59)$$

Thus, results obtained for gravity anomalies in the error analysis may be directly applied to deflections of the vertical as well, when the previously mentioned "conversion factor" of 6.7 mgal/arc sec is used.

To get error estimates an exponential ("Markov") model $C_{\Delta h \Delta h}(r) = \sigma_{\Delta h}^2 e^{-r/D}$ will be assumed for the topography covariance function. By (7.50) and (7.57) the error variance will be

$$\begin{aligned} \sigma_{\epsilon}^2 &= \frac{1}{2\pi} \int_0^{\infty} \omega \phi_{\epsilon\epsilon}(\omega) d\omega \\ &= (2\pi G\rho)^2 \sigma_{\Delta h}^2 \int_0^{\infty} \omega \left(1 - 2 \frac{J_1(a\omega)}{a\omega}\right)^2 e^{-2\omega H} \frac{D^2}{[1+\omega^2 D^2]^{3/2}} d\omega \end{aligned} \quad (7.60)$$

It is convenient to normalize the parameters with respect to D , introducing a dimensionless averaging parameter $a' = \frac{a}{D}$ and elevation $H' = \frac{H}{D}$. Then by shift of variable $t = \omega D$:

$$\sigma_{\epsilon}^2 = (2\pi G\rho)^2 \sigma_{\Delta h}^2 F^2(a', H') \quad (7.61)$$

$$F^2(a', H') = \int_0^{\infty} \left(1 - 2 \frac{J_1(a't)}{a't}\right)^2 e^{-2tH'} \frac{t}{[1+t^2]^{3/2}} dt \quad (7.62)$$

This integral has no simple analytical expression. It has been integrated numerically, using a standard adaptive numerical integration subroutine and using polynomial expansions for $J_1(t)$ given by Abramowitz and Stegun (1965). The result (i.e. the function F , square root of 7.62) is shown in Figure 17.

The r.m.s. computation error σ_{ϵ} at elevation H should ordinarily be compared to the "actual" r.m.s. terrain effect $\sigma_{\Delta g}(H)$ at elevation H . The

relative r.m.s. effect at altitude will be given simply by the integral (7.62) without the Bessel function term, i.e. as the limit of F for large a' , additionally shown on Figure 17.

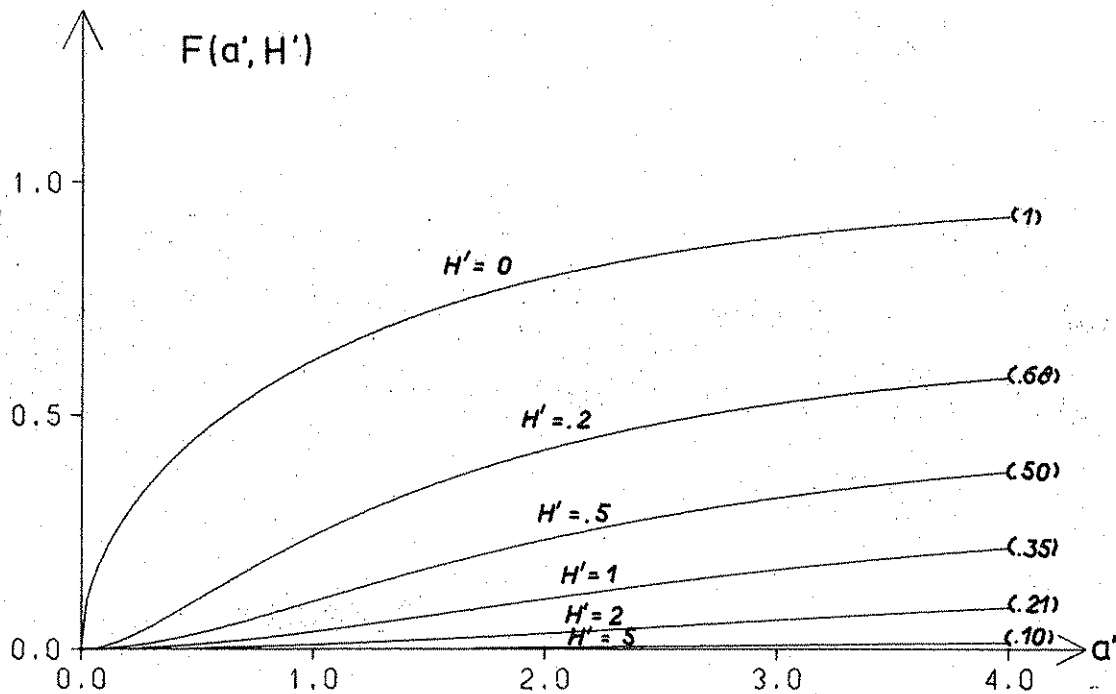


Figure 17 R.m.s. error integral (7.62) for terrain reduction of gravity and deflections. The graphs show the ratio between the r.m.s. computation error σ_ϵ and $2\pi G\rho \sigma_{\Delta h}$ as a function of normalized averaging radius for various normalized elevations. Asymptotic values shown at left.

To give an example of application of the error curves, consider the Smoky Mountains area, a typical "mild" mountainous area. From the topography covariance function (Figure 15) we have $\sigma_{\Delta h} \sim 305$ m, correlation length $X_{1/2} \sim 7.6$ km and thus $D = 11.0$ km. First consider stations at the level of the topography, $H' = 0$. The r.m.s. variation of the residual terrain effect will be 34 mgal and 5.2" for gravity and deflections respectively. To compute terrain effects with a 6.6mgal/1" r.m.s. error ($F \sim 0.19$), Figure 16 gives $a' \sim 0.008$ and by (7.51) $\Delta x = \Delta y \sim 1.6$ km. Hence, a digital terrain model with a grid spacing around 1.6 km will be needed to give 1"-deflections. At altitude, say $H = 10$ km, the r.m.s. terrain effect is seen to be only ~ 13 mgal. To get e.g. a 1 mgal error (i.e. $F \sim 1/34$), the

figure indicates $a' \sim 0.7$ and thus the resolution of the digital terrain model needs to be only 13-14 km.

For geoid undulations similar error curves may be computed. In the linear approximation height anomaly residual terrain effects at the surface of the topography will be

$$\tilde{\zeta} = \frac{2\pi G\rho}{\gamma} \frac{1}{\omega} \Delta h \quad (7.63)$$

Analogously to gravity and deflections the following expressions for the height anomaly variance and error variance are obtained

$$\sigma_{\zeta}^2 = \left(\frac{2\pi G\rho}{\gamma}\right)^2 \sigma_{\Delta h}^2 D^2 \int_0^{\infty} \frac{1}{\omega[1+\omega^2 D^2]^{3/2}} d\omega \quad (7.64)$$

$$\sigma_{\epsilon_{\zeta}}^2 = \left(\frac{2\pi G\rho}{\gamma}\right)^2 \sigma_{\Delta h}^2 D^2 \int_0^{\infty} \left(1 - 2 \frac{J_1(a\omega)}{a\omega}\right)^2 \frac{1}{\omega[1+\omega^2 D^2]^{3/2}} d\omega \quad (7.65)$$

The variance σ_{ζ}^2 computed by (7.64) is infinite (opposed to the finite $\sigma_{\epsilon_{\eta}}^2$). This is a phenomena analogous to the infinite potential effect of the Bouguer plate: very long wavelengths in the topography results in very large geoid effects. However, although the simple Markov covariance model used has energy at long wavelengths, this will not be the case for "real" residual terrain reduction with respect to a 180 x 180 reference surface. Ideally, no power should remain below the "reference" frequency $\omega_0 = \frac{180}{R}$. Thus, a better, less conservative estimate of the "local" height anomaly variation is obtained by integrating from ω_0 rather than 0 in (7.64) and (7.65)

$$\sigma_{\epsilon_{\zeta}}^2 = \left(\frac{2\pi G\rho}{\gamma}\right)^2 \sigma_{\Delta h}^2 D^2 G_1^2(D, a') \quad (7.66)$$

$$G_1^2(D, a') = \int_{\omega_0 D}^{\infty} \left(1 - 2 \frac{J_1(a't)}{a't}\right)^2 \frac{1}{t[1+t^2]^{3/2}} dt \quad (7.67)$$

where the substitution $t = \omega D$, $a' = a/D$, has been used again. The function

G_1 is shown in Figure 18. Note that the error variance is nearly insensitive to the omission of the low frequencies.

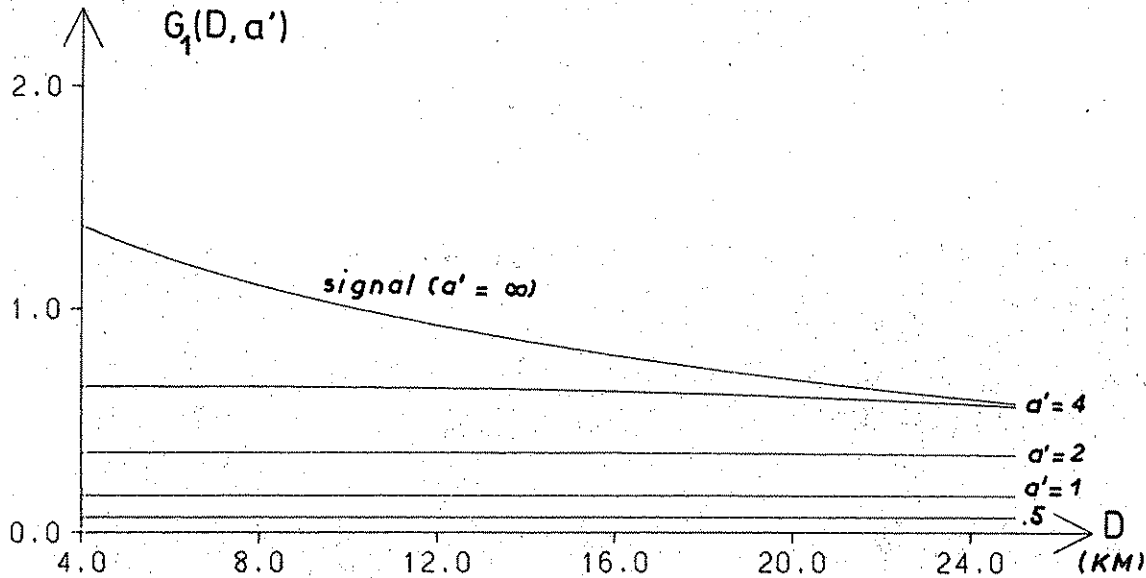


Figure 18 R.m.s. error integral (7.67) for height anomaly residual terrain effects with respect to a 180 x 180 spherical harmonic reference surface.

For isostatic reductions the "full" height anomaly variance will be well defined. At the accuracy levels of the linear approximation, the isostatic reduction may be viewed as a mass plane compensation at depth T . Then the isostatic reduction transfer function will be simply

$$\tilde{\zeta} = \frac{2\pi G_0}{\gamma} \frac{1}{\omega} (1 - e^{-\omega T}) \tilde{h} \quad (7.68)$$

where it is now the elevation h and not the residual elevation Δh which is used. The isostatic error variance integral then becomes

$$\sigma_{\epsilon_\zeta}^2 = \left(\frac{2\pi G_0}{\gamma} \right)^2 \sigma_{\Delta h}^2 D^2 G_2^2(a', T') \quad (7.69)$$

$$G_2^2(a', T') = \int_0^\infty \left(1 - 2 \frac{J_1(a't)}{a't} \right)^2 (1 - e^{-tT'})^2 \frac{1}{t[1+t^2]^{3/2}} dt$$

again through the substitution $t = \omega D$, $T' = \frac{T}{D}$, $a' = \frac{a}{D}$. The dimensionless function G_2 is shown in Figure 19.

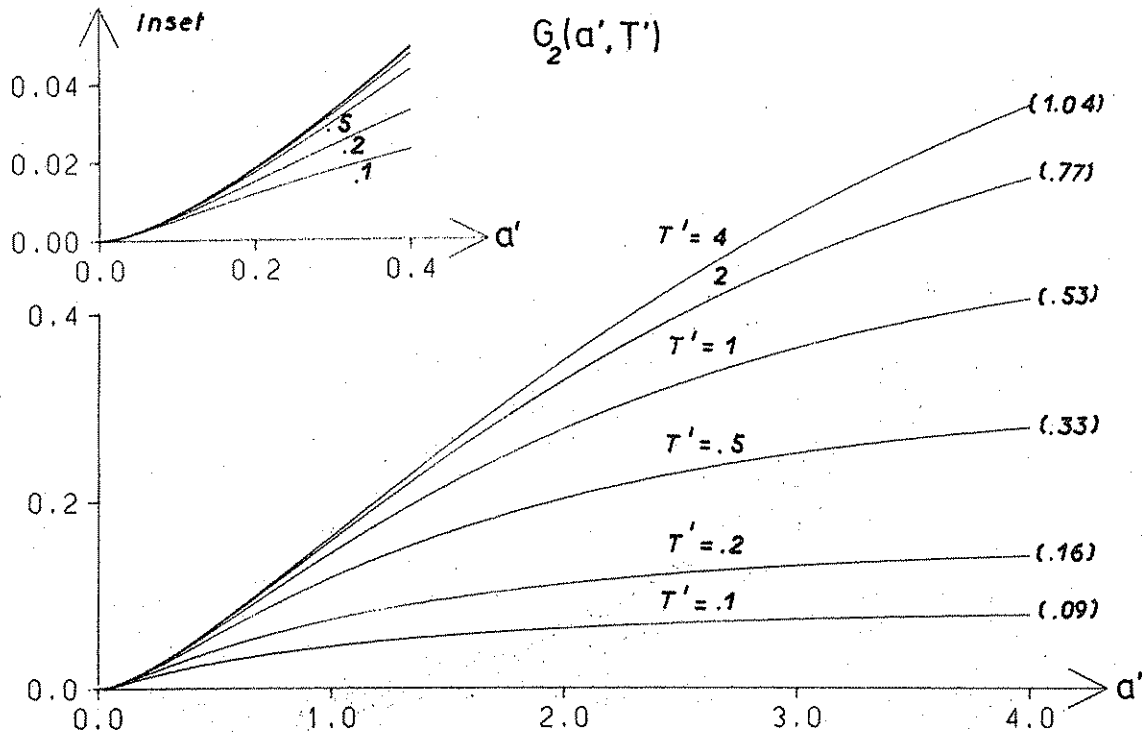


Figure 19 R.m.s. error integral for isostatic height anomaly reductions. Asymptotic values for large a' (i.e., the variance integral) shown in brackets at right.

For a RTM-reduction example, consider again the Smoky Mountains area, $D = 11$ km, $\sigma_{\Delta h} = 305$ m. From Figure 18 and (7.66) the r.m.s. variation of the RTM height anomalies is seen to be only ~ 38 cm, which verifies the earlier claimed advantage of the RTM reduction: terrain effects on the geoid are very small. Now, say if an accuracy of 10 cm is wanted for the geoid terrain effects, Figure 18 shows that $a' \sim 2$ will be sufficient, corresponding to a necessary gridspacing of $\Delta x = \Delta y \cdot \frac{2}{0.56} \cdot 11 \text{ km} \sim 40 \text{ km}$, again demonstrating the insensitivity of geoid terrain effects to the very local topography.

To give an example of application of the error analysis in oceanic areas, an empirical bathymetric covariance function for a $10^\circ \times 10^\circ$ trench area in the Pacific is shown in Figure 20. In this area the mean depth is 3.2 km, $\sigma_h \sim 1553$ m

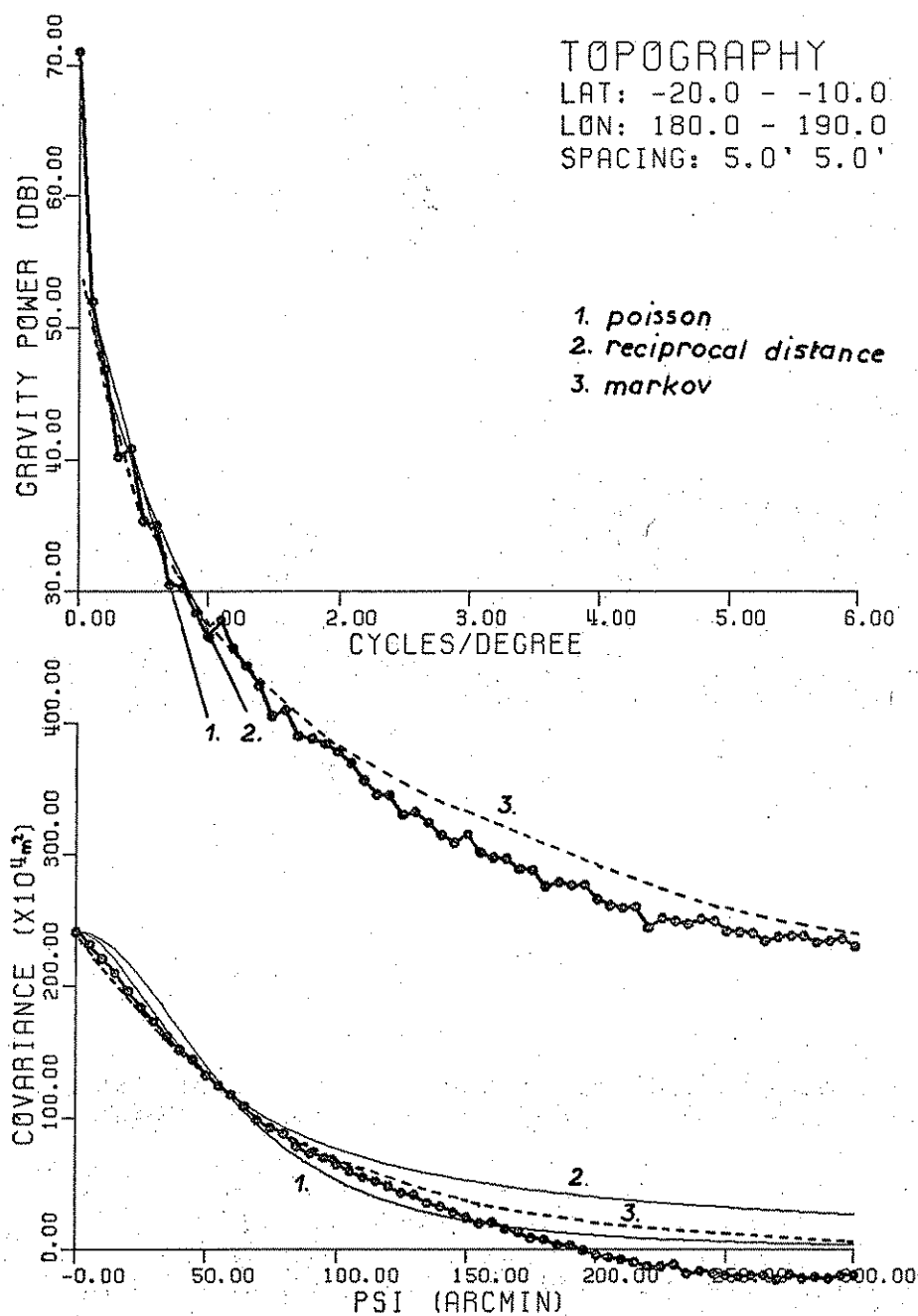


Figure 20 Power spectrum and covariance function for bathymetry in a $10^\circ \times 10^\circ$ area around the Tonga trench. No reference elevations have been subtracted. Again the exponential Markov model is seen to give the best fit of the simple covariance models. (power spectrum has been plotted for $\rho = 2.67$. To get $\rho = 1.64$ results, simply subtract 2 dB from given values).

and $X_{1/2} \sim 107$ km, giving $D \sim 155$ km. For a trench area the isostatic compensation is known to be partly based on density anomalies in the upper mantle, and therefore a fairly deep isostatic compensation level T must be chosen. Assume e.g. $T = 40$ km. Then $T' \sim 0.26$ and from Figure 19 and (7.69) with $\rho = -1.64$ the variance of the isostatic geoid effect is seen to be $\sigma_z \sim 3.4$ m (a direct computation of the

isostatic effects have yielded $\sigma_{\zeta} = 3.1$ m, thus validating the error analysis approach, cf. next chapter). To compute the isostatic geoid effect with an accuracy comparable to SEASAT satellite altimetry, say $\sigma_{\epsilon_{\zeta}} \sim 10$ cm, then we must have $G_2 \sim 0.006$ and hence $a' \sim 0.09$, giving necessary grid spacing $\Delta x \sim 25$ km.

An "inverse" example may also be given: recently a global 5'x5' mean bathymetry data set (SYNBAPS) was released, covering most of the earth's oceans between 75° N and 75° S. In the "rough" Tonga trench area, the SYNBAPS data corresponds to $a' \sim 0.033$, giving an r.m.s. isostatic computation error $\sigma_{\epsilon_{\zeta}} \sim 3$ cm. However, it should be remembered that this number corresponds to the linear approximation and mass plane condensation, and assumes the mean elevations to be error free. Therefore SYNBAPS derived isostatic geoids might be significantly more in error, naturally especially in areas of poor bathymetric data coverage.

8. Spectral Characteristics and Covariance Functions for Local Topography and Terrain Effects

In the present section key parameters describing the statistical behavior of the local topography will be investigated for a number of different sample areas, representing various types of topography, from nearly flat to alpine areas in the United States.

Power spectrum and covariance functions have been estimated from available 0.5'x0.5' elevations, supplied by the National Geodetic Survey, using a simple FFT approach.

With this approach, the residual topography power spectrum (power spectral density) is obtained from the discrete fourier transform (7.37) of Δh by

$$\phi_{\Delta h \Delta h}(u, v) = \frac{nm}{\Delta x \Delta y} |\tilde{h}(u, v)|^2 \quad (8.1)$$

where $\Delta x, \Delta y$ are grid spacing of the $n \times m$ given elevation grid. The power spectrum $\phi_{\Delta h \Delta h}$ will be defined in a frequency square between the Nyquist fre-

quencies (7.40) $\pm u_N, \pm v_N$. It will be symmetric with respect to the zero-frequency: $\phi(u, v) = \phi(-u, -v)$. By the inverse fourier transform (7.38) the 2-dimensional covariance function is obtained:

$$C_{\Delta h \Delta h}(x, y) = \frac{\Delta x \Delta y}{nm} \tilde{\phi}_{\Delta h \Delta h}^{-1}(u, v) \quad (8.2)$$

This function will be defined within the square $\pm \frac{n}{2} \Delta x, \pm \frac{m}{2} \Delta y$, and will again exhibit symmetry with respect to (0,0).

In the sequel ϕ and C will be investigated in a number of cases for both topography, terrain corrections and observed gravity and geoid. Since we are mainly concerned with isotropic processes, the results will be averaged along circles, to give the "isotropic" covariance function $C(r)$ and power spectrum $\phi(\omega)$. However, to get an idea of the anisotropy, a contour plot of the 2-dimensional covariance function will be given as well. For gravity also degree-variances will be given, based on formula (7.54).

The power estimate (8.1) may be improved by taking the finite extent of the given data into account through the use of window filters. For tests, a two-dimensional Hanning window has been applied in the frequency domain (see e.g. Engelis, 1983), the main effect being a less "noisy" $\phi(u, v)$. The discrete Hanning window in the frequency domain is nothing but a simple smoothing, with a filtered frequency value given as a weighted mean of the value itself and the adjacent frequencies. Since this smoothing already to some degree is performed by the radial smoothing (and the prime interest is in the overall shape of the curves) I have found no practical need for windowing, and thus the spectral estimates represent "raw", unfiltered FFT-results.

Examples of results have already been shown in Figures 15 and 20. The power spectra will be given in units of $\text{mgal}^2 \text{degree}^2$ (1 degree \sim 111 km), where elevations have been converted to gravity using the simple Bouguer factor for $\rho = 2.67 \text{ g/cm}^3$.

$$g_m = 2\pi G_p \Delta h \sim 0.1119 \text{ [mgal/m]} \cdot \Delta h \quad (8.2)$$

and results are shown logarithmic in dB

$$\phi \text{ [dB]} = 10 \log_{10} (\phi \text{ [mgal}^2\text{degree}^2]) \quad (8.3)$$

as a function of the frequency $\nu = \frac{\omega}{2\pi}$ in units cycles/degree.

The anisotropy will be indicated through a small contour plot of the normalized 2-dimensional covariance function at levels $C(r) = 1.0, 0.8, 0.6, \dots$ (Figure 21). To get a quantitative measure of the anisotropy, an anisotropy index will be defined as

$$\text{anisotropy index} = \frac{\text{maximal } X_{1/2}}{\text{minimal } X_{1/2}} \quad (8.4)$$

where $X_{1/2}$ is the correlation length in a certain direction, i.e. the distance from origo for which the covariance is half its zero-value C_0 . An isotropic field will have an anisotropy index of 1.

The second-order gradient variance G_0 will be used in the sequel as a measure of high-frequency content. As shown by Moritz (1980), G_0 will be given as the curvature of the (gravity) covariance function at origo. It will be estimated directly from the empirical covariance function, using a symmetrical spline interpolation procedure. The result must be used with some caution, especially for the topography where the applied Bouguer-approximation is very crude for second-order gradients. Since the spline curvature determination will be directly dependent on the data grid spacing, G_0 will merely represent a lower limit of the gradient variance, giving the gradient variance of some smooth, filtered version of the actual gradient field. The gradient variances will be given in E^2 ,
 $1E = 10^{-9} \text{ s}^2 = 0.1 \text{ mgal/km}.$

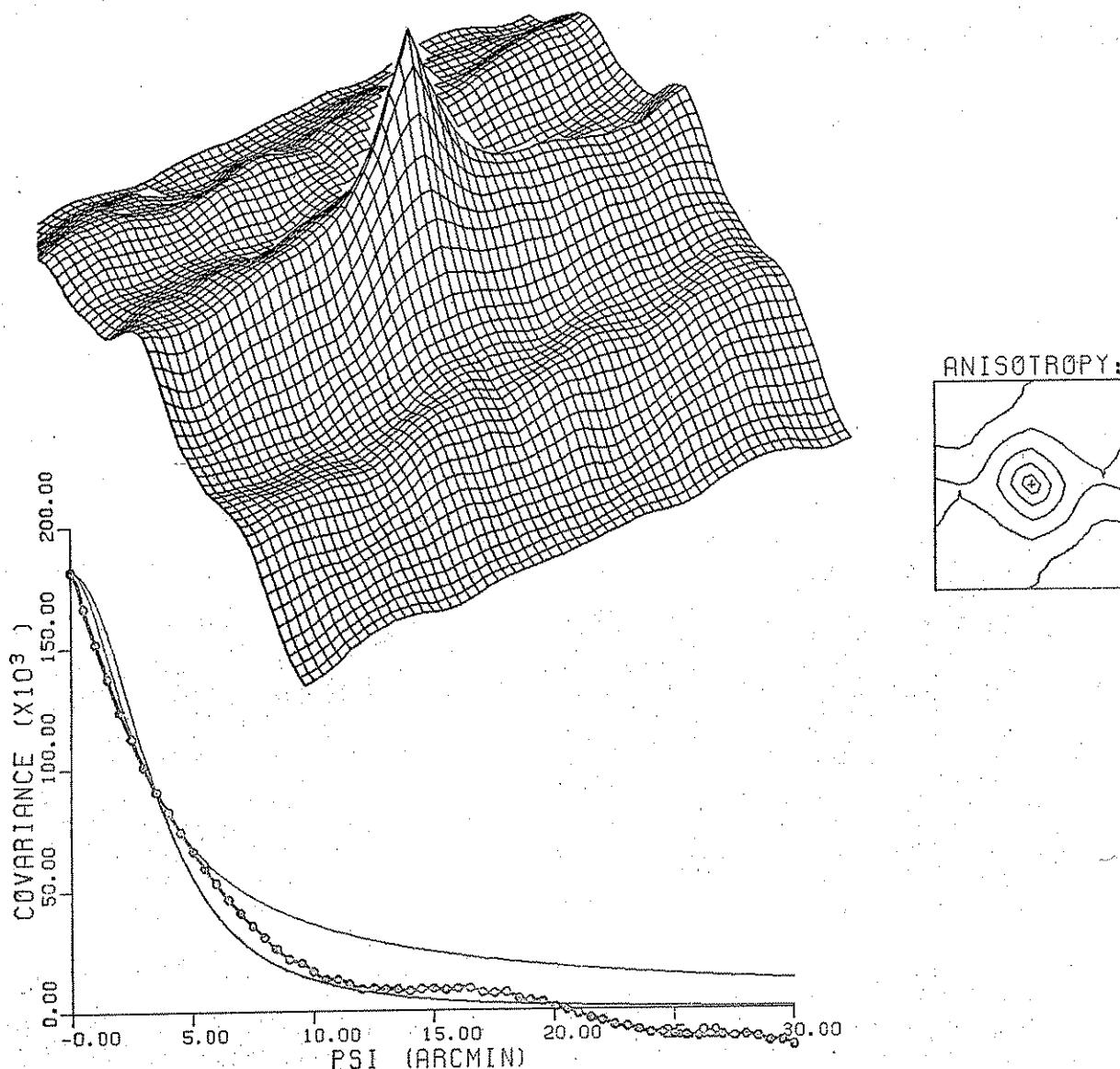


Figure 21 Empirical residual elevation covariance function for the Colorado Rocky Mountain test area of Figure 12 ($1^\circ \times 1^\circ$ block, latitude 39° to 40° N, longitude 107° to 106° W).
TOP: 2-dimensional covariance function from FFT,
RIGHT: same, but shown with $0.2 C_0$ contour interval (and only to ± 15 arcmin),
BOTTOM: radially averaged covariance function. Poisson and reciprocal distance covariance models also shown (again an exponential model would give a better fit, cf. Figure 15)

8.1 Topographic Covariance Functions for U.S. Sample Areas

A number of $1^\circ \times 1.2^\circ$ nearly square blocks (each containing 120x144 elevation points) have been analyzed using 0.5'x0.5' (~1 km) elevations from the NGS data base. Each analysis, with FFT, plotting etc., used c.5 sec CPU-time on The Ohio State University's Amdahl computer.

The areas are shown in Figure 22, and represent various types of topography: alpine (Colorado, Sierra Nevada), alpine-mountainous with volcanoes (Washington), mountainous plains (New Mexico), older mountains (Smoky Mountains) and flat to hilly lowland (Ohio). The two 1° New Mexico blocks comprise most of the "White Sands" New Mexico test area for comparison of gravity field modelling techniques, see e.g. (Tscherning and Forsberg, 1983).

All elevations analyzed are residual elevations $\Delta h = h - h_{ref}$, where the 180x180 spherical harmonic expansion of the earth's topography of Rapp (1982) has been used as reference elevation. The Bouguer-derived topographic gravity is thus to first order the RTM 180 terrain effect.

Results are shown in Figures 23, 24, and Table 4. Despite the different types of topography, the results are amazingly similar, with the prime variation being in the r.m.s. variation of C_0 , less in the shape of the curves and the correlation length. The correlation length varies in the range 6.5-12.2 km, while the r.m.s. residual elevations varies from 45 m to 785 m. For the eight test areas, maximal and minimal roughness of RTM-terrain effect field is obtained in the Sierra Nevada and Ohio blocks respectively: for gravity the r.m.s. terrain effect will be 88 and 5 mgal respectively, for deflections 13" and .8" and for height anomalies 96 cm and 5 cm, using the results of section 7.8. The degree of anisotropy is seen in some cases to be nil, in other cases rather severe. Since the observed gravity field will be dominated by the topographic effects in mountainous blocks, the same degree of anisotropy will be expected in the gravity covariance function, thus stressing the need for utilization of terrain reduction methods.

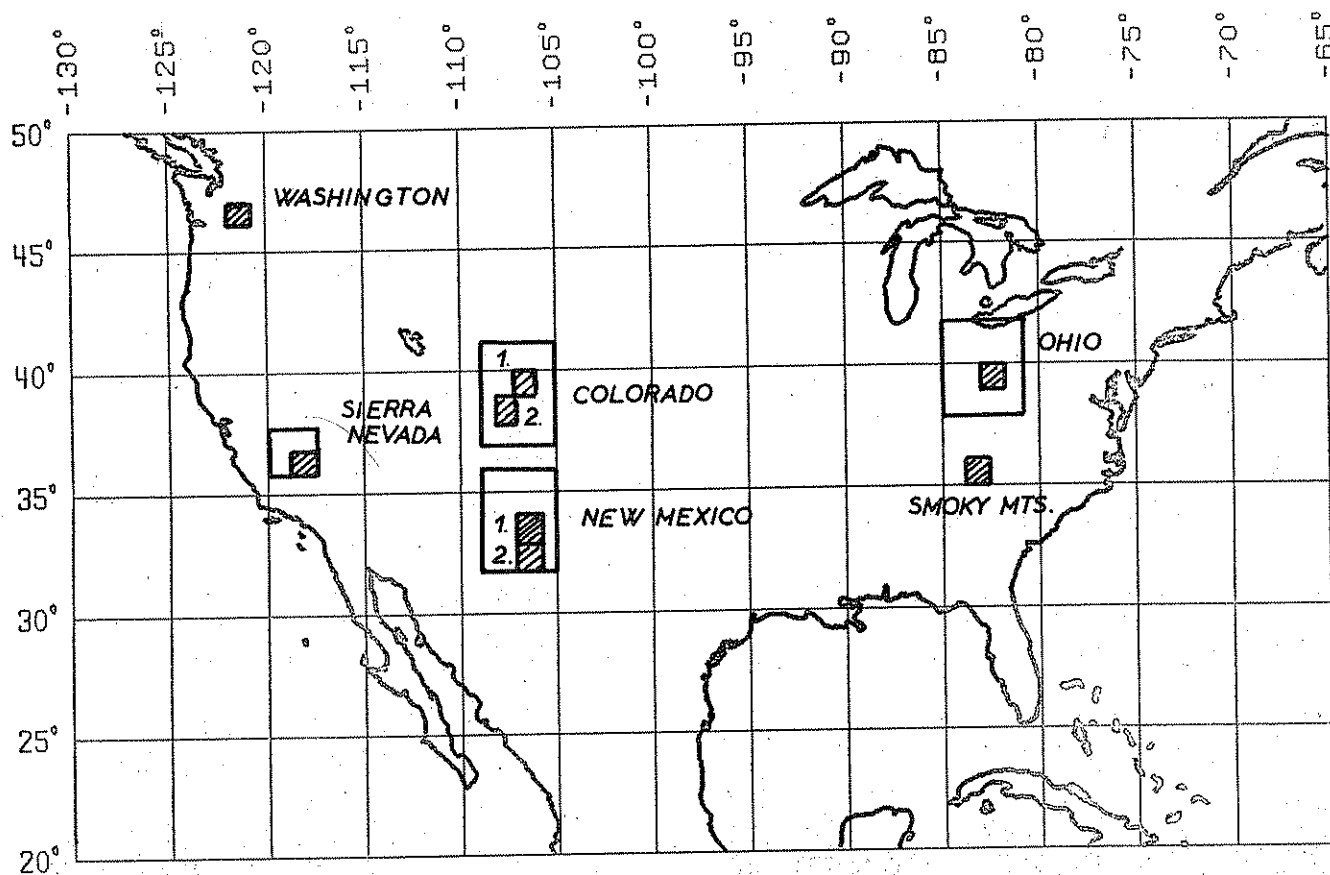


Figure 22 $1^\circ \times 1.2^\circ$ sample areas for topographic covariance functions and power spectra (hatched small rectangles) and gravity analysis sample areas (large rectangles) in the United States.

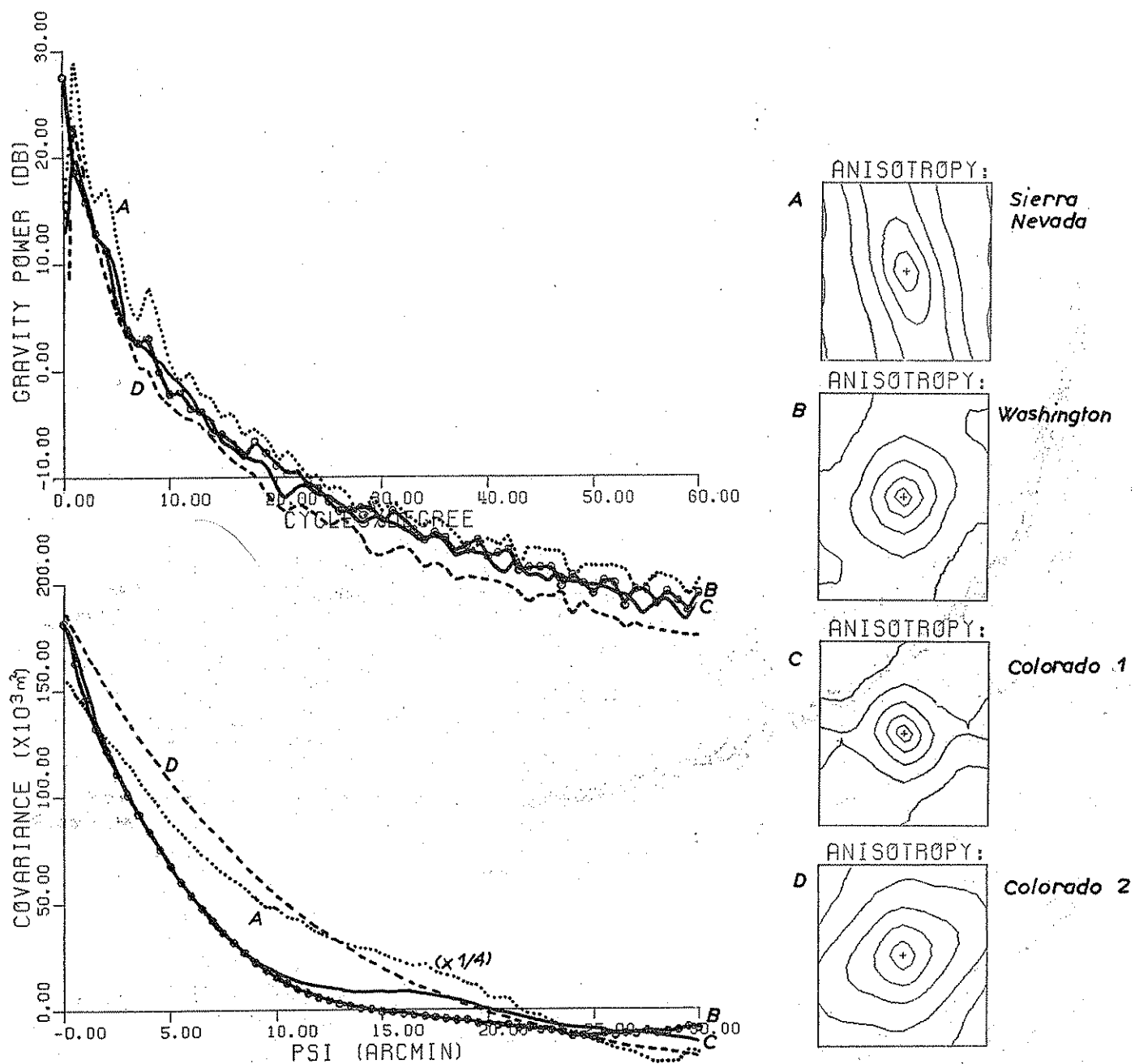


Figure 23 Empirical power spectra (top) and covariance functions (bottom and right) for residual topography in selected $1^\circ \times 1.2^\circ$ mountainous blocks of western U.S.

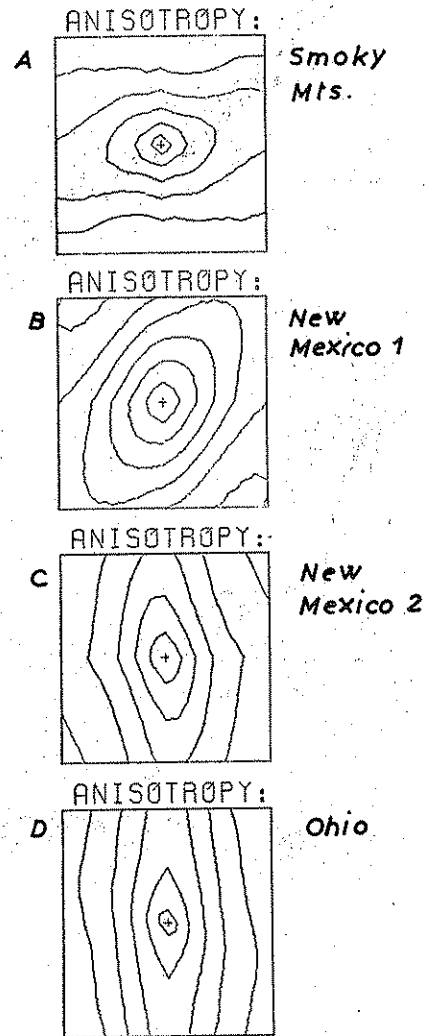
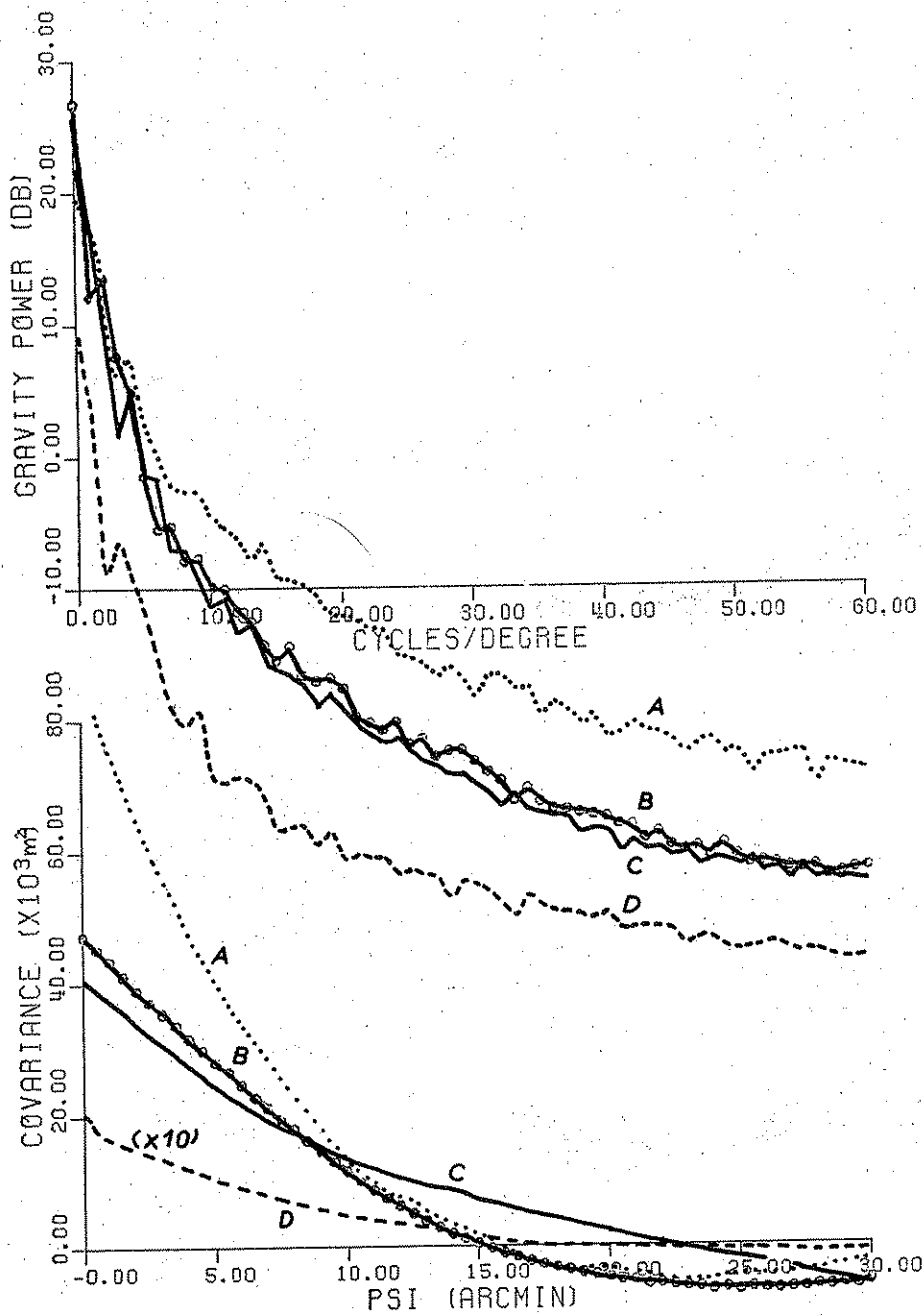


Figure 24 Empirical power spectra and covariance functions for residual topography in selected, relatively less mountainous $1^\circ \times 1.2^\circ$ blocks.

Table 4
Statistical Parameters for Residual Topography, 1°x1.2° Blocks, 0.5'x0.5' Sampling

Area (lat. N, lon, W)	Highest point. (m)	Topography (m) mean std.dev.	Residual topo- graphy mean	C ₀ (m ²)	$\sqrt{C_0}$ (m)	X _{1/2} (arcmin)	$\sqrt{G_0}$ (E)	Aniso- tropy index
California/Sierra Nevada 36-37, 119-117.8	Mt. Whitney 4417	1697 784	37	615954	785	6.1'	366	2.7
Washington/Cascades 46-47, 122-120.8	Mt. Rainier 4392	950 356	234	181332	426	3.6'	305	1.0
Colorado I 39-40, 107.1-105.9	Mt. Elbert 4399	3005 468	39	181229	426	3.5'	276	1.2
Colorado II 38-39, 108.1-106.9	Uncompahgre Pk. 4361	2627 534	-10	187749	433	6.1'	214	1.2
Smoky Mountains 35-36, 84-82.8	Clingman Dome 2025	754 292	90	93023	305	4.1'	228	1.6
New Mexico I 33-34, 107.1-105.9	Sacramento Mts. c. 3600	1583 264	-194	47176	217	6.3'	99	1.5
New Mexico II 32-33, 107.1-105.9	San Andres Mts. 2511	1364 211	-134	40797	202	6.6'	89	2.2
Ohio 39-40, 83.1-81.9	Hocking Hills c. 400	256 35	-29	2044	45	5.0'	40	3.0

8.2 Magnitude of the Gravimetric Terrain Correction - Colorado Area

In the previous sections emphasis has been on the dominant terrain effect on gravity anomalies - the "Bouguer" term $-2\pi G\rho\Delta h$. To get the complete terrain effect, the additional terrain correction is needed. However, it will usually be one order of magnitude smaller than the Bouguer term - in the present section the actual magnitudes will be investigated for the Colorado areas.

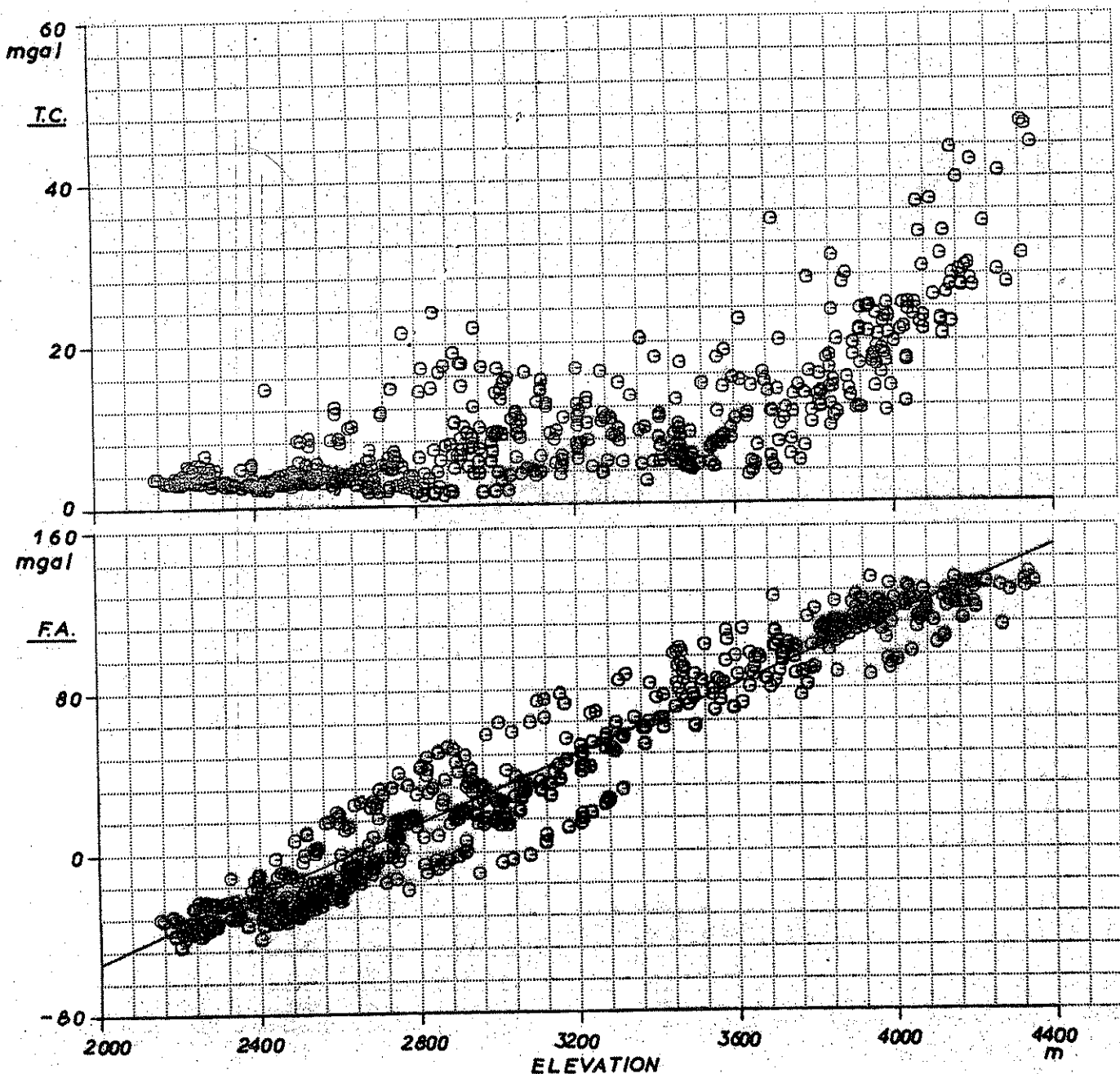


Figure 25 Terrain corrections (top) and free-air anomalies (bottom) for gravity stations in a $\frac{1}{2}^\circ \times \frac{1}{2}^\circ$ Colorado area (lat. $38.5-39^\circ$ N, lon. $106.5-106^\circ$ W). Note the different scale used in the plots.

Figure 25 shows an example of actual gravity data and terrain corrections for a small ($\frac{1}{2}^\circ \times \frac{1}{2}^\circ$) block (NGS data). The terrain corrections are seen to be in the range of 0-40 mgal, opposed to a Bouguer RTM-effect range of roughly -120 to 120 mgal. For such a rather small area, the free-air anomalies correlate well with elevation, the slope being essentially a measure of the topographic density. However, since the terrain corrections have a tendency to be large for the higher stations, the free-air slope will give too low density values: in the case of Figure 25 $\rho \sim 2.1$, which is unrealistic. Therefore, while terrain corrections might be neglected in connection with e.g. error studies, omission in other cases implies serious systematic errors, especially when used for density determination as outlined in Section 5.

To study further the terrain correction, computation of terrain corrections was done in a $2' \times 3'$ grid for the two $1^\circ \times 1^\circ$ Colorado blocks of the last section (and on a $2' \times 2'$ grid for the $\frac{1}{2}^\circ \times \frac{1}{2}^\circ$ area of Figure 25), using the prism integration programme of the appendix. The choice of the rather coarse computation grid size was necessary to avoid excessive computation times (on the OSU Amdahl system CPU-time requirements were c. 0.2 sec/station). Figure 26 shows the result for the northeastern block. By comparing to the topographic map (Figure 12) it is clear that some degree of undersampling is done by only computing on a $2' \times 3'$ grid, so some aliasing might be expected in the power spectra of the terrain correction signals, shown in Figure 27.

At the $2'$ resolution level, the terrain correction covariance functions (Figure 27) might be described as a "white noise" signal with very short correlation length plus a smaller long wavelength signal (remote zone effects). Compared to the main "Bouguer" terrain effect, the terrain corrections are indeed seen to be smaller, as shown in Table 5 - however, large outliers and non-normal error distribution makes it important to use the best possible terrain corrections for gravity field modelling, using even more detailed elevation data than the presently used $0.5' \times 0.5'$ heights.

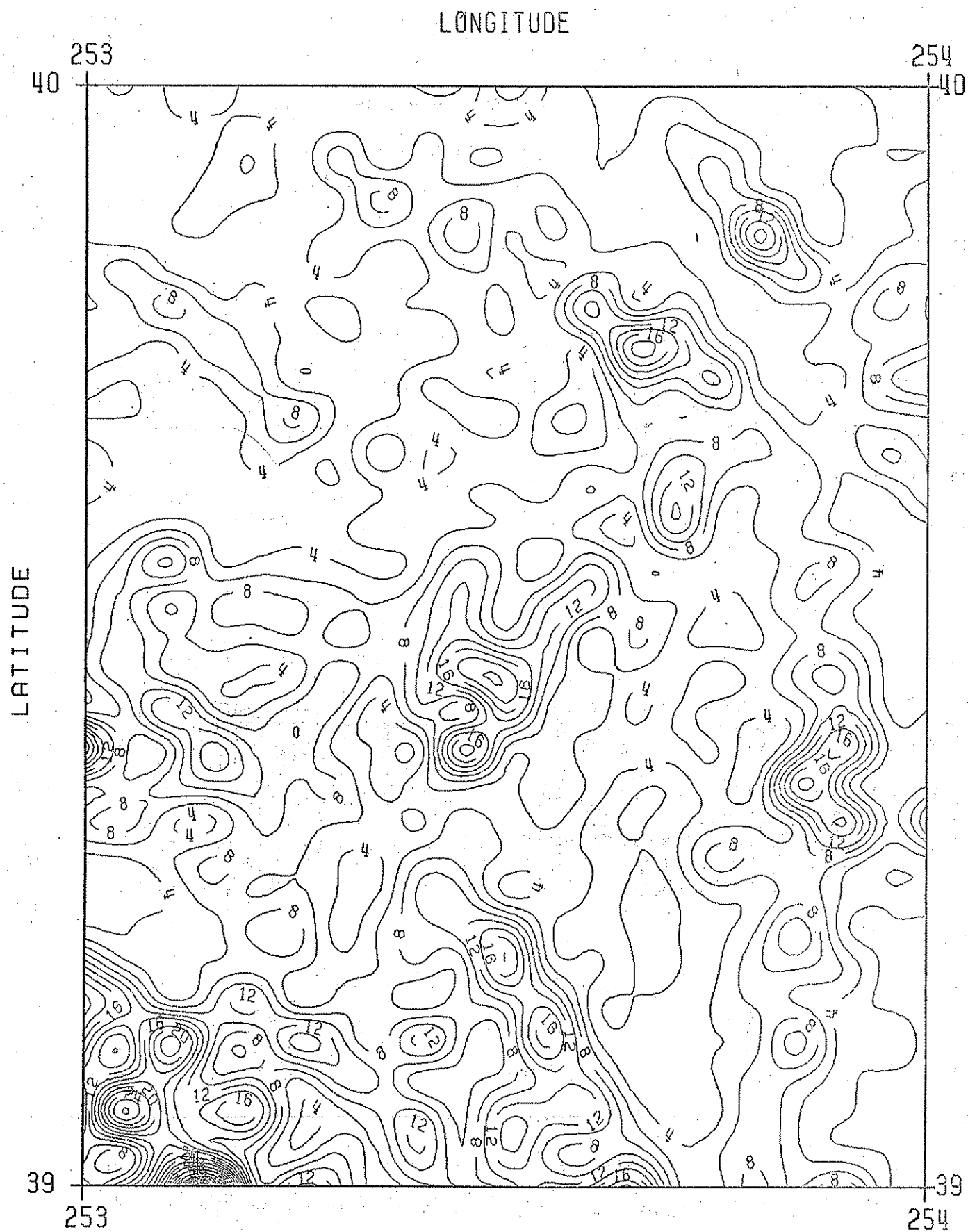


Figure 26 Terrain corrections in mgal for "Colorado I" 1°x1° block, computed on a 2'x3' grid. A topographic map of the same area is shown in Figure 12.

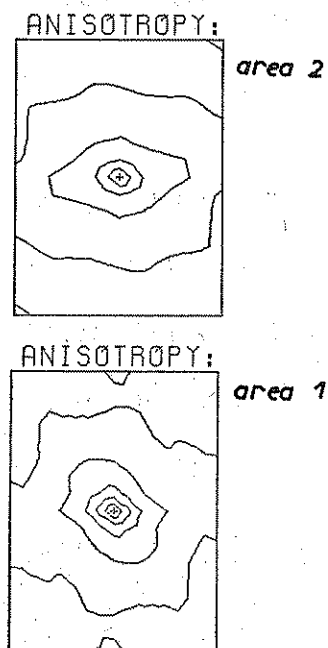
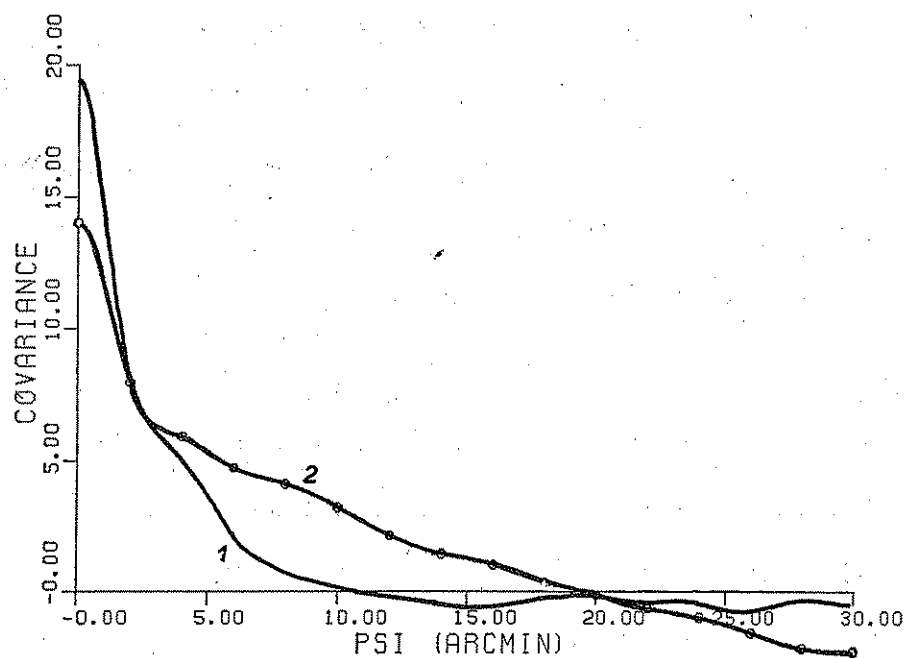
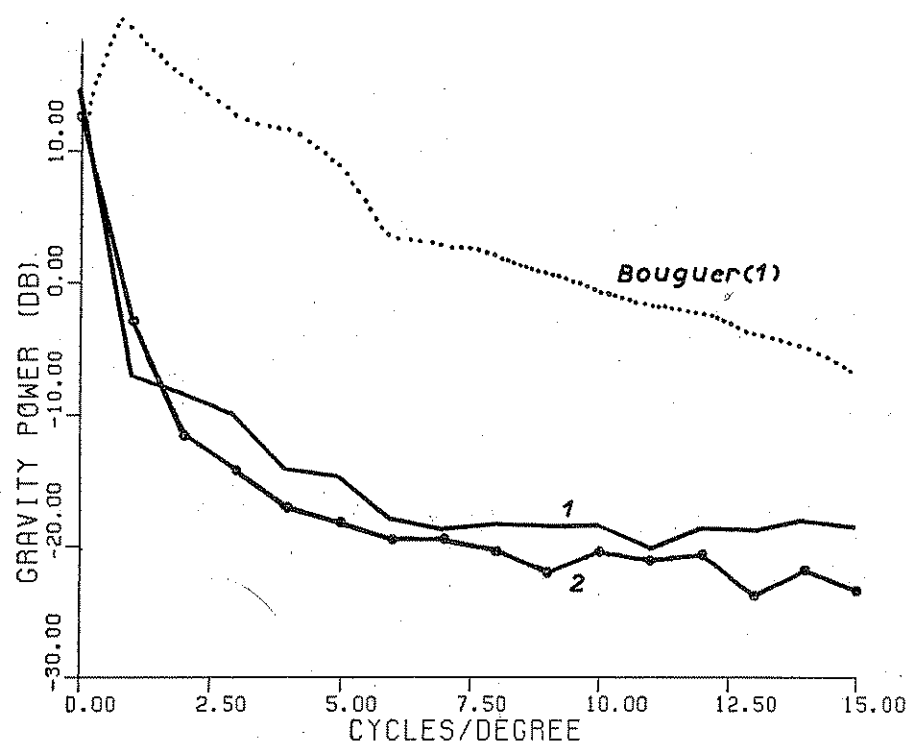


Figure 27 Power spectra and covariance function for the gravimetric terrain correction in two $1^\circ \times 1^\circ$ blocks of Colorado. The main terrain effect additionally shown with dots, cf. Figure 23.

Area	RTM Bouguer term (mgal)		Terrain corrections (mgal)			
	r.m.s.	$\chi_{1/2}$	mean	std. dev.	max	$\chi_{1/2}$
I (39-40° N, 107-106° N)	47.7	3.5'	6.4	4.4	55	1.8'
II (38-39° N, 108-107° N)	48.5	6.1'	4.8	3.7	29	2.4'
III (38.5-39° N, 106.5-106° W)	51.9	4.6'	6.4	4.4	27	2.4'

Table 5 Gravity terrain corrections, Colorado areas.

The obtained mean terrain corrections may be used to test Sünkel's approximate formula (cf. Section 7.2):

$$\text{mean terrain correction} \sim 3\pi G_D \frac{\sigma_h^2}{\chi_{1/2}} \quad (8.5)$$

For the three areas, values of 4.7 mgal, 2.8 mgal and 4.2 mgal are obtained.

The mean terrain corrections obtained by (8.5) are thus seen to be somewhat too low (this deficiency is primarily a consequence of the tendency of the topographic covariance functions to be exponential: for such covariance function the integral formula underlying (8.5) is undefined, cf. Sünkel, 1981a, p. 62).

8.3 RTM Geoid Effects - Colorado Area

When using a residual terrain reduction with respect to a 180x180 spherical harmonic elevation reference surface, the study of section 7.8 showed the terrain geoid effects to be fairly small. In this section, an example of actual magnitudes encountered in an extreme case - the mountainous part of Colorado - will be given. The 4°x4° block of Figure 22 - comprising essentially all of Colorado west of Denver - will be studied based on 4'x5' mean elevations.

Figure 28 shows the residual topography covariance function for the 4'x5' elevations. RTM geoid undulations were computed from this grid in a "fixed-area" reduction taking only into account the 4°x4° square. The geoid effects varied from 1 to -3 m with a mean of -80 cm and an r.m.s. variation of 87 cm with respect

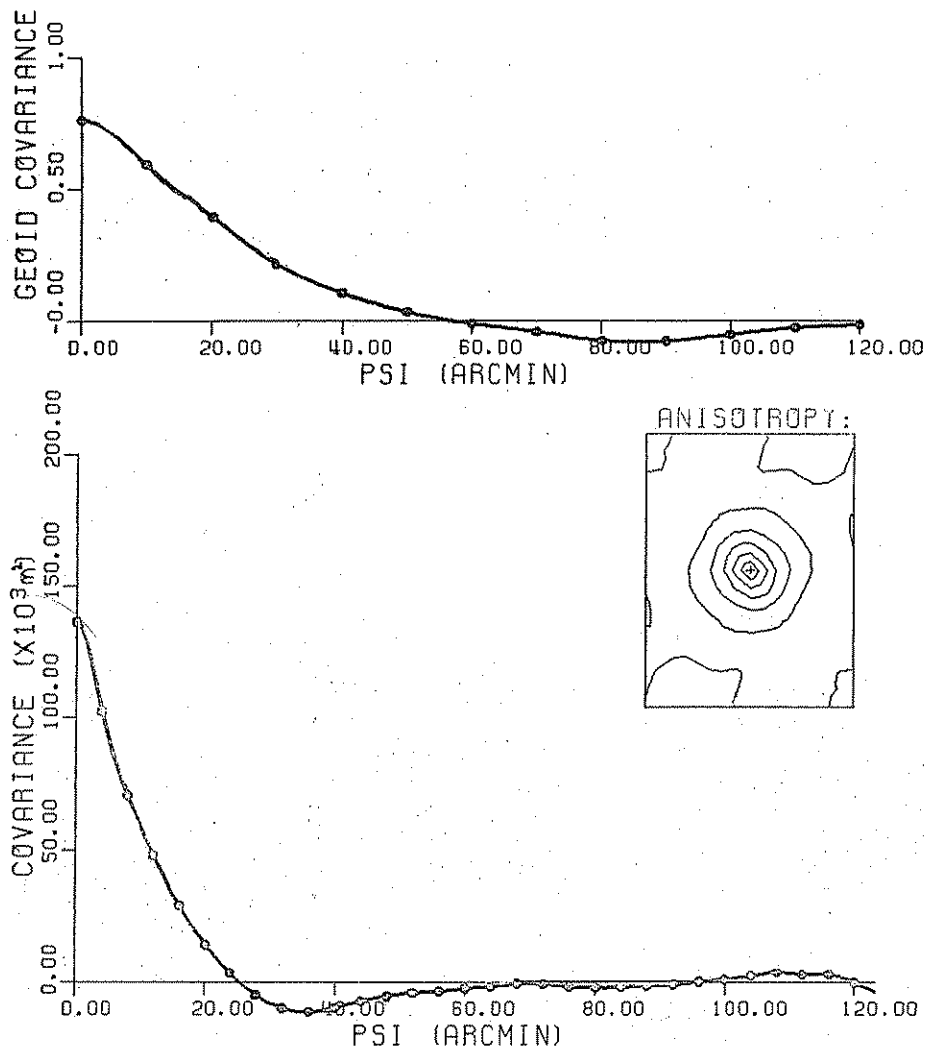


Figure 28 Covariance functions for residual topography (lower) and computed RTM-180 geoid effects (upper) for the mountainous part of Colorado. The 180x180 reference elevation surface is seen to give a good fit in Colorado, the height covariances being near zero for $\psi > 1^\circ$.

to the mean (Figure 29), corresponding to indirect effects on gravity anomalies below 1 mgal. For comparison, using the statistical study of Section 7.8, the elevation covariance parameters ($\sigma_{\Delta h} = 369$ m, $X_{1/2} = 8.4'$) yields an r.m.s. geoid variation of 66 cm, the slightly too low value being primarily due to the remaining small long-wavelength geoid effects, evident from Figure 28.

LONGITUDE

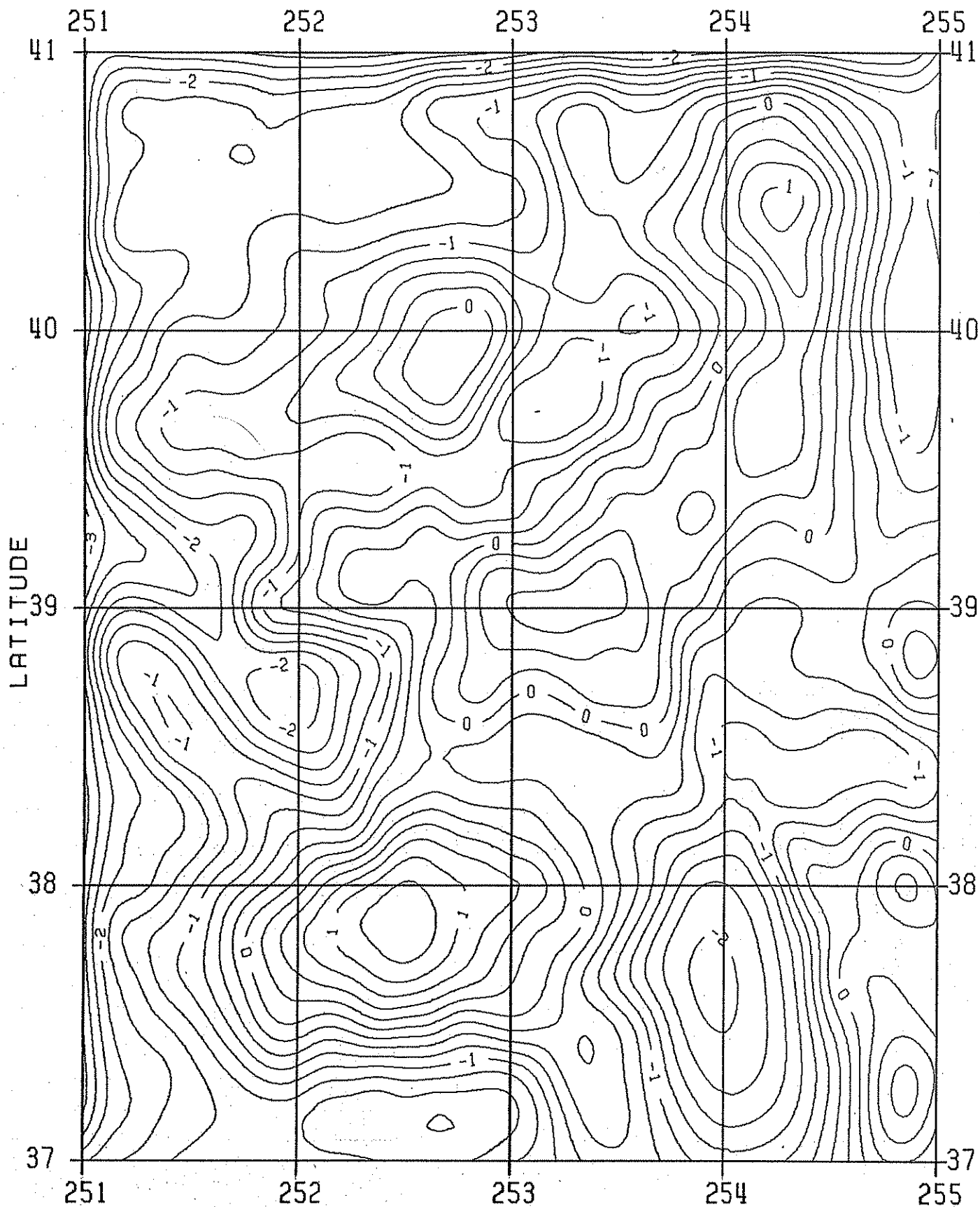


Figure 29 Residual terrain effects on height anomalies in the mountainous part of Colorado (elevation range 1300 - 4400 m). Countour interval 0.25 m.

9. Terrain Reductions: Spectral Characteristics and Covariance Functions for Local Gravity

By using known density anomalies in gravity field modelling, the purpose is to obtain a more smooth field, more suitable for interpolation and prediction. In this section the actual smoothing obtained using the residual terrain reduction will be studied for a number of U.S. sample areas, shown in Figure 22, each representing various types of topography and geologic setting: the 2°x2° Sierra Nevada block contains the highest part of the Sierra Nevada mountains plus a part of the California Valley, and is characterized by a large horizontal gravity gradient, relating to changes in crustal and upper mantle structures. The 4°x4° Colorado block has high mountains all through, and a thick crust giving rise to very low Bouguer anomalies. The 4°x4° New Mexico block has both mountains and plateau-type topography, and major density anomalies associated with the Rio Grande rift system. Finally, the 4°x4° Ohio area represents lowlands and an area geology of primarily thick paleozoic sediments.

The 4 areas have a reasonable coverage of terrestrial gravity anomalies in the NGS data base. To obtain covariance functions and power spectra of the data, the terrain-corrected Bouguer anomalies were gridded in a 4'x5' (ca. 7.5x7.5 km) grid, using a truncated collocation gridding algorithm (Cruz, 1983) where the value at a point is obtained from the 5 closest neighboring points (used subsequent to an initial thin-out screening, where only one data point per 1'x1' "pixel" was retained). An example of the obtained Bouguer anomaly grid is shown in Figure 30.

To obtain RTM-gravity anomalies, relating to a 180x180 spherical harmonic expansion, use is made of (7.5):

$$\text{RTM anomaly } \Delta g^C = \Delta g - \Delta g_{\text{RTM180}} = \Delta g - 2\pi G\rho (h - h_{\text{ref}}) + t_c \quad (9.1)$$

For local gravity field modelling, a 180x180 spherical harmonic gravity reference field corresponds as earlier mentioned to the RTM reduction. Thus, by (9.1) the terrain-reduced gravity anomalies, referred to a 180x180 reference gravity field,

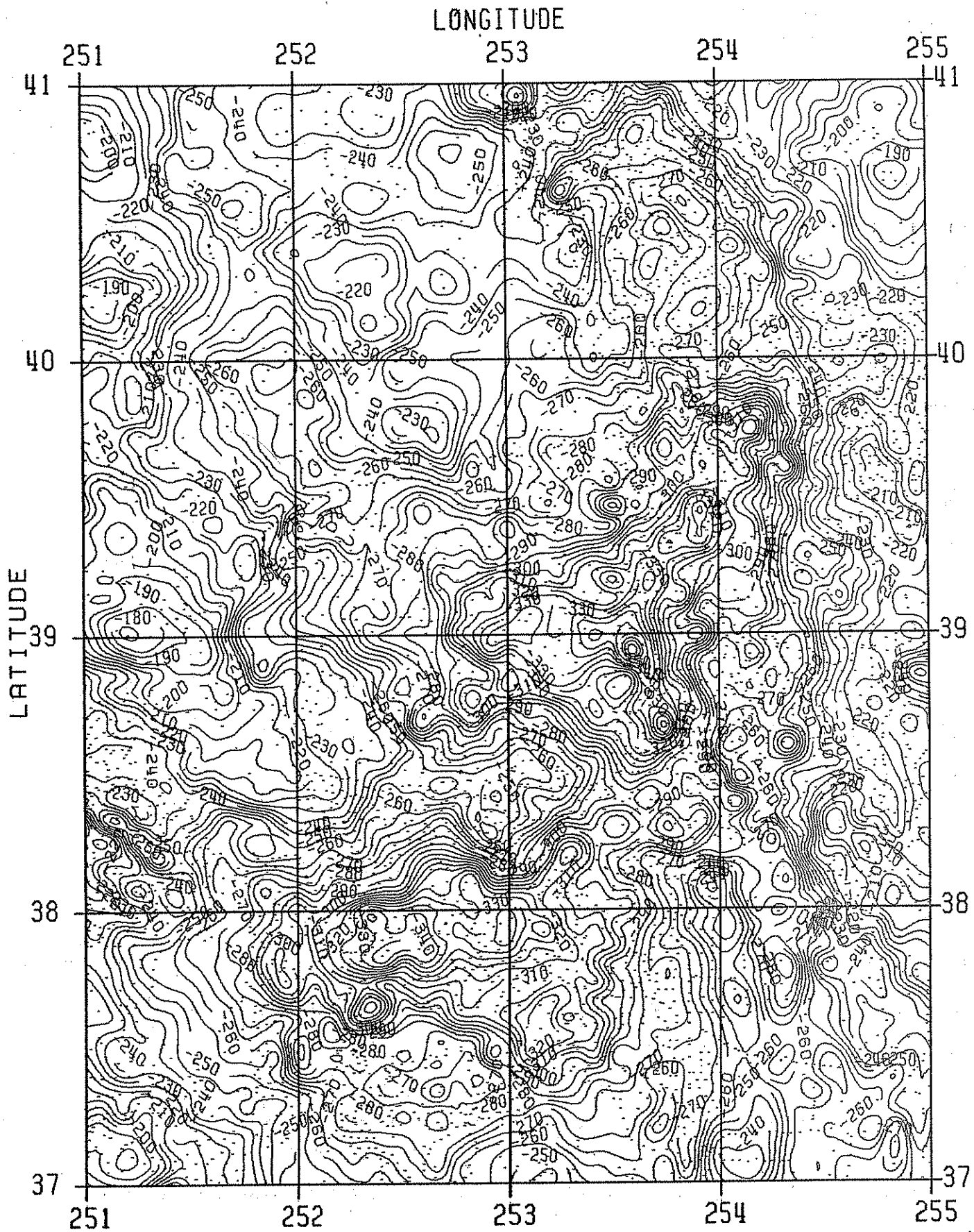


Figure 30 Bouguer anomalies in the Colorado block, shown with 5 mgal contours. Gravity station locations shown with dots.

is simply obtained by

$$\Delta g^{\text{residual}} = (\Delta g - \Delta g_{\text{ref}}) - \Delta g^{\text{C}} = \Delta g^{\text{Bouguer}} - \Delta g_{\text{ref}}^{\text{Bouguer}} \quad (9.2)$$

i.e. as the difference between the usual terrain-corrected Bouguer anomalies and the reference field Bouguer anomaly $\Delta g_{\text{ref}}^{\text{Bouguer}} = \Delta g_{\text{ref}} - 2\pi G \rho h_{\text{ref}}$, cf. Figure 31.

From the gridded, residual gravity anomalies, gridded free-air anomalies have been reconstructed by a simple "inverse" Bouguer reduction, neglecting the terrain correction, which - as demonstrated in section 8.2 - is small compared to the "main" terrain effect.

The data have been spectral analyzed using FFT, to obtain power spectra and covariance functions, as described in section 8. The power spectra have additionally been converted to normalized degree-variances, using the formula (7.54). This allows a comparison of the variability of the gravity field to global spherical harmonic degree-variance models, e.g.

$$\text{Kaula's rule: } \sigma_{\ell} \sim 0.7 \cdot 10^{-10} \frac{2\ell+1}{\ell^4} \quad (9.3)$$

$$\text{Tscherning-Rapp's model: } \sigma_{\ell} \sim 4.47 \cdot 10^{-10} \frac{1}{(\ell-1)(\ell-2)(\ell+24)} (0.999617)^{\ell+1} \quad (9.4)$$

see e.g. Moritz (1980). These models may be viewed as "average" earth models, and for a particular area they may be used as indications of the smoothness of the gravity field, compared to the global behavior.

An example of the obtained two-dimensional covariance function is shown in Figure 32, results are shown for Colorado in Figure 33 and for the other areas in Figure 34. Table 6 outlines the main statistical parameters, analogous to Table 4.

The results are seen to confirm what intuitively should be expected: in mountainous areas the use of terrain reductions significantly reduces the variance of the gravity field, especially for the shorter wavelengths, where the decrease

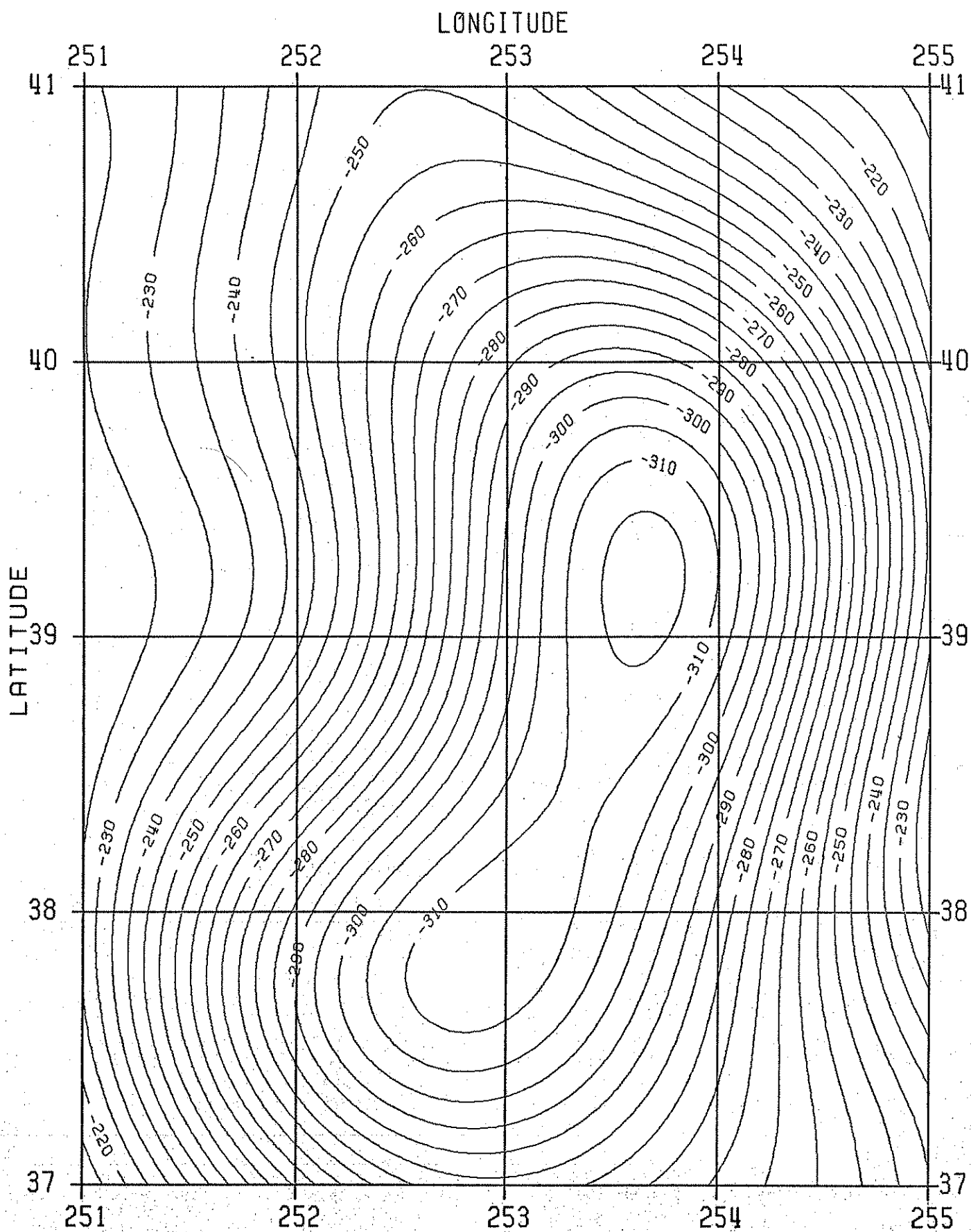


Figure 31 Spherical harmonic reference Bouguer anomalies in Colorado, obtained from gravity and topography expansions of Rapp (1981, 1982), complete to degree and order 180. Contour interval 5 mgal.

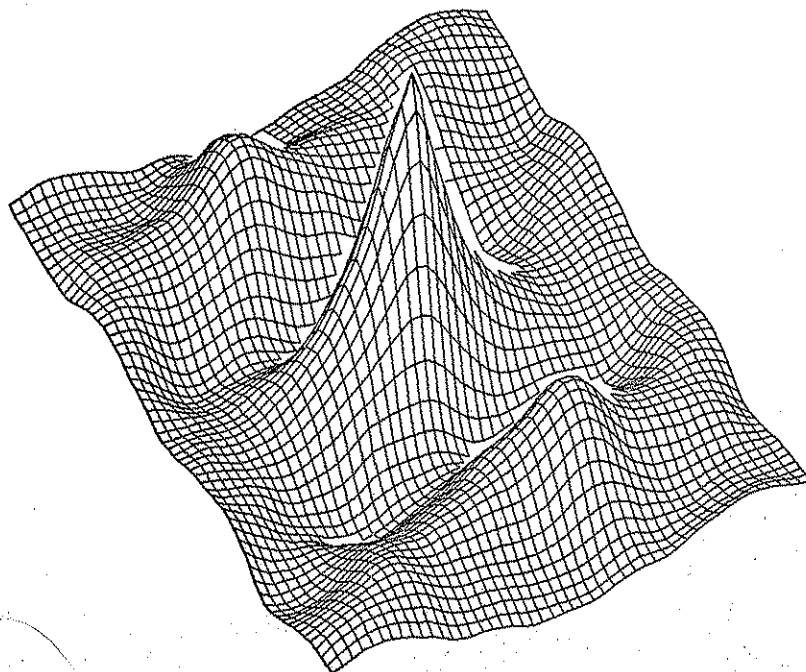
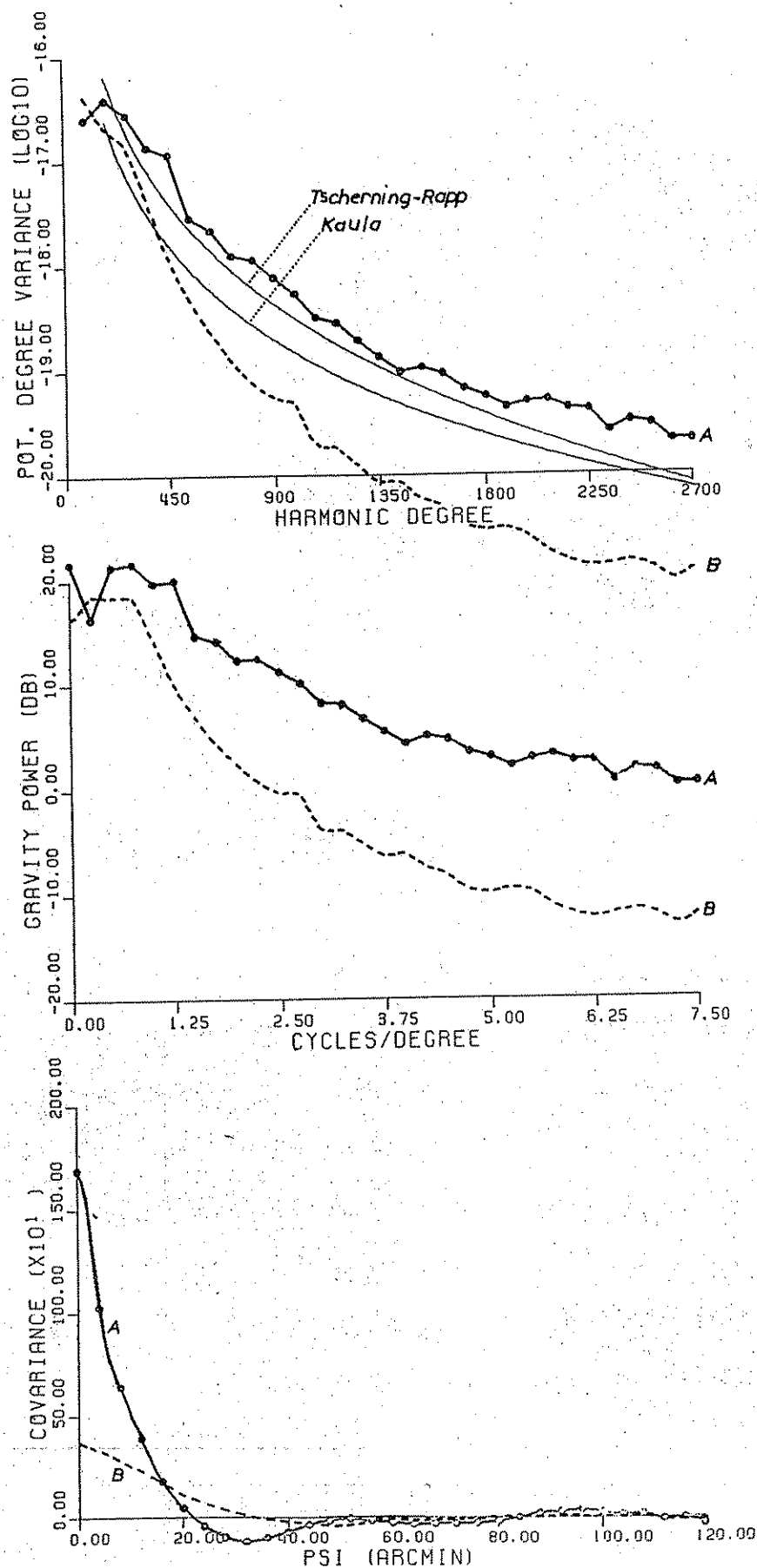


Figure 32 Two-dimensional covariance function for the Colorado block for terrain-reduced, residual gravity anomalies (argument interval: -2° to 2° in latitude and longitude).

in power in the present test areas is around 12 dB, corresponding to a factor of c.16 in power or 4 in r.m.s. variation. After reduction the spectra are fairly similar to the lowland gravity spectrum of Ohio, although they still contain somewhat more energy (this should not be too surprising, since mountainous areas naturally are areas of tectonic activity and thus large geologic density anomalies).

Also, the correlation length is seen to increase and the anisotropy seems to decrease significantly for terrain-reduced data, quite as expected. A typical correlation length for the RTM-reduced data seems to be around 15'.

Comparing to the global degree-variance models (which in principle also contains the effect of an "average" topography) the reduced gravity data lies significantly below in power for the higher wavelengths. This illustrates the general need for always "adapting" covariance functions to particular gravity field modelling



GRAVITY
LAT: 37.0 - 41.0
LON: 251.0 - 255.0
SPACING: 4.0' 5.0'

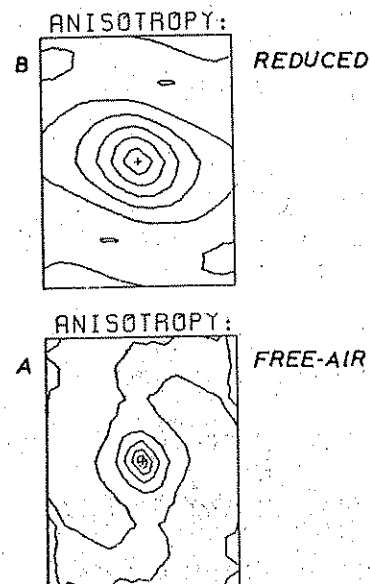
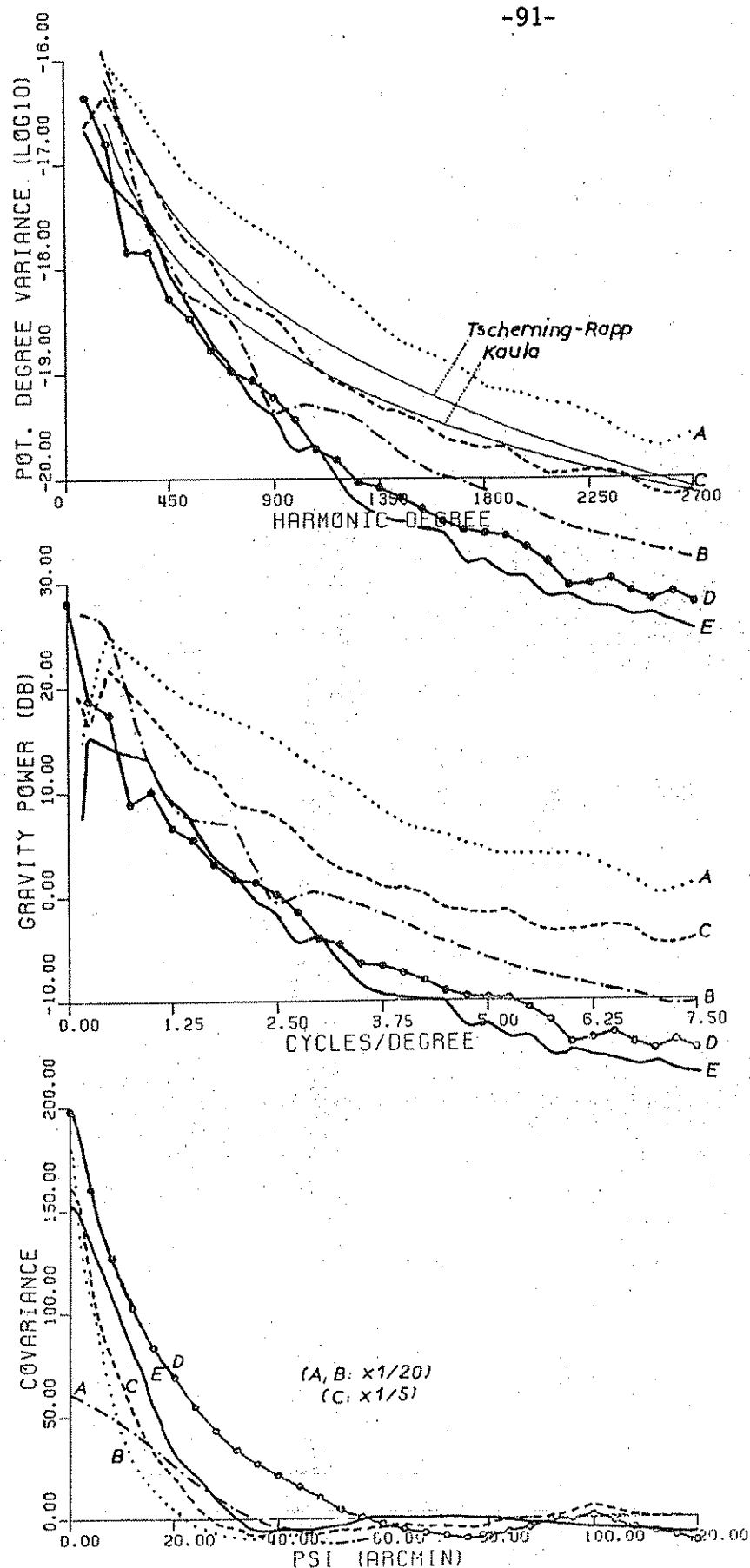


Figure 33 Degree variances, power spectra and covariance functions for terrain-reduced and unreduced gravity data in Colorado (180x180 reference field subtracted).



GRAVITY

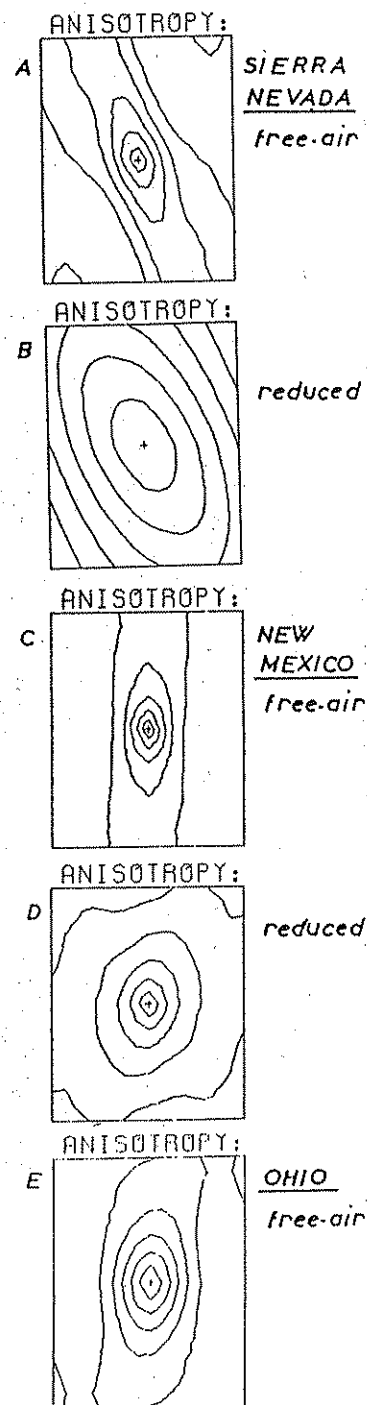


Figure 34 Degree variances, power spectra and covariance functions for gravity data for U.S. test areas. (Note: scale of anisotropy plots A and B are double the scale of C, D, and E.)

Table 6 Statistical Parameters for Gravity Data in Various U.S. Areas
(FA: without terrain reduction; BA: with Bouguer/RTM terrain reduction) Units: mgal

Area (lat. N, lon. W)	"Observed" gravity data		Residual gravity referred to 180x180 reference fields						
	mean	std. dev.	mean	C_0 (mgal ²)	$\sqrt{C_0}$ (mgal)	$X_{1/2}$ (arcmin)	$\sqrt{G_0}$ (E)	anisotropy index	
Colorado (37-41°, 109-105°)	FA	28.2	45.4	3.4	1688.4	41.1	5.3'	68	1.3
	BA	-253.0	33.2	1.8	365.9	19.1	14.1'	18	1.2
Sierra Nevada (36-38°, 120-118°)	FA	15.4	70.8	0.9	3628.7	60.2	5.6'	85	3.2
	BA	-162.7	73.2	13.6	1226.0	35.0	17.9'	23	2.0
New Mexico (32-36°, 109-105°)	FA	14.2	30.9	3.4	816.3	41.1	5.3'	40	1.8
	BA	-194.2	28.2	6.9	197.8	19.1	14.1'	15	1.3
Ohio * (38-42°, 85-81°)	FA	-13.2	16.7	0.1	153.0	12.4	13.2'	12	1.7
	BA	-42.8	15.4	0.1	152.3	12.3	12.9'	10	1.6

*For Ohio the Bouguer anomaly grid was constructed from 4'x4' gridded free-air anomalies.
The difference FA - BA for Ohio might therefore be somewhat under estimated.

area: the global covariance models must generally be modified to have less power at higher frequencies. For the free-air gravity data, only the New Mexico block is seen to be of fairly typical "global" type. This block is thus a good representative test area for gravity field modelling experiments.

The general conclusions of this section supports the results of the extensive study of North American gravity covariance functions by Lachapelle, Mainville and Schwarz (1983). That study, based on 5'x5' gravity data and using a completely different approach than here, shows parameters in good agreement with relevant parts of Table 6., e.g. for "block 11" of that study, covering most of Colorado, a free-air C_0 -value of 2071 mgal² is given, opposed to the 2061 mgal² obtained here. For the gravity gradient variance G_0 , the average for "block 11" is c. 1750 E² compared to 4620 E² of Table 6 for unreduced data, and c. 400 E² versus 324 E² for "terrain-reduced" data.

These G_0 -values are probably much too low, the spacing of the data being simply too large. An example: for the 2°x2° Colorado area 38-40° N, 107-105° N (which has a dense gravity coverage), a computation of G_0 based on 2'x2.5' data have yielded G_0 -values of 14100 and 1006 E² for unreduced and reduced data respectively - and by utilizing the topography results of Table 4, a 0.5'x0.5' data grid would be predicted to yield G_0 -values around 60000 E² for free-air anomalies! This shows, that the G_0 -quantity is nearly meaningless in mountainous areas - only combined with a suitable filtering through well-defined mean value operators or upward continuation do the second-order gradients have well-behaved statistical parameters.

10. Isostatic Reductions of Satellite Altimetry Data in Two Areas of the Pacific

Many of the features of the ocean bathymetry are of such dimensions, that use of a kind of "residual" terrain effect with respect to a 180×180 reference surface would simply miss the bulk of the geoid effects associated with these features. In this section, emphasis will therefore be on isostatic reductions and their relationship to geoid heights determined by satellite altimetry.

A recently released global bathymetric data set - SYNAPS - covering nearly all of the earth's oceans from 75° N to 75° S with $5' \times 5'$ mean depths, provides a very convenient data set for the computations of ocean isostatic geoid effects. As investigated in section 7.8, the resolution of the SYNAPS data allows ocean "terrain reductions" to be computed with r.m.s. errors at the cm-level. An example of the SYNAPS data is shown in Figure 35.

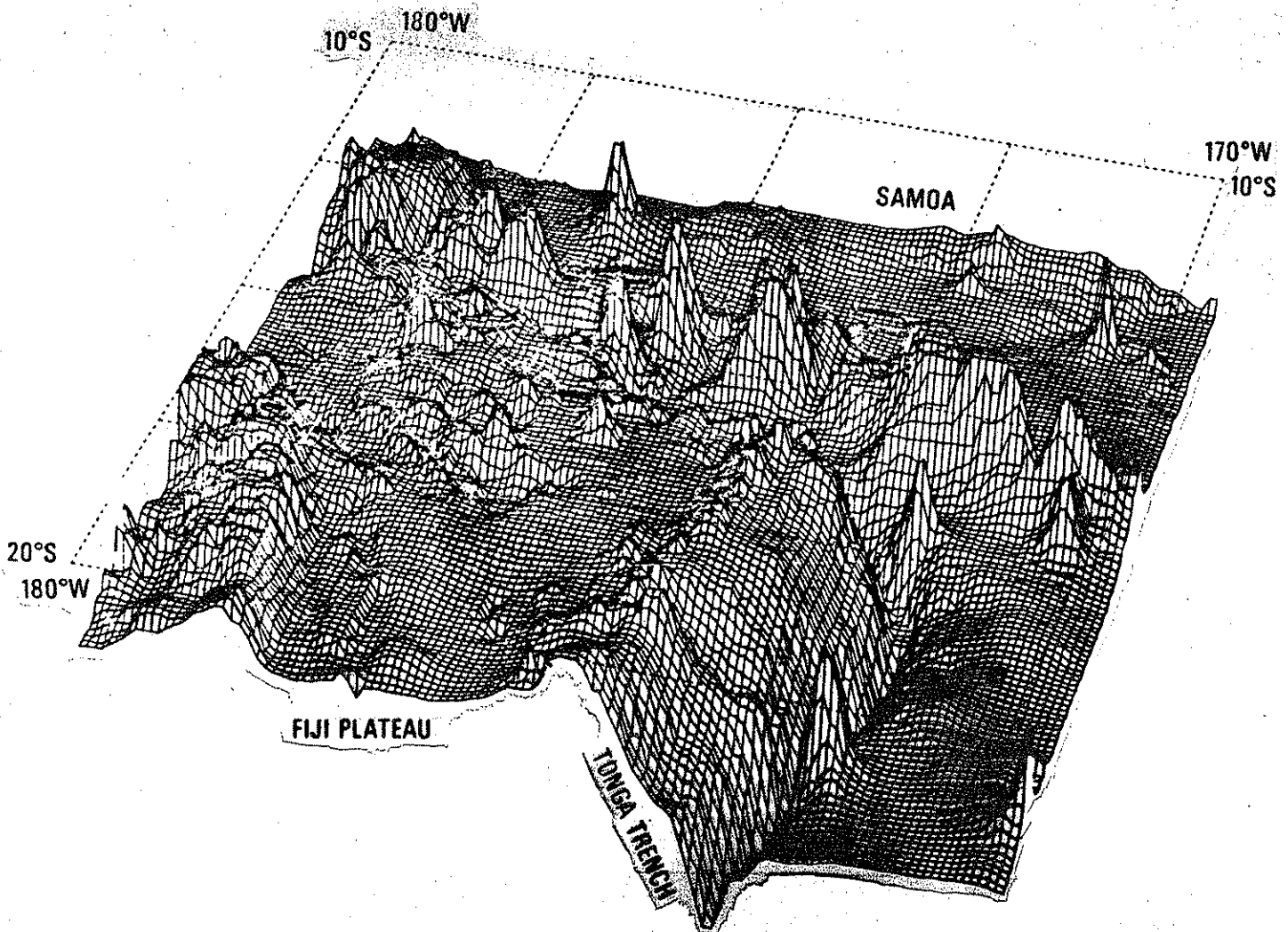


Figure 35 SYNAPS $5' \times 5'$ Bathymetry in the $10^\circ \times 10^\circ$ Tonga Block

The bathymetric data was used to compute isostatic geoid undulations by the "tc"-programme system for two $10^\circ \times 10^\circ$ areas of the Pacific:

"TONGA": a trench area of extreme bathymetry, shown in Figures 35 and 36.
and

"TAHITI": a mid-plate island area to the NE of Tahiti, shown in Figure 37.

For both these types of areas traditional Airy isostasy is expected to have limited applicability - especially for the trenches, where isostatic compensation is partially absent, and the existing compensating density anomalies occur at rather deep levels, associated with downgoing slabs etc. The failure of "traditional" isostasy at trenches is evident from a simple numerical consideration: for a normal crust thickness $T = 30$ km and density contrast of 0.6 g/cm^3 , commonly applied continental values, the isostatic mantle "anti-roots" will end above the ocean bottom at depths greater than 8000 m! Also, the implied average oceanic crustal thickness of 13-14 km is too thick by a factor of nearly 2.

Isostatic reductions are, however, very useful as an empirical mathematical tool, irrespective of whether or not the physical reality may be described by simple models. In the sequel, three simple types of isostatic compensation will be tested:

- A) conventional Airy isostasy, $T = 30$ km, $\Delta\rho = 0.6$ (With average oceanic depths around 4000 m, this corresponds to some degree to a mass plane condensation $T \sim 12$ km).
- B) a compensation in the upper mantle in depth ranges 20-60 km, described as a mass plane compensation at depth $T = 40$ km.
- C) compensation in deeper parts of the upper mantle and lithosphere, approximated by a mass plane compensation at depth $T = 70$ km.

For each of the areas, bathymetry will be taken into account for a fixed area extending 2° outside the $10^\circ \times 10^\circ$ area, i.e. for a $14^\circ \times 14^\circ$ area. By using such a fixed-area isostatic reduction, the computed effects will have a varying (arbitrary) bias. It is therefore only the variation with respect to the mean which is indicative of the "fit" of the isostatic models.

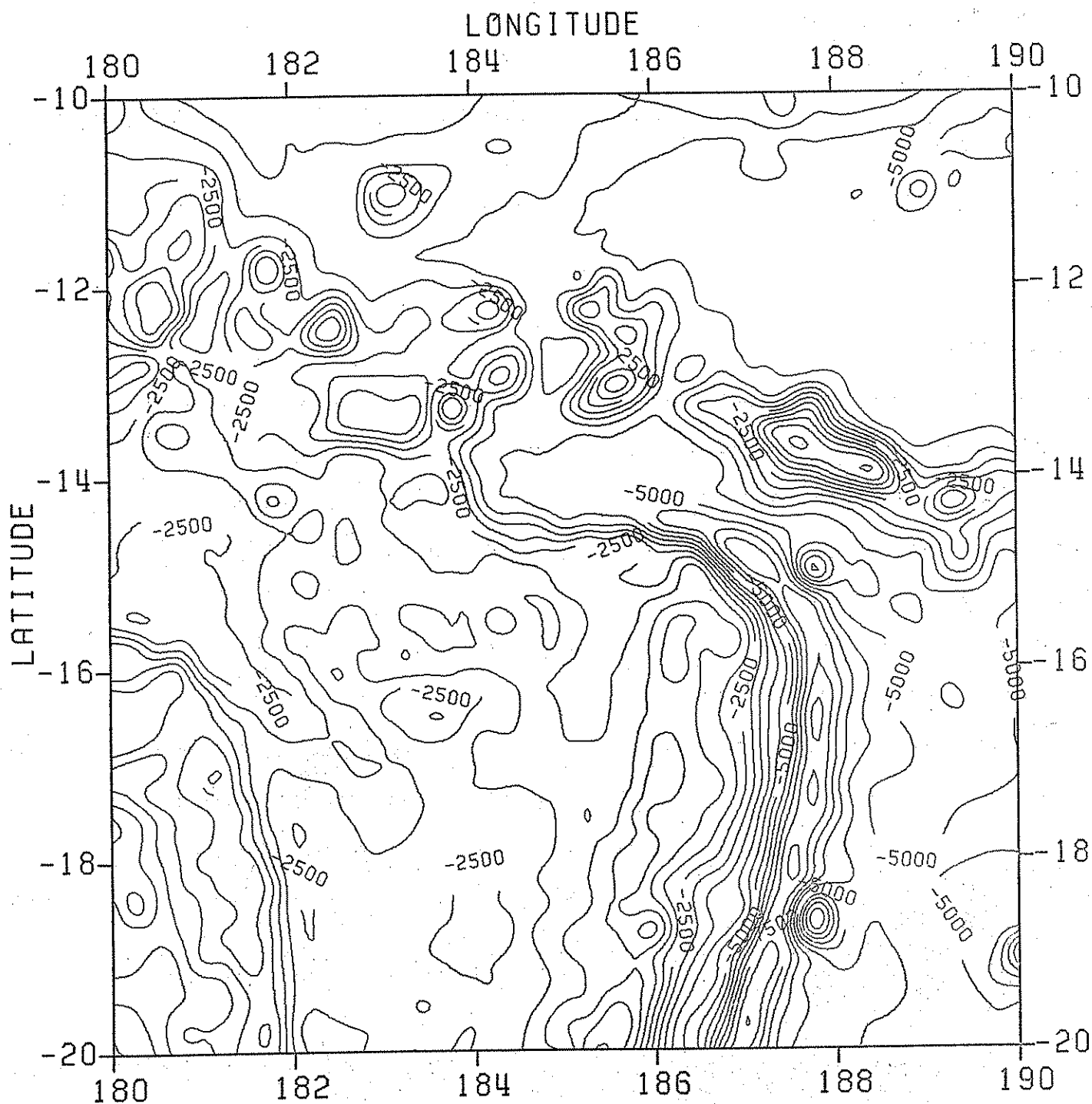


Figure 36 15'x15' bathymetry in the Tonga block. Contour interval: 500 m.

Geoid undulations for the two areas were derived from the combined SEASAT-GEOS-3 satellite altimeter data base, available at The Ohio State University (Liang, 1983). Sea surface heights with respect to GRS80 were identified with geoid undulations, and were gridded in a 15'x15' grid using the truncated collocation procedure (5 closest points), analogous to the gravity gridding of section 9.

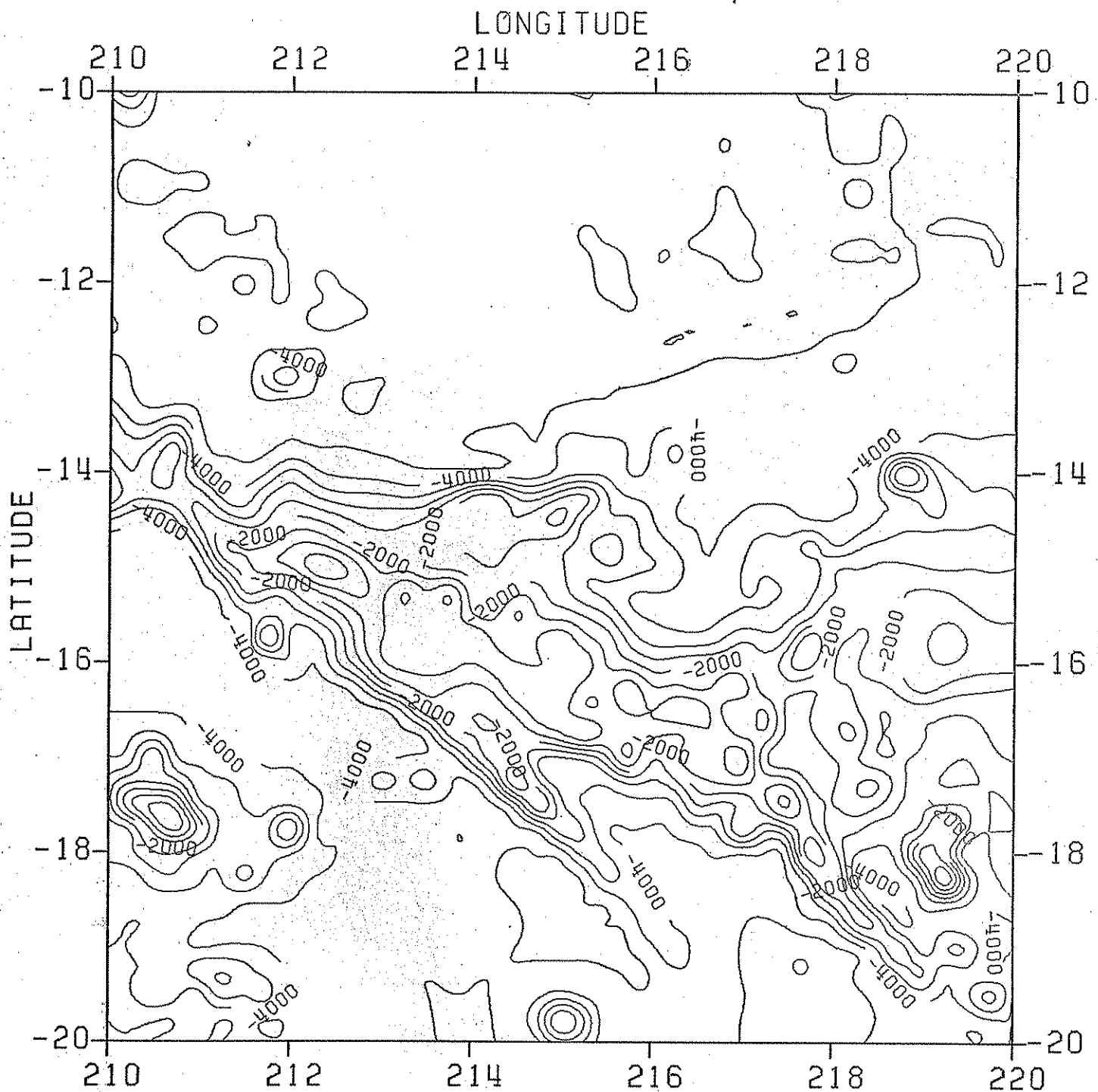


Figure 37 15'x15' bathymetry in the Tahiti block (Tahiti is in lower left and the Tuamotu Islands are in the center). Contour interval: 500 m.

The obtained altimeter geoids are shown in Figures 38 and 39. The correlation to the bathymetry is obvious in both cases, the Tonga Trench having e.g. an impressive asymmetric negative geoid anomaly of nearly 20 m, whereas the islands have associated positive geoid anomalies of some meters. Degree variances, power spectra

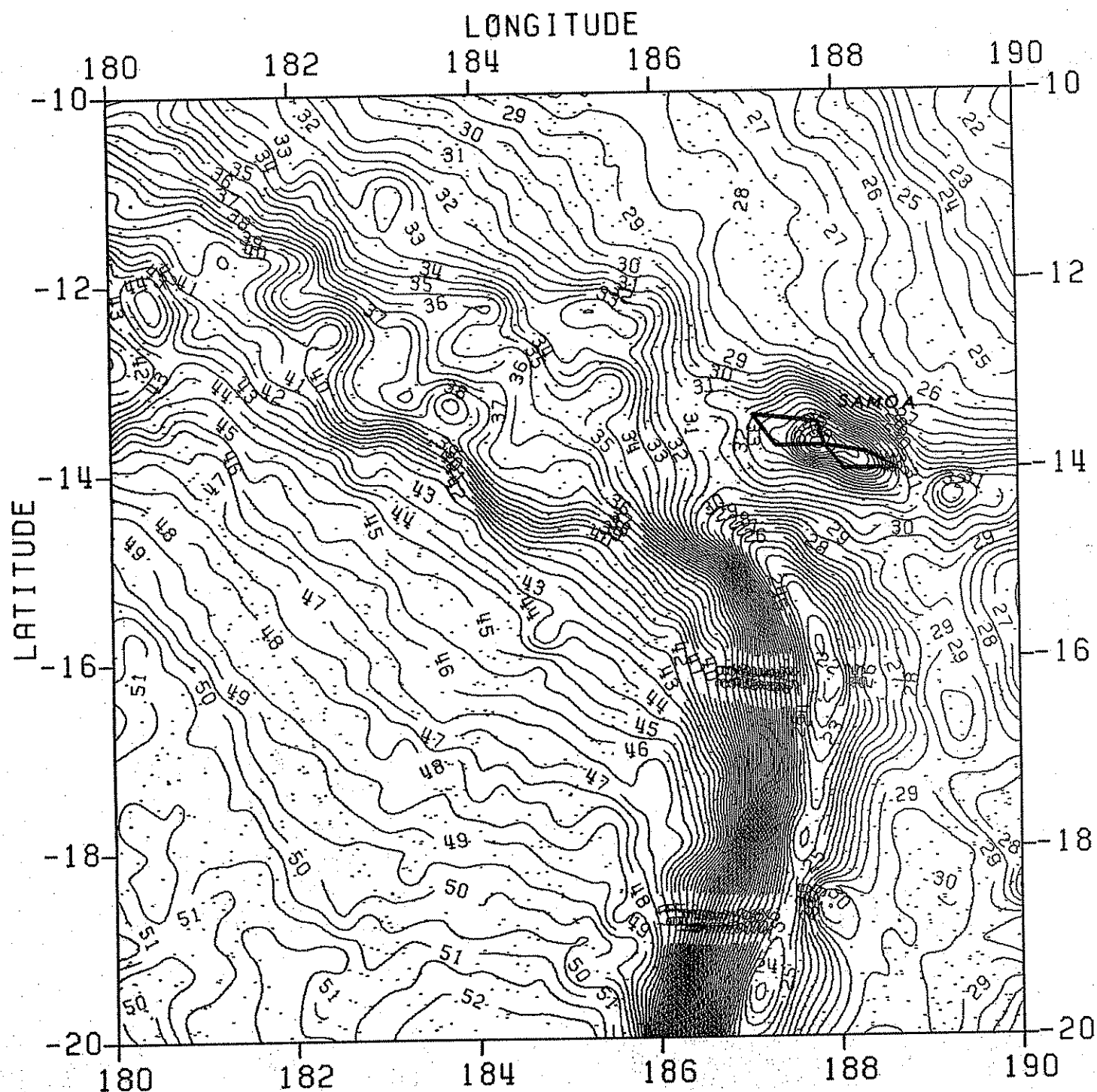


Figure 38 15'x15' combined SEASAT/GEOS-3 satellite altimetry geoid in the Tonga area, referred to GRS80. Contour interval 0.5 m. Altimeter sea surface height points used in prediction of gridded values shown with dots.

and covariance function for the geoids are shown later in Figure 47.

Topographic/isostatic effects computed from the "shallow" Airy isostasy (A), the intermediate depth compensation (B) and deep compensation (C) for the Tonga area are shown in Figures 40-42. From these figures it is seen that the trench

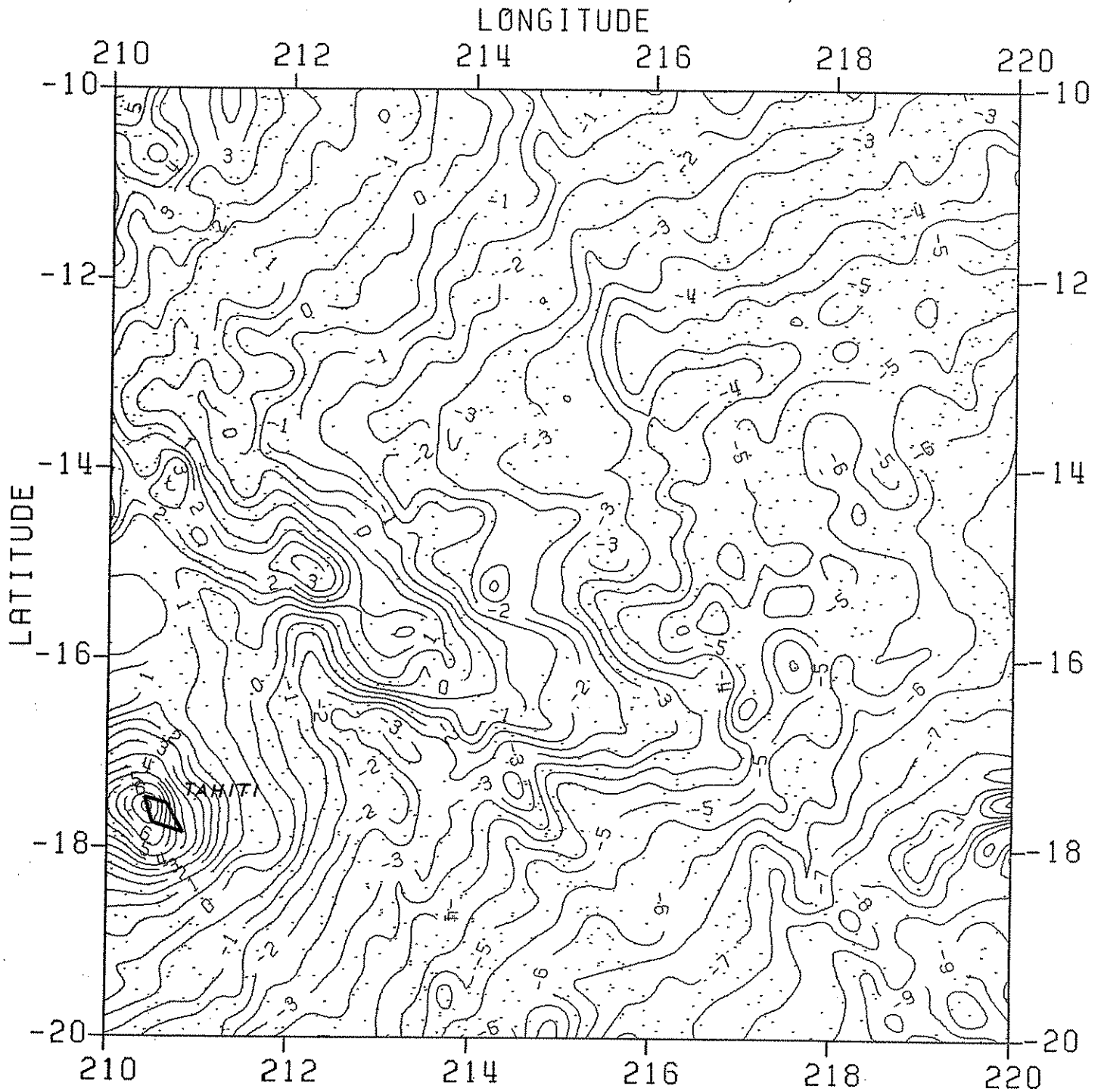


Figure 39 SEASAT/GEOS-3 altimeter geoid in the Tahiti block

itself is partially uncompensated, i.e. a very deep compensation level is needed to reproduce the large geoid anomaly across the trench. This is also shown in Figure 43. On the other hand, some features (e.g. most of the islands) seem to be compensated at much more shallow levels. There is therefore no simple general isostatic principle which is applicable in this area.

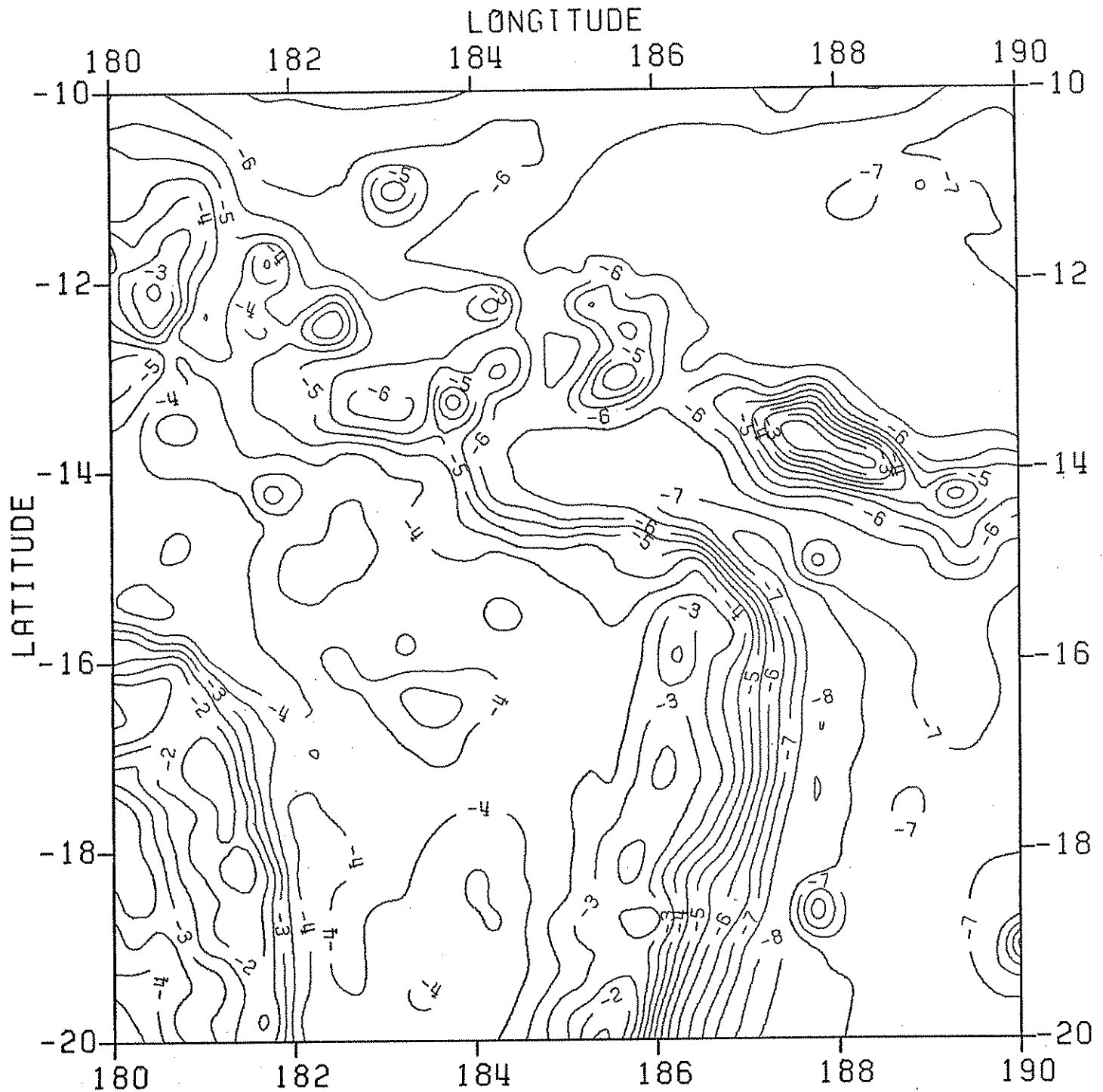


Figure 40 Isostatic geoid "A" in the Tonga area, conventional Airy isostasy (power spectra and degree variances shown in Figure 47)

For the Tahiti block, an example of an isostatic geoid, derived from the bathymetry is shown in Figure 44. By comparing to the satellite geoid (Figure 39), it is seen that the central Tuamotu Islands area is well represented by the conventional

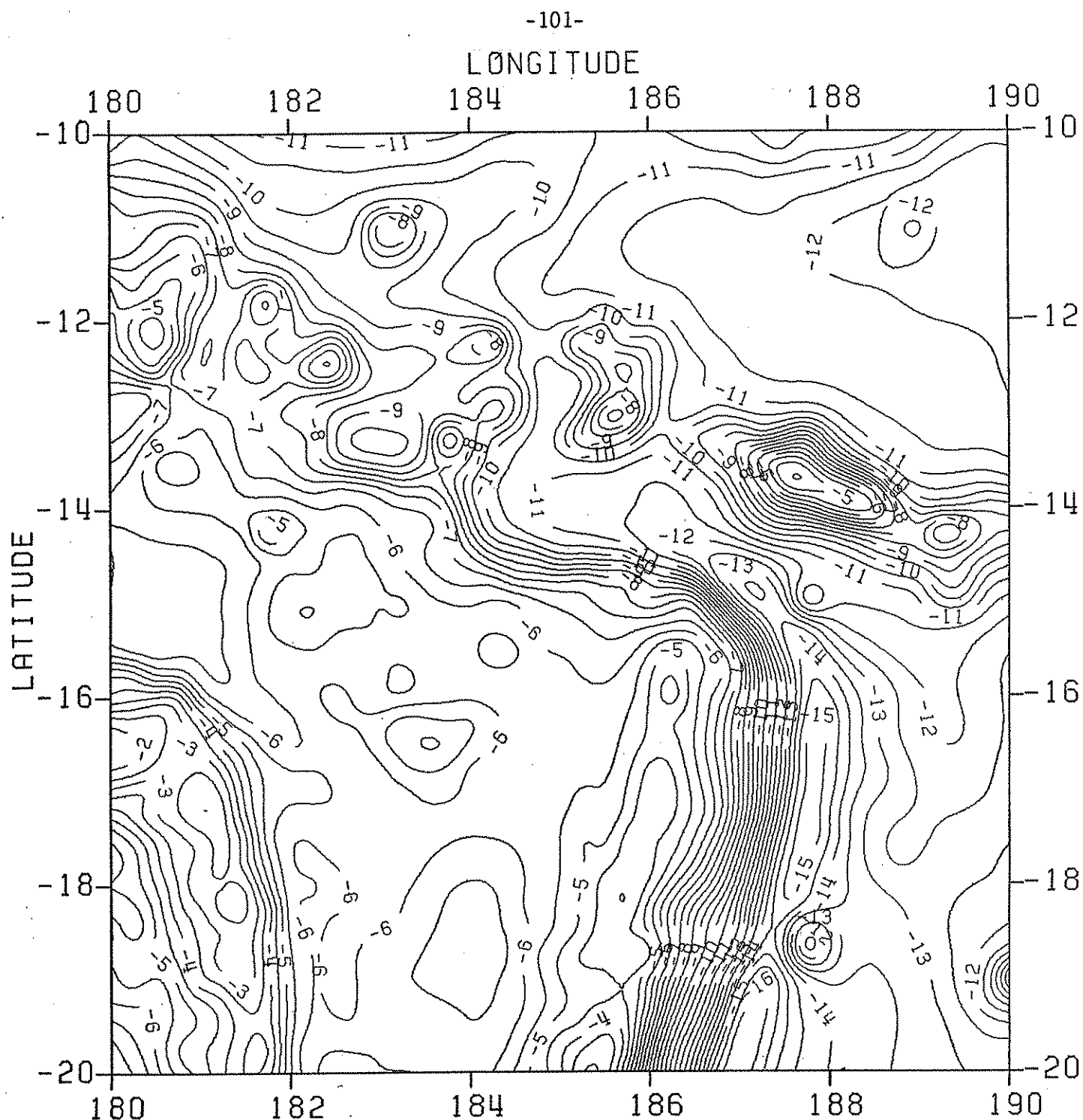


Figure 41 Isostatic geoid "B" in the Tonga area (mass plane compensation in depth 40 km)

Airy isostasy, while the smaller Tahiti islands apparently are compensated at deeper levels (Figure 45), or - rather - is partially uncompensated. By subtracting the computed isostatic geoids from the altimetry geoids, smoother "terrain-reduced"

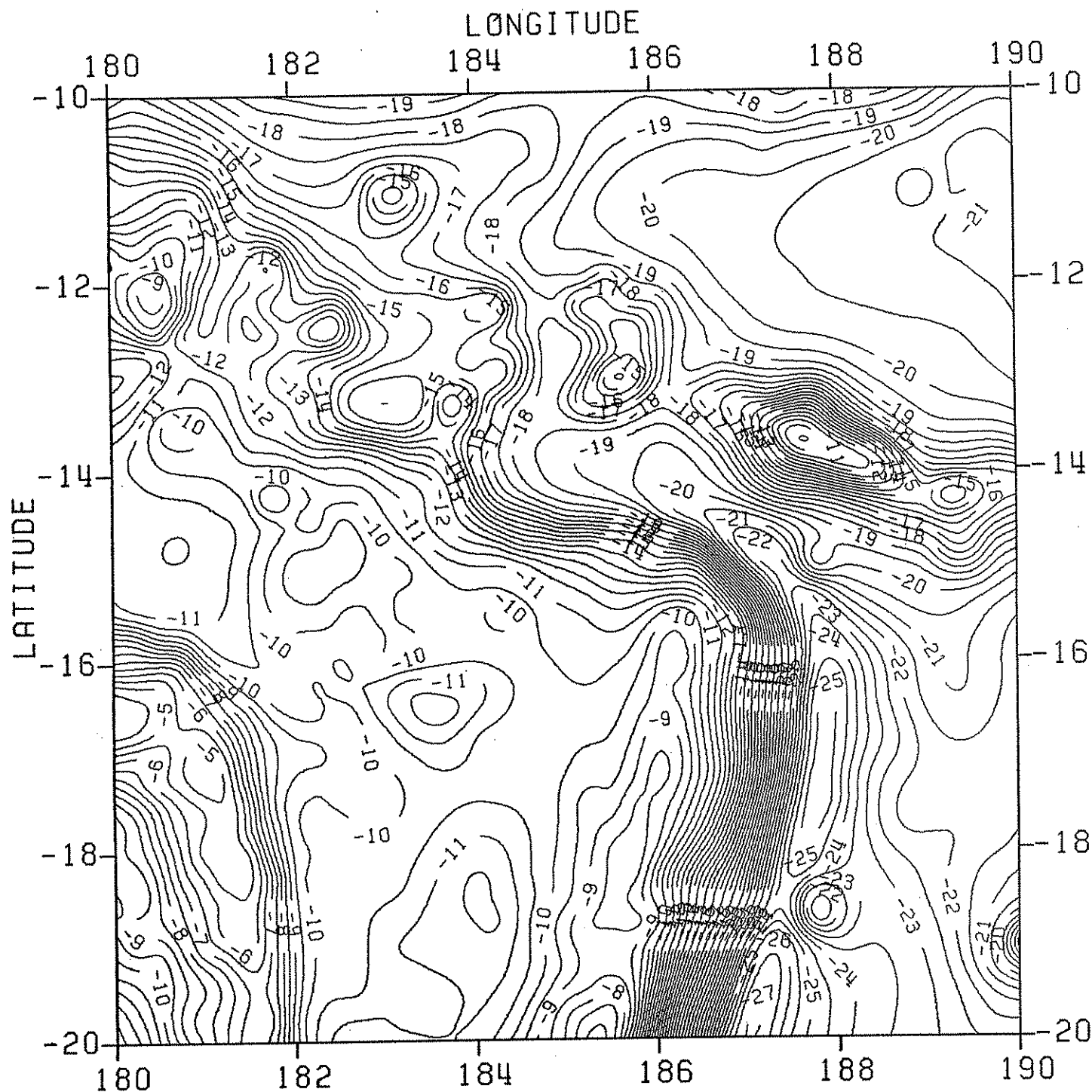


Figure 42 Isostatic geoid "C" in the Tonga area (mass plane compensation in depth 70 km)

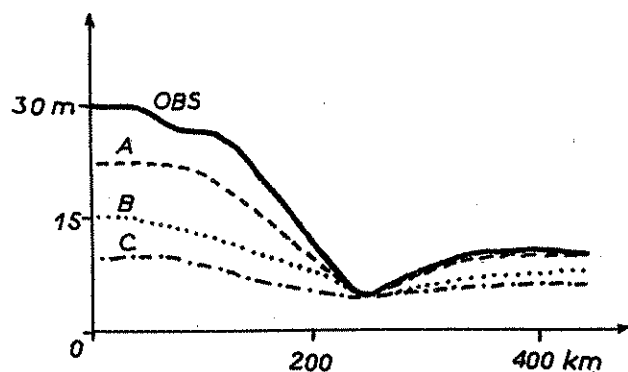


Figure 43 Interpolated observed sea surface heights and computed isostatic geoid profiles across the Tonga trench in a W-E profile at 18° S (arbitrary bias).

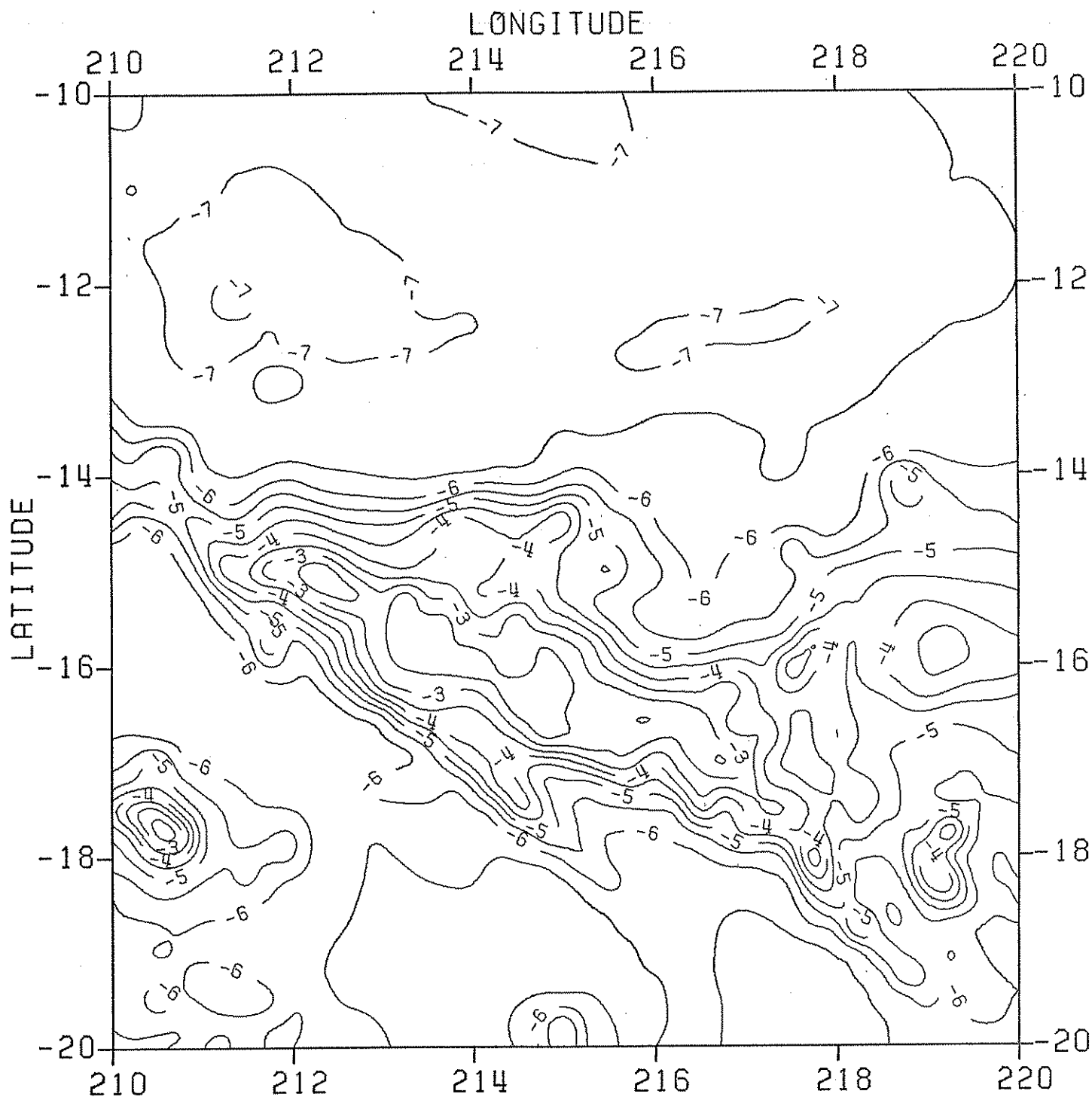


Figure 44 Airy isostatic geoid ("A") in the Tahiti block. (Power spectrum and degree variances shown in figure 47).

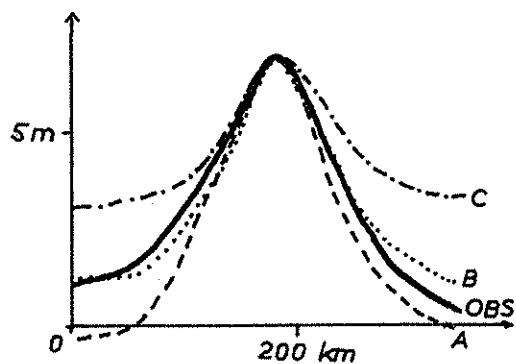


Figure 45 Satellite altimetry geoid undulation in an N-S profile across Tahiti (lower left of area) at longitude 210.5°, and computed isostatic geoids.

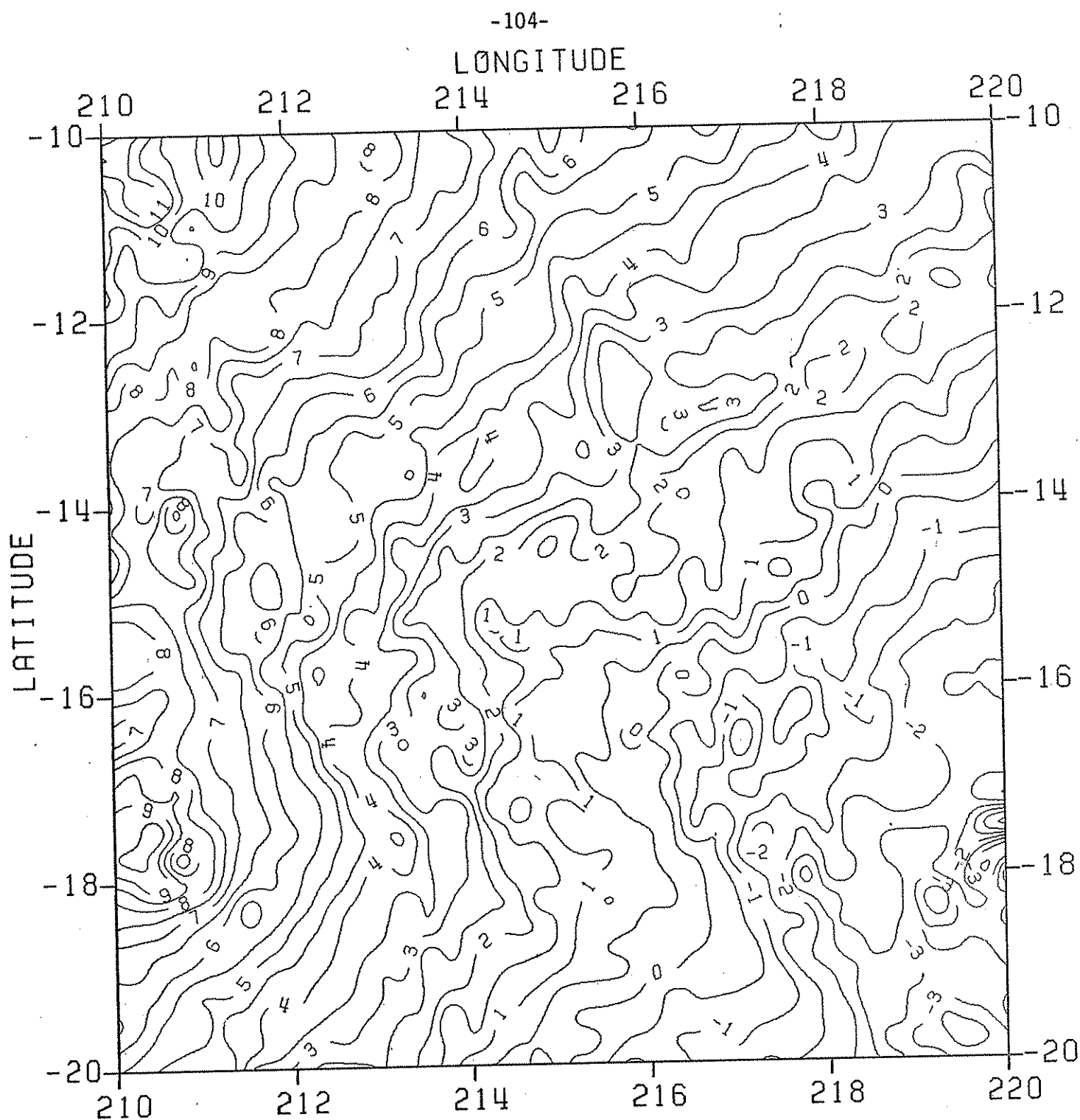


Figure 45 Isostatically reduced altimetry geoid in the Tahiti area. Airy isostasy ("A").

geoids are obtained (Figure 45). Statistics of these residuals are shown in Table 7. Since the geoid itself is dominated by long wavelength trends, uncorrelated to the bathymetry and probably originating in the deeper mantle, the comparison has also been done against a "high-pass" filtered geoid, obtained by subtracting the GEM9 spherical harmonic expansion (complete to degree and order 20) from the altimeter geoids.

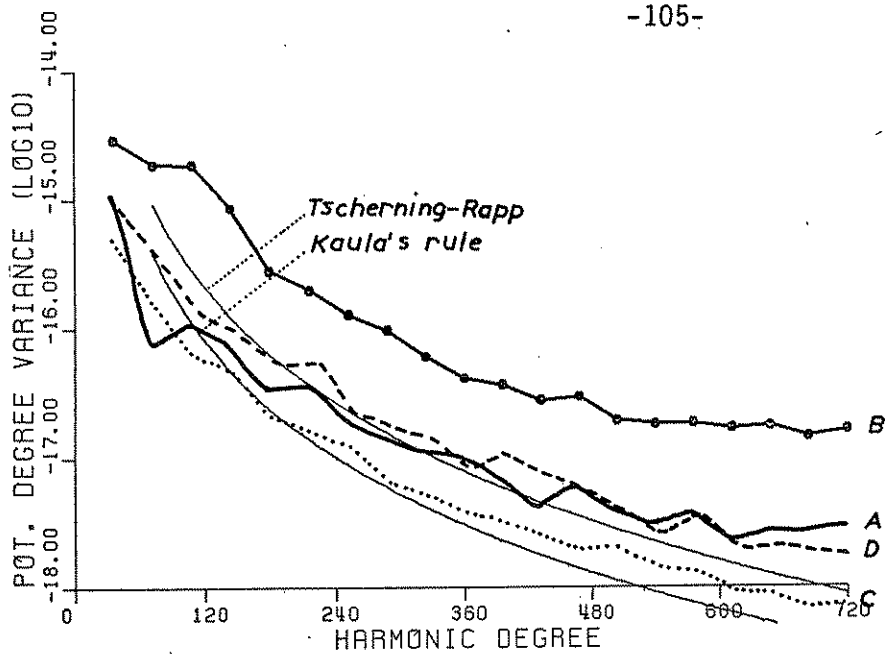
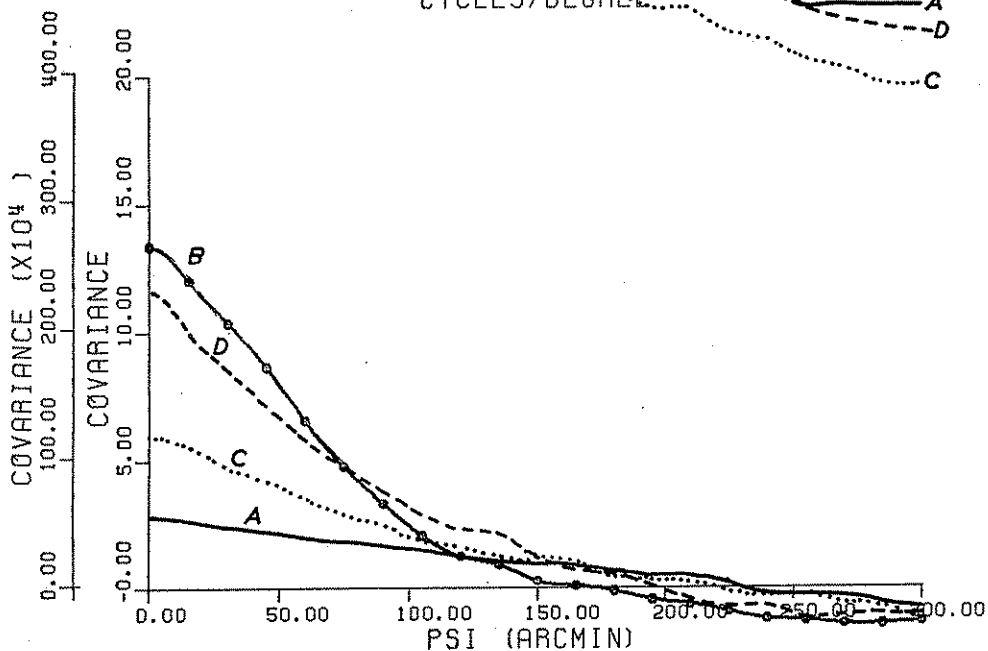
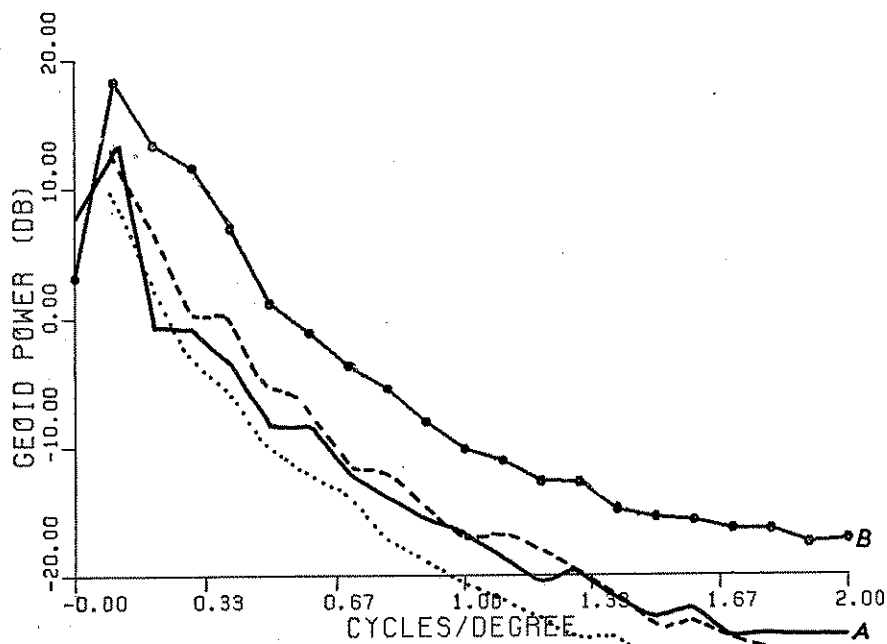
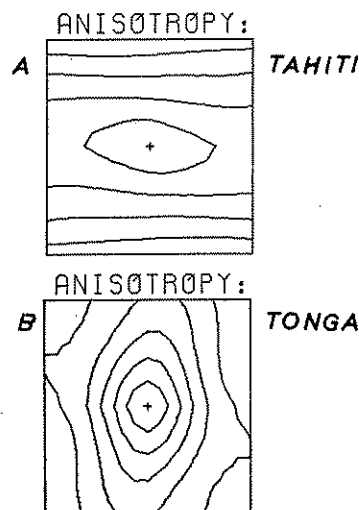


Figure 47 Degree-variances, power spectra and covariance for the satellite altimetry geoid (minus GEM9) and iso-static geoid effects (conventional Airy isostasy) for the two $10^\circ \times 10^\circ$ areas of the Pacific. Covariance functions C and D are for the bathymetry directly (left scale on abscissa).



GEOID - GEM9



BATHYMETRY

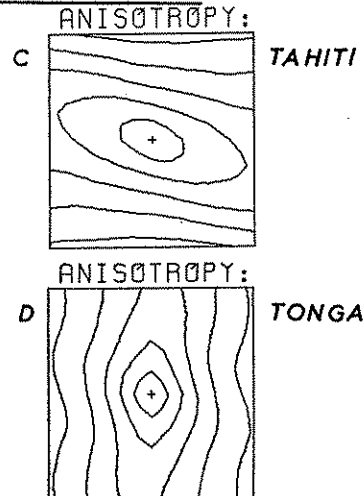


Table 7 Geoid undulation variation for various isostatic reductions.
(A: T = 12 km, B: T = 40 km, C: T = 70 km, massplane comp.)

Area	Geoid	Geoid Variation mean std. dev.		Isostatic Geoid std. dev.			Reduced Geoid std. dev.		
				A	B	C	A	B	C
TONGA	Altimetry	37.61	9.34				7.93	6.59	4.84
	Alt.-GEM9	-0.18	3.60	1.61	3.12	5.17	2.91	2.97	4.21
TAHITI	Altimetry	-2.80	3.15				3.41	4.00	4.82
	Alt.-GEM9	-0.19	1.69	1.18	2.16	3.49	1.04	1.23	2.28

By inspecting the numbers of the table it is seen that the "smoothing" effect of the terrain reduction is not very marked, and it is apparently mainly related to the shorter wavelengths (alt.-GEM9). However, by inspecting the isostatic geoids and comparing them to the "actual" geoid, it is clear that many features of the ocean geoid are essentially nothing but bathymetric/isostatic effects, but they do not show up very well in the statistics because the geoid signal is dominated by effects from deeper sources (cf. Figure 47). Also, error sources such as orbit errors, sea surface topography and errors in SYNBAPS might play some role.

From the statistics there seems to be a slight favorization of the conventional Airy isostasy, in spite of the obvious deficiencies for the trench (this would be a good case for utilizing a "geologic" density anomaly model, e.g. a dipping slab). For global studies, the geoid anomalies observed over trenches carry a very high weight due to their magnitude, and when solving for "optimal" compensation depths somewhat too deep levels might be obtained.. A recent global study by Rapp (1982) suggests for the "best" Airy-isostasy a compensation depth of 50 km rather than the conventional 30 km, a probable effect of the trenches.

The primary purpose of this section of the report has been to demonstrate the practical use of the SYNBAPS-bathymetry data for ocean geoid studies. The

primitive approach taken here should be improved for future studies, and of particular interest would be to utilize the global coverage of the data to make a comprehensive analysis of global oceanic isostasy, e.g. through the use of empirical bathymetry (geoid transfer functions), classifying different tectonic ocean areas. Results of such an analysis could then be used for the important "inverse" problem - to determine bathymetry from satellite altimetry in unsurveyed areas.

11. Summary and Conclusions

In the present report, many different topics have been treated. In spite of the somewhat diverse composition, I hope that the reader still has felt some kind of continuity in the contents - the idea was to provide the general background of gravity field modelling using topographic/geologic information, stress the similarities to and possible uses of geophysical inversion methods, stress the practical benefits of using spherical harmonic reference fields and then finally go into details on terrain reductions and provide the theoretical background for the FORTRAN programme published with this report.

In the first part of the report (sections 2-5), the necessary theoretical background was outlined, including the concept of density anomalies. Opposed to physical densities, density anomalies attain both positive and negative values. In spite of the basic ambiguity of potential field theory, it is still very meaningful to work with density anomalies, even without having defined the "normal" density distribution explicitly: it may simply be taken as an average "expected" geophysical model.

Known density anomalies - topography, isostasy, geology etc. - may be taken into account by a "remove-restore" technique. Then values of anomalous density etc. are assumed to be known. For unknown densities, geophysical inversion methods may be used to provide better models of geologic structures or to provide

"optimal" density anomaly values, e.g. finding a best density for terrain reductions. Furthermore, it was outlined how the "ultimate" combination of generalized inversion and gravity field modelling by collocation in principle could be done, to allow incorporation of e.g. "non-gravity" geophysical information in gravity field modelling. In the second part of the report (sections 6-7), emphasis was on terrain reductions. Formulas for the gravity field around the rectangular prism - the natural "building stone" when elevations are given as digital terrain models - were given and evaluated. The basic "types" of terrain reductions were then reviewed:

- Bouguer reduction, removal of the visual topography
- Isostatic reductions, removal of the visual topography and the isostatic compensation
- Residual reductions, removal only of the short-wavelength, "noisy" topography

The terrain correction, frequently treated in the literature, should not be viewed as a terrain reduction, but rather just as an important mathematical auxiliary quantity. The programme "TC" - given in the appendix - may be used to compute any of these types of reductions for gravity, deflections and height anomalies. The development and implementation of "TC" represents the bulk of "practical" work associated with this report.

For error studies and FFT-methods, an approximative terrain reduction formulation - the "linear approximation" - plays a key role. The accuracy of the approximation was investigated both for a theoretical model and for actual data, with the conclusion that the approximation is usually acceptable. However, care should be exercised in alpine areas, especially for deflections of the vertical.

Assuming the validity of the linear approximation, effective FFT-methods for terrain effect computations were outlined, and finally a key topic - DTM resolution requirements - were studied. Curves were given to compute r.m.s. errors for terrain effects for gravity, deflections and height anomalies, based on spacing of the given elevations and on topography covariance functions.

Finally in the report, empirical data were investigated, to give actual empirical information on

- topography covariance functions for various types of areas (they turned out to be generally exponential)
- magnitudes of terrain corrections
- magnitudes of RTM geoid effects (they are actually so small that the indirect effect on gravity anomalies may be neglected)
- degree of smoothing obtained using terrain reductions for actual gravity data (as expected variance decreased, correlation length increased and anisotropy was diminished)
- relationship of altimetry derived ocean geoids to geoids computed solely from bathymetric data (including bathymetry covariance functions).

The main empirical results - covariance functions for topography and gravity - are contained in Figures 23-24, 33-34 and Tables 4 and 6.

Unfortunately the duration of the author's stay at The Ohio State University was too short to allow the implementation and practical evaluation of some key topics of the report. Therefore, natural extensions of the present study would be

- implementation of hybrid geophysical inversion/collocation, with test in an area of well-known geology with large density anomalies, e.g. a salt-dome province, shelf area, etc.
- implementation of a "hierarchial" FFT terrain effect computation system, with comparison to results e.g. obtained by "TC" in a suitable test area.

Other directions for future research could be the extension of the analysis of the covariance functions for topography and gravity, to include more regions of different types. Ideally, a classification of "covariance provinces", based e.g. on existing geographical landscape classification systems, could be attempted.

The availability of the global detailed bathymetric data set SYNBAPS opens as just mentioned possibilities for extensive studies of the relationship between the ocean geoid and the bathymetry. Ocean isostasy could be studied for many types of areas through (FFT) cross-covariance analysis. With the results it could then e.g. be possible to design optimum filters to derive the bathymetry

from satellite altimetry in poorly surveyed areas. Another application would be to "enhance" geoid variations not associated directly with bathymetry, such as isostatic geoid anomalies being obviously of great interest for geophysicists.

APPENDIX

TC - A Program for General Terrain Effect Computations

The terrain effect computations mentioned in the present report have been done using the Fortran Program "TC", outlined in the sequel. This program - which is written in structured Fortran (FORTRAN 77) - has been developed and implemented at the Amdahl system at The Ohio State University, and has been tested against "synthetic" topography (cones, cylinder segments) and results from an older, somewhat different ALGOL program at the Danish Geodetic Institute.

The program uses a set of digital terrain models (DTM's) to calculate gravity, deflections of the vertical or height anomalies at specific points, using the formulas of the rectangular prism, outlined in section 6.1. Four different mass model types may be specified: topography, topography and isostatic compensation, terrain corrections or residual terrain effects. The computations may either be done out to a certain distance R, or a specified fixed area may be taken into account. A fixed density of 2.67 for the topography ($h > 0$) and 1.64 for the bathymetry ($h < 0$) is used presently, but it may be changed easily in the start of the program. For the isostatic compensation, an Airy isostasy with Moho density contrast 0.4 g/cm^3 and normal crust thickness 32 km is used, in accordance with accepted "best" continental values.

The curvature of the earth is taken into account to the second order, through the use of the "super elevation".

$$\text{SUPELV} = \frac{1}{2} \frac{s^2}{R_{\text{earth}}}$$

which gives the z-shift of a prism in distance s below the tangential plane at the computation station S. This approximation is valid for distances up to several thousand kilometers. The superelevation is also utilized for terrain corrections, so for very large computation radii terrain corrections must be combined with

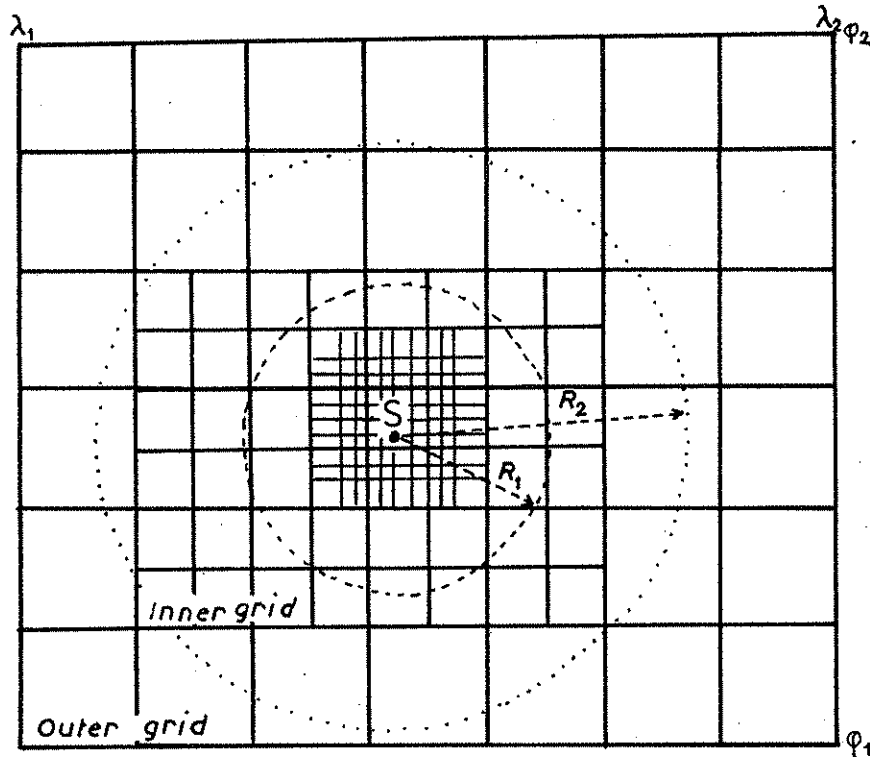


Figure 48 The use of the two DTM's in "TC" terrain effect computations. Elevations from the detailed inner grid is used in the outlined rectangle covering the circle of radius R_1 , centered at the computation point S , the coarse grid being utilized outside this rectangle. In the inner-most 3×3 grid elements (the "inner-zone") the digital terrain model may be densified using a bicubic spline interpolation.

the spherical Bouguer plate formulas rather than just the plane formula ($2\pi G_p h$) to give the complete topographic effects.

Two digital terrain models are ordinarily used for the terrain effect computations in "TC" (although both are not necessary). A detailed grid (say $1 \text{ km} \times 1 \text{ km}$ point elevations) is used out to a computation distance R_1 , and then a coarse grid (say $10 \times 10 \text{ km}$ mean elevations) is used for the remaining "remote zones", see Figure 48. A distance specification R_1 of the order of magnitude twice the outer grid spacing is usually sufficient. In addition to the "detailed" and "coarse" DTM, an additional reference DTM must be specified for residual terrain reductions. This DTM is used together with a parabolic hyperboloid (bilinear) interpolation scheme to define the mean elevation surface.

Each DTM must be stored in a separate file, for which a simple standard format is used. A DTM file is initiated by a

Label: $\phi_1, \phi_2, \lambda_1, \lambda_2, \Delta\phi, \Delta\lambda$ (REAL*4)

defining the coverage and grid spacing of the DTM, followed by the

Elevations: $h_1, h_2, h_3, h_4, \dots$ (INTEGER*2)

scanned in west to east stripes, starting from the north. Each "stripe" is one record. The first elevation in the sequence is thus the NW-point, the last the SE-point. The limits of the DTM ($\phi_1, \phi_2, \lambda_1, \lambda_2$) is specified by geographical coordinates of the outer limits of the rectangular grid "compartments" (viewed as mean elevations), see Figure 47. Thus for point elevations, half the grid spacing must be added/subtracted from the limits to get the correct limits for the label.

For the inner grid, an alternative NGS format may be used. This format, used for data obtained from the National Geodetic Survey, consists of 0.5'x0.5' point elevations, partitioned in 7.5'x1° blocks each containing 1800 elevations, the blocks stored sequentially as

ϕ, λ (REAL*4), $h_1, h_2, \dots, h_{1800}$ (INTEGER*2)

where (ϕ, λ) specifies the SE-point of the block.

The program demands the inner and outer grids to be consistent, that is, the outer grid spacings must be multipla of the inner grid spacings, and the gridlines of the outer grid must be grid lines also in the inner grid (ideally the outer grid should be simple averages of the inner grid). If this is not the case the program will terminate with an error message. This will also happen if too small arrays are available for storing elevations. (The program only stores elevations for the smallest possible area internally, but the dynamic storage is done common for all stations to save time and I/O transfers. It will therefore be advantageous

to "block" the computations, reducing widely separated station groups in different runs).

Each grid "compartment" and its elevation defines a rectangular prism, the effect of which is summed up to give the complete terrain effect. The shift between exact and approximative prism formulas is automatic, defined through the ratio distance to prism/grid spacing, cf. Figure 7. The speed of the program may be increased by reducing this ratio ("R2EXAC", "R2MACM" in subroutine "PRISM1"), however at a price of degraded computation accuracy. The values used in the program represent a reasonable trade-off, determined from Figure 7 and practical experiments.

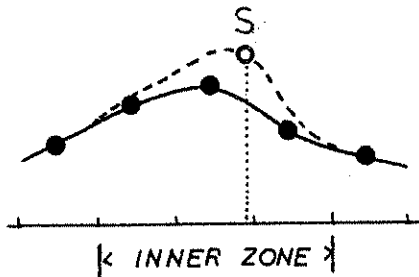


Figure 49 Spline interpolation of elevations in an inner zone and possible modification to give the "correct" elevation at computation point s.

The "innermost" topography, surrounding the computation point, is of critical importance for both gravity and deflections. Through an input variable "IZCODE" it is possible to govern how the inner zone (3x3 elements, cf. Figure 48) is taken into account. For stations at altitude no special actions will usually be needed (IZCODE 3), otherwise the elevations are interpolated using a bicubic spline interpolation to dense, non-equidistant inner-zone grid, used for summing up inner-zone effects. When a station is known to be on the earth's surface and has a given elevation, a discrepancy between the "model" elevation and actual elevation at S is unavoidable. For deflections and undulations this discrepancy is unimportant, and the terrain effect should be computed at the "model" elevation (IZCODE 0 or 2). For gravity, however, the topographic or RTM-effects are correlated directly

with the model elevation, so in this case the terrain model should be modified to reproduce the elevation of S (IZCODE 1). This modification is done smoothly within the inner-zone (Figure 49), assuming the discrepancy to be due to erroneous (biased) DTM elevations. Since the physical mass model is changed independently for each individual station, some care should be exercised when using this option, especially for large values of the DTM grid spacings.

In the sequel the programme is listed, more detailed information may be found in the introductory or "en-route" comments. The programme is modular constructed, with subroutines "TC" giving effect in one station, "DTC" effect for one grid compartment and "PRISM 1" giving prism formulas. Station input/output should be modified (in the beginning of the program) to satisfy the particular needs of the user. Typical computation times at the OSU Amdahl system is around 4-5 points/second. An input example is given at the end of the program listing.

[illegible]

```

C FIL, F12, LA1, LA2  FIXED MAXIMUM AREA FOR WHICH TER-
C RAIN EFFECT IS COMPUTED, IRRESPECTIVELY OF THE
C SPECIFIED COMPUTATIONAL RADII.
C
C R1  MINIMUM COMPUTATION DISTANCE OF INNER GRID (METER).
C THE INNER GRID IS ACTUALLY USED IN THE SMALLEST
C 'SUBSQUARE' OF THE COARSE GRID, COVERING A CIRCLE
C OF RADIUS R1.
C
C R2  MAXIMAL RADIUS OF COMPUTATION (METER). IF R2 = 0
C NO OUTER GRID IS USED. IF A FIXED-AREA COMPUTATION
C IS WANTED 'R2' MUST BE SUFFICIENTLY LARGE.
C
C THE COMPUTATION IS PERFORMED IN 'N' STATIONS, DEFINED BY A
C LISTING OF LATITUDE AND LONGITUDE (IN DEGREES) AND ELEVATION.
C
C GRID OPTION (N=0):
C COMPUTATIONS ARE PERFORMED IN THE POINTS OF A GRID, DEFINED BY
C LATITUDES 'LATIN' TO 'LATMAX' AND LONGITUDES 'LONMIN' TO
C 'LONMAX', WITH SPACING 'DLAT' AND 'DLON' SPECIFIED IN A R C -
C M I N U T E S. ELEVATION OF POINTS: 'ELEV', UNLESS IZCODE=1.
C INB: GRID RESULTS ARE P.T. ALSO OUTPUT ON UNIT 30 - BUT ONLY
C FOR ONE QUANTITY. SHOULD BE CHANGED TO LOCAL FORMAT NEEDS.)
C
C NOTE: IF THE TERRAIN GRIDS DOES NOT COVER THE 'COMPUTATION
C AREA' AS DEFINED BY THE MAXIMUM ZONE AND THE RADII, ELEVATION
C ZERO WILL BE ASSUMED FOR THE MISSING ELEVATIONS - WITHOUT WAR-
C NING. IF THE INNER GRID IS TOO SMALL TO ALLOW COMPUTATION TO
C DISTANCE 'R1' COMPUTATION WILL BE DONE USING OUTER GRID DATA
C WHERE DATA IS LACKING.
C
C PROGRAMMER: RENE FORSBERG, OHIO STATE UNIVERSITY / DANISH
C GEODETIC INSTITUTE, JULY 1983.
C LAST UPDATED: NOVEMBER 1983.
CCCCCCCCCCCCCCCCCCCCCCCCCCCCCCCCCCCCCCCCCCCCCCCCCCCCCCCC
C IMPLICIT REAL*8 (A-G, L, O-Z), INTEGER*2 (H)
C LOGICAL DG, DFV, HA, NCGRD2, STGRID
C DIMENSION LAT(1000), LCN(1000), ELEV(1000), GRES(1000)
C REAL*4 GLAB(6)
C
C COMMON /CPAR/ ITYPE, IKIND, IZCODE, DG, DFV, HA, R1, R2, R1SQ, R2SQ,
C RHO0, RHGISO, OPTISO, FKTIISO
C COMMON /RESULT/ SUMDG, SUMKSI, SUMETA, SUMHA, NPRISM, NPRIEX,
C DIMELV
C COMMON /HGRID/ F101, LA01, DF11, DLAI, NF11, NLAI, F102, LA02, DF12,
C DLAI, NF12, NLAI, IHD1M1, IHD2M1, IHD2M2
C COMMON /HREF/ F10REF, LA0REF, DF1REF, DLAREF, NF1REF, NLAREF,
C IHRD1M1, IHRD2M1
C
C SIZES OF ARRAYS USED TO HOLD ELEVATIONS ADJUSTED HERE
C
C DIMENSION H1 (481, 431), H2 (61, 61), HREF (30, 30)
C IHD1M1 = 481

```

```

481
IHD1M2 =
IHD2M1 =
IHD2M2 =
IHRD1M1 =
IHRD2M1 =
IHRD2M2 =
30
30
61
61
61
61
READ(5, *) ITYPE, IKIND, IZCODE, IGTYP1, F11, F12, LA1, LA2,
R1, R2, N
DG = (ITYPE.EQ.1.OR.ITYPE.EQ.4)
DFV = (ITYPE.EQ.2.OR.ITYPE.EQ.4.OR.ITYPE.EQ.6)
HA = (ITYPE.EQ.3.OR.ITYPE.EQ.5)
NCGRD2 = (R2.LE.0)
IF (LA1.LT.0.AND.LA2.LT.0) THEN
LA1 = LA1 + 360.0
LA2 = LA2 + 360.0
ENDIF
C
C DENSITY AND ISOSTATIC PARAMETERS
C
C RHO0 = 2.67
C RHOISO = -0.4
C OPTISO = 32000
C FKTIISO = DABS(1/RHCISO)
C
C READ STATION LIST AND FIND MAX AND MIN OF COORDINATES
C
C IF (N.GT.0) THEN
C STGRID = .FALSE.
C F1MIN = 360.0
C F1MAX = -360.0
C LAMIN = 360.0
C LAMAX = -360.0
C DO 11 I = 1, N
C READ(5, *) FI, LA, SH
C LAT(I) = FI
C IF (LA.LT.0) LA = LA + 360.0
C LON(I) = LA
C ELEV(I) = SH
C IF (LAT(I).LE.F1MIN) F1MIN = LAT(I)
C IF (LAT(I).GE.F1MAX) F1MAX = LAT(I)
C IF (LCN(I).LE.LAMIN) LAMIN = LCN(I)
C IF (LCN(I).GE.LAMAX) LAMAX = LCN(I)
C CONTINUE
C ELSE
C STGRID = .TRUE.
C READ(5, *) F1MIN, F1MAX, LAMIN, LAMAX, DFIS, OLAS, ELEVS
C IF (LAMAX.LT.0) THEN
C LAMIN = LAMIN+360.0
C LAMAX = LAMAX+360.0
C ENDIF
C DFIS = CFIS/60.0
C OLAS = CLAS/60.0
C NNS = (F1MAX-F1MIN)/DFIS+1.5
C NES = (LAMAX-LAMIN)/OLAS+1.5
C N = NNS*NES

```

```

C
K = 0
DO 20 I = NNS, 1, -1
DO 20 J = 1, NES
  K = K+1
  LAT(K) = FMIN + (I-1)*DFIS
  LON(K) = LAMIN + (J-1)*DLAS
  ELEV(K) = ELEVS
20 CONTINUE
ENDIF

WRITE(6, 8999)
8999 FORMAT('0===== TC TERRAIN EFFECT COMPUTATION =====')
9000 WRITE(6, 9000) ITYPE, IKIND, IZCODE, IGTYP1, FI1, FI2, LA1, LA2, R1, R2
9000 FORMAT(' - INPUT CODES: ', 4I2, ' ', MAXAREA: ', 4F7.2, ' ', RADII: ', 2F7.0)
WRITE(6, 9001) N, FMIN, FMAX, LAMIN, LAMAX
9001 FORMAT(' - STATIONS: ', 13, ' ', IN AREA: ', 4F9.4)
IF (STGRID) WRITE(6, 9009) NNS, NES, DFIS, DLAS
9009 FORMAT(' STATION GRID: ', 2I5, ' ', SPACING: ', 2F9.4)

C
C READ IN SUFFICIENT ELEVATIONS TO COVER STATION AREA WITH THE
C THE GIVEN CALCULATION RADII
C
RADEG = 180/3.1415926535900
F1 = 1.0DC/6371000*RADEG
F2 = F1/DCOS(FMIN/RADEG)
DO 12 I = 1, 2
  IF (I.EQ.1) THEN
    IF (IGTYP1.EQ.1) THEN
      READ(21) GLAB
      BACKSPACE(20)
      DRI = DMAX1(GLAB(5)/F1, GLAB(6)/F2)
    ELSE
      DRI = DMAX1(1.0D0/120/F1, 1.0D0/120/F2)
    ENDIF
  ENDIF
  IF (ICGRD2) THEN
    DR2 = 0
  ELSE
    READ(21) GLAB
    BACKSPACE(21)
    DR2 = DMAX1(GLAB(5)/F1, GLAB(6)/F2)
  ENDIF
  R = DMAX1(R1 + DR2, 2*GR1) + 0.001*DRI
ELSE
  R = R2
  IF (ICGRD2) THEN
    FI02 = FI01
    LA02 = LA01
    DF12 = DF11
    DLA2 = DLA1
    GC TO 12
  ENDIF
ENDIF
FLOW = DMAX1(FI1, FMIN-R*F1)
FIUP = DMIN1(FI2, FMAX+R*F1)
LALOW = DMAX1(LA1, LAMIN-R*F2)
LAUP = DMIN1(LA2, LAMAX+R*F2)

C
IF (I.EQ.1) THEN
  IF (.NOT. NOGRD2 .AND. IGTYP1.EQ.1) IGTYP1 = 0
  CALL RDELEV(20, IGTYP1, FILOW, FIUP, LALOW, LAUP,
    FI01, LA01, DF11, DLA1, NF11, NL1, IH1DM1, IH1DM2)
  CALL FINFO(FI01, LA01, DF11, DLA1, NF11, NL1, IH1DM1, IH1DM2)
ELSE
  CALL RDELEV(21, 1, FILOW, FIUP, LALOW, LAUP,
    FI02, LA02, DF12, DLA2, NF12, NL2, IH2DM1, IH2DM2)
  CALL FINFO(FI02, LA02, DF12, DLA2, NF12, NL2, IH2DM1, IH2DM2)
ENDIF
12 CONTINUE
C
C CHECK RELATIVE POSITION CF GRIDS
C
Q1 = DF12/DF11
Q2 = DLA2/DLA1
S1 = (FI01-FI02)/DF11
S2 = (DLA1-LA02)/DLA1
IF (DABS(Q1-IFRAC(Q1+.5))) .GT. 0.01 .OR. DABS(Q2-IFRAC(Q2+.5))) .
  .GT. 0.01 .OR. DABS(S1-IFRAC(S1+.5)) .GT. 0.01 .OR.
  .DABS(S2-IFRAC(S2+.5)) .GT. 0.01 WRITE(6, 9005)
9005 FORMAT('0*** WARNING *** OUTER AND INNER GRID DO NOT FIT ***')
C
C READ MEAN ELEVATION GRID
C
IF (IKIND.EQ.4) THEN
  READ(22) GLAB
  BACKSPACE(22)
  CALL RDELEV(22, 0, FILOW-GLAB(5)/2, FIUP+GLAB(5)/2,
    LALOW-GLAB(6)/2, LAUP+GLAB(6)/2,
    FI0REF, LA0REF, DF1REF, DLAREF, NF1REF, NLAREF,
    HREF, IH0DM1, IH0DM2)
  CALL FINFO(FI0REF, LA0REF, DF1REF, DLAREF, NF1REF, NLAREF,
    HREF, IH0DM1, IH0DM2)
ENDIF
WRITE(6, 9006)
9006 FORMAT('0===== RESULTS =====')
WRITE(6, 9002) FI LA H DTMELV HA
  . DG KSI ETA HA
C
DG 13 I = 1, N
  CALL TC(LAT(I), LON(I), ELEV(I), H1, H2, HREF)
  IF (ITYPE.EQ.5) SUMDG = SUMDG + 0.314*SUMHA
  WRITE(6, 9003) LAT(I), LON(I), ELEV(I), DTMELV, SUMDG, SUMKSI,
    SUMETA, SUMHA
9003 FORMAT(2F11.4, 2F8.2, ' ', 4F11.6)
  IF (ITYPE.EQ.1 .OR. ITYPE.GE.4) GRES(I) = SUMDG
  IF (ITYPE.EQ.2) GRES(I) = SUMKSI
  IF (ITYPE.EQ.3) GRES(I) = SUMHA
13 CONTINUE
C
C OUTPUT GRAVITY GRID ON UNIT 30
C

```



```

9001 WRITE(6, 9001) FI, LA
      FORMAT('---** TC WARNING ** STATION ', 2F10.4,
      * OUTSIDE OUTERGRID **')
      SPLINT = .FALSE.
      ELSEIF (RF1-LT-10-0.001-OR-RF1-GT-10+NF1+0.001-
      *OR-RLA-LT-10-0.001-OR-RLA-GT-10+NL1+0.001) THEN
        WRITE(6, 9002) FI, LA
        FORMAT('---** TC WARNING ** STATION ', 2F10.4,
        * OUTSIDE INNERGRID **')
        SPLINT = .FALSE.
        ELSEIF (SPLINT-AND-((11-LT-11-OR-112-GE-12-
        *OR-JJ1-LT-11-OR-JJ2-GE-12)) THEN
          WRITE(6, 9003) FI, LA
          FORMAT('---** TC WARNING ** STATION ', 2F10.4,
          * TOO NEAR GRID BOUNDARY FOR SPLINE **')
          SPLINT = .FALSE.
          ENDF

C CHECK BOUNDARIES FOR OUTSIDE STATIONS
C
C IF (R2-GT-0-AND-((11-GE-12Y-OR-11Y-GE-J2Y)) RETURN
C IF (11-GE-12-OR-11-GE-J2) THEN
  SPLINT = .FALSE.
  I1 = I2Y
  I2 = I2Y
  J1 = J2Y
  J2 = J2Y
  ENDF

C COMPUTATION OF INNER GRID WITHOUT SPLINE DENSIFICATION
C
C IF (.NOT.SPLINT) THEN
  I1 = IFRAC(RF1)+1-10
  JJ = IFRAC(RLA)+1-J0
  IF (11-LT-1-OR-11-GT-NF1-OR-JJ-LT-1-OR-JJ-GT-NLA1) THEN
    DTMLV = 0
  ELSE
    DTMLV = H1(11, JJ)
  ENDF
  IF (12CODE.EQ.0) STNELV = DTMLV
  DO 9 I = 11+1, I2
    DO 9 J = J1+1, J2
      CALL DTC(1-0.500, J-0.500, 1.00, 1.00, H1(1-10, J-J0), HREF)
    CONTINUE
  9 CONTINUE

C COMPUTATION OF INNER GRID WITH SPLINE DENSIFICATION
C
C NPCINT = 2*NSPL - 1
  DO 10 I = 1, NSPL
    S = SPODEF(I)
    VOIV(I) = (RF1-111)*S
    XOIV(I) = (RLA-JJ1)*S
    VOIV(NPCINT+2-1) = 3.00 - (112-RF1)*S
    XOIV(NPCINT+2-1) = 3.00 - (JJ2-RLA)*S
  10 CONTINUE

C COMPUTE ELEVATIONS AT HORIZONTAL SPLINE LINES
C
C DO 11 J = 1, 5
  DO 11 I = 1, 5
    A(I) = H1(1+11-10-1, J+JJ1-J0-1)
    CCNTINUE
    CALL INITSP(A, 5, R, Q)
    DO 11 I = 1, NPCINT
      RV = (VOIV(1+1)+VOIV(I))/2
      HSPL(I, J) = SPLINE(RV+1.500, A, 5, R)
    11 CONTINUE

C SCAN HORIZONTAL LINES, START WITH STATION TO GET MODEL HEIGHT
C
C DTMLV = 599999
  DO 12 I = NSPL, NSPL+NPCINT-1
    I1 = I
    IF (1-GT-NPCINT) I1 = I - NPCINT
    RV = (VOIV(I1+1)+VOIV(I1))/2
    DO 12 J = 1, 5
      A(J) = HSPL(I1, J)
      CALL INITSP(A, 5, R, Q)
    CCNTINUE
    DO 12 J = NSPL, NSPL+NPCINT-1
      JJ = J
      IF (J-GT-NPCINT) JJ = J - NPCINT
      RX = (XOIV(JJ+1)+XOIV(JJ))/2
      H = SPLINE(RX+1.500, A, 5, R)
      IF (DTMLV.EQ.599999) THEN
        DTMLV = H
        IF (12CODE.EQ.0) STNELV = DTMLV
      ENDF
      CALL DTC(RY+11, RX+JJ1, VOIV(I1+1)-VOIV(I1),
      * XOIV(JJ+1)-XOIV(JJ), H, HREF)
    12 CONTINUE

C COMPUTE REST OF INNERGRID
C
C DO 21 I = 11+1, I1
  DO 21 J = J1+1, J2
    CALL DTC(1-0.500, J-0.500, 1.00, 1.00, H1(1-10, J-J0), HREF)
  21 CONTINUE
  DO 24 I = 11+1, I12
    DO 24 J = J1+1, JJ1
      CALL DTC(1-0.500, J-0.500, 1.00, 1.00, H1(1-10, J-J0), HREF)
    CCNTINUE
  22 DO 23 J = JJ2+1, J2
    CALL DTC(1-0.500, J-0.500, 1.00, 1.00, H1(1-10, J-J0), HREF)
  23 CCNTINUE
  24 CONTINUE
  DO 25 I = 112+1, I2
    DO 25 J = J1+1, J2
      CALL DTC(1-0.500, J-0.500, 1.00, 1.00, H1(1-10, J-J0), HREF)
    CCNTINUE
  25 CONTINUE
  ENCF

```

[illegible]

```

C
C      WRITE(6,8000) RI-DI/2,RI-DI/2,RJ-DJ/2,RJ-DJ/2,H,HBASE,
C      .NPRISM,NPRIEX,STNELV,SUPELV
C8000 FORMAT(' *DTC* ELEM ',4F2.2,' H HBASE ',2F7.1,' * ',2I5,2F8.1)
C
C      DX = DJ*FAKT*F
C      DY = DI*YFAKT
C      DZ = H - HBASE
C      ZM = HBASE-STNELV-SUPELV+DZ/2
C
C      CALL PRISM1(RHO,XM,YM,ZM,DX,DY,DZ,DIST2+ZM**2)
C
C      EFFECT OF ISOSTATIC COMPENSATION
C
C      IF (IKIND.EQ.2) THEN
C        DZ = RHO*FKTISO*H
C        ZM = -STNELV-SUPELV-DPTISO-DZ/2
C        CALL PRISM1(RHOISO,XM,YM,ZM,DX,DY,DZ,DIST2+ZM**2)
C      ENDIF
C
C      RETURN
C      END
C
CCCCCCCCCCCCCCCCCCCCCCCCCCCCCCCCCCCCCCCCCCCCCCCCCCCCCCCCCCCCCCCC
C      SUBROUTINE PRISM1
C
C      COMPUTES GRAVITY FIELD IN ORICE FROM RECTANGULAR PRISM WITH
C      COORDINATES OF CENTER (XM, YM, ZM) AND SIDELENGTHS (DX, DY, DZ).C
C      EXACT OR APPROXIMATIVE FORMULAS ARE USED DEPENDING ON THE PRISM C
C      GEOMETRY.
C
CCCCCCCCCCCCCCCCCCCCCCCCCCCCCCCCCCCCCCCCCCCCCCCCCCCCCCCCCCCCCCCC
C      SUBROUTINE PRISM1(RHO, XM, YM, ZM, DX, DY, DZ, RSQ)
C
C      IMPLICIT REAL*8 (A-H, D-Z)
C      LOGICAL DG, DFV, HA
C      COMMON /CPAR/ ITYPE,IKIND,IZCODE,DG,DFV,HA,R1,R2,R1SQ,R2SQ,
C      RHO,RHOISO,DPTISO,FKTISO
C      COMMON /RESULT/ SUMDG,SUMKSI,SUMETA,SUMHA,SUMHA,NPRIEX,
C      DTWELV
C      DIMENSION X(2), Y(2), Z(2)
C      REAL*8 K(2,2,2), H(2,2,2), KK(2,2)
C
C      DATA R2EXAC, R2MACH / 6.0, 50.0 /
C      DATA G, GDFV, GHA / 0.00667, 0.001403, 6.5408D-9 /
C
C      SELECT APPROPRIATE FORMULAS
C
C      IF (DABS(DZ).LE.0.001) RETURN
C      NPRISM = NPRISM + 1
C      DR2 = DX**2 + DY**2 + DZ**2
C      F2 = RSQ/DR2
C      IF (F2.LT.R2EXAC) GO TO 100
C
C      PGINT MASS/MAC MILLAN

```

```

R = DSQRT(RSQ)
R3 = R*RSQ
FAKT = RHO*DX*DY*DZ
IF (DG) SUMDG = -G*FAKT*ZM/R3 + SUMDG
IF (DFV) THEN
  SUMKSI = -FAKT*GDFV*YM/R3 + SUMKSI
  SUMETA = -FAKT*GDFV*XM/R3 + SUMETA
ENDIF
IF (HA) SUMHA = FAKT*GHA/R + SUMHA
IF (F2.GT.R2MACH) RETURN
C
C      MC MILLAN EXPANSION
C
C      ALFA = 3*DX**2 - DR2
C      BETA = 3*DY**2 - DR2
C      GAMMA = 3*DZ**2 - DR2
C      ABG = ALFA*XM**2 + BETA*YM**2 + GAMMA*ZM**2
C      FAKT = FAKT/24/RSQ/R3
C      IF (DG) SUMDG = FAKT*G*ZM*(GAMMA - 5*ABG/RSQ) + SUMDG
C      IF (DFV) THEN
C        SUMKSI = FAKT*GDFV*YM*(BETA - 5*ABG/RSQ) + SUMKSI
C        SUMETA = FAKT*GDFV*XM*(ALFA - 5*ABG/RSQ) + SUMETA
C      ENDIF
C      IF (HA) SUMHA = FAKT*GHA*ABG + SUMHA
C      RETURN
C
C      EXACT PRISM FORMULAS
C
C      100 NPRIEX = NPRIEX + 1
C      X(1) = XM-DX/2
C      X(2) = XM+DX/2
C      Y(1) = YM-DY/2
C      Y(2) = YM+DY/2
C      Z(1) = ZM-DZ/2
C      Z(2) = ZM+DZ/2
C      IF (DG.OR.DFV) THEN
C        DO 11 I1 = 1, 2
C        DO 11 I2 = 1, 2
C        DO 11 I3 = 1, 2
C          K(I1, I2, I3) = DSQRT(X(I1)**2+Y(I2)**2+Z(I3)**2)
C        CONTINUE
C      11 CONTINUE
C
C      IF (DG) SUMDG = RHO*G*GZIX,Y,Z,K) + SUMDG
C
C      IF (DFV) THEN
C        DO 12 I1 = 1, 2
C        DO 12 I2 = 1, 2
C        DO 12 I3 = 1, 2
C          H(I1, I2, I3) = K(I2, I3, I1)
C        CONTINUE
C      12 SUMKSI = RHO*GDFV*GZ(Z, X, Y, H) + SUMKSI
C        DO 13 I1 = 1, 2
C        DO 13 I2 = 1, 2
C        DO 13 I3 = 1, 2
C          H(I1, I2, I3) = K(I3, I1, I2)

```


[illegible]

REFERENCES

- Abramowitz, M. and I.A. Stegun: Handbook of Mathematical Functions. Dover, New York, 1965.
- Bhattacharyya, B.K.: Magnetic anomalies due to prism-shaped bodies with arbitrary polarization. *Geophysics*, 29, p. 517-53.
- Burkhard, N. and D.D. Jackson: Application of stabilized linear inverse theory to gravity data. *Journ. Geoph. Res.*, 31, no. 8, pp. 1513-1518, 1976.
- Cruz, J: Experiences with altimeter data gridding. Report no. 347, Department of Geodetic Science and Surveying, The Ohio State University, 1983.
- Dorman, L.M. and B.T.R. Lewis: Experimental Isostasy, 1. Theory of the determination of the earth's isostatic response to a concentrated load. *JGR*, 75, 17, pp. 3357-3365, 1970.
- Dziewonski, A.M., A.L. Hales and E.R. Lapwood: Parametrically simple earth models consistent with geophysical data. *Phys. Earth and Plan. Int.*, 10, pp. 12-48, 1975.
- Engelis, T.: Analysis of sea surface topography using SEASAT altimeter data. Report no. 343, Department of Geodetic Science and Surveying, The Ohio State University, 1983.
- Forsberg, R. and F. Madsen: Geoid prediction in Northern Greenland using collocation and digital terrain models. *Ann. Geophys.*, 37, pp. 31-36, 1981.
- Forsberg, R. and C.C. Tscherning: The use of height data in gravity field approximation by collocation. *Journal Geophys. Res.*, 86, no. 9, pp. 7843-7854, 1981.
- Haddon, R.A.W. and Bullen, K.E.: An earth model incorporating free earth oscillation data. *Phys. Earth and Plan. Int.*, 2, 35, 1969.
- Heiskanen, W.A. and H. Moritz: *Physical Geodesy*. Freeman, San Francisco, 1967.
- Jung, K.: *Schwerkraft verfahren in der Angewandten Geophysik*, Akademisches Verlag, Leipzig, 1961.
- Kanasewich, E.R.: *Time Sequence Analysis in Geophysics*. University of Alberta Press, Edmonton, 1975.
- Lachapelle, G., A. Mainville and K.P. Schwarz: Empirical investigations on the anisotropy of the free-air gravity anomaly covariance function. *Boll. Geod. Sci. Aff.*, 42, no. 1, 1983.
- Lerch, F.J., B. Putney, C. Wagner and S. Klosko: Goddard earth models for oceanographic applications. *Marine Geodesy*, 5, no. 2, pp. 145-187, 1981.
- Liang, C.: The adjustment and combination of Geos-3 and Seasat altimeter data. Report no. 346, Department of Geodetic Science and Surveying, The Ohio State University, 1983.

- MacMillan, W.D.: Theoretical Mechanics, vol. 2, The theory of the potential. Dover, New York, 1958.
- Moritz, H.: Linear solutions of the geodetic boundary value problem. Report no. 79, Department of Geodetic Science and Surveying, The Ohio State University, 1966.
- Moritz, H.: On the use of the terrain correction in solving Molodensky's problem. Department of Geodetic Science, Report no. 108, The Ohio State University, 1968a.
- Moritz, H.: Density distributions for the equipotential ellipsoid. Department of Geodetic Science, Report no. 115, The Ohio State University, 1968b.
- Moritz, H.: Least squares collocation as a gravitational inverse problem. Department of Geodetic Science and Surveying, Report no. 249, The Ohio State University, 1976.
- Moritz, H.: Advanced physical geodesy. Herbert Wichmann Verlag, Karlsruhe, 1980.
- Nash, R.A. and S.K. Jordan: Statistical geodesy - an engineering perspective. Proc. IEEE, 66, no. 5, pp. 532-550, 1978.
- Papoulis, A.: Systems and transformations with applications in optics. McGraw-Hill, New York, 1968.
- Pedersen, L.B.: Constrained inversion of potential field data. Geoph. Prosp., 27, pp. 726-748, 1979.
- Rapp, R.H.: The earth's gravity field to degree and order 180 using SEASAT altimeter data, terrestrial gravity data, and other data. Reports of the Department of Geodetic Science and Surveying, no. 322, The Ohio State University, 1981.
- Rapp, R.H.: Degree variances of the earth's potential, topography and its isostatic compensation. Bull. Geod. 56, pp. 84-94, 1982.
- Rapp, R.H.: Problems in the development of improved high degree spherical harmonic expansions of the gravity field. Paper presented at the workshop "Gravity field modelling on a local basis", The Ohio State University, October 1983.
- Rummel, R., K.-P. Schwarz and M. Gerstl: Least squares collocation and regularization. Bull. geod., 53, pp. 343-361, 1979.
- Sanso, F. and C.C. Tscherning: Mixed collocation, a proposal. Quaterniones Geodaeiae, 3, no. 1, 1982.
- Sideris, M.G.: Computation of terrain corrections using the fast fourier transform. IAG SSG 4.91 handout, January 1984.
- Sünkel, H.: The estimation of free-air anomalies. Reports of the Department of Geodetic science and Surveying, Report no. 315, The Ohio State University, 1981a.

Sünkel, H.: Point mass models and the anomalous gravity field. Reports of the Department of Geodetic Science and Surveying, Report no. 328, The Ohio State University, 1981b.

Tscherning, C.C.: Some simple methods for the unique assignment of a density distribution to a harmonic function. Reports of the Department of Geodetic Science and Surveying, Report no. 213, The Ohio State University, 1974.

Tscherning, C.C. and R. Forsberg: Prediction test using least squares collocation and residual terrain reduction. In K.-P. Schwarz (ed.): Techniques to predict gravity anomalies and deflections of the vertical in mountainous areas, Department of Surveying Engineering, report 30004, University of Calgary, Alberta, 1983.

Tscherning, C.C.: A brief introduction to geoid modelling using collocation with some results from Scandinavia and Greenland. Preprint, submitted to Marine Geodesy, 1983.

